NSWC/WOL/TR 75-134

NSWC/WOL/TR 75-134

NSWC

TECHNICAL REPORT

WHITE OAK LABORATORY

A SUMMARY OF METHODS FOR COMPUTING THE DEGRADATION OF STRUCTURAL ELEMENTS DUE TO THE THERMAL AND THERMAL-BLAST EFFECT OF NUCLEAR WEAPONS

BY
Donald M. Wilson

26 MARCH 1976

NAVAL SURFACE WEAPONS CENTER
WHITE OAK LABORATORY
SILVER SPRING, MARYLAND 20910

- Approved for public release; distribution unlimited.

NAVAL SURFACE WEAPONS CENTER
WHITE OAK, SILVER SPRING, MARYLAND 20910

UNCLASSIFIED

SECURITY CLASSIFICATION OF THIS PAGE (When Data Entered)

REPORT DOCUMENTATION PAGE		READ INSTRUCTIONS BEFORE COMPLETING FORM
1. REPORT NUMBER NSWC/WOL/TR 75-134	2. GOVT ACCESSION NO.	3. RECIPIENT'S CATALOG NUMBER
4. TITLE (and Subtitle) A SUMMARY OF METHODS FOR COMPUTING THE DEGRADATION OF STRUCTURAL ELEMENTS DUE TO THE THERMAL AND THERMAL-BLAST EFFECT OF NUCLEAR WEAPONS		5. TYPE OF REPORT & PERIOD COVERED 6. PERFORMING ORG. REPORT NUMBER
7. AUTHOR(s) Donald M. Wilson		8. CONTRACT OR GRANT NUMBER(s)
9. PERFORMING ORGANIZATION NAME AND ADDRESS Naval Surface Weapons Center White Oak Laboratory White Oak, Silver Spring, Maryland 20910		10. PROGRAM ELEMENT, PROJECT, TASK AREA & WORK UNIT NUMBERS See Block 18
11. CONTROLLING OFFICE NAME AND ADDRESS		12. REPORT DATE 26 March 1976 13. NUMBER OF PAGES 97
14. MONITORING AGENCY NAME & ADDRESS(if different from Controlling Office)		15. SECURITY CLASS. (of this report) UNCLASSIFIED 15a. DECLASSIFICATION/DOWNGRADING SCHEDULE

16. DISTRIBUTION STATEMENT (of this Report)
Approved for public release; distribution unlimited

17. DISTRIBUTION STATEMENT (of the abstract entered in Block 20, if different from Report)

18. SUPPLEMENTARY NOTES
This research was sponsored by the Defense Nuclear Agency under Subtask #V99QAXND015, Operational Impact Assessment, Work Unit 03, Thermal Radiation - Operational Consequences.

19. KEY WORDS (Continue on reverse side if necessary and identify by block number)
Air Blast Effects
Thermal Radiation
Nuclear Weapons Effects

20. ABSTRACT (Continue on reverse side if necessary and identify by block number)
This report reviews and summarizes an existing large body of work on the effects of thermal radiation alone and thermal radiation combined with air blast effects on military structures or systems. All nuclear weapon phenomena were considered in order to find the ranges where thermal and thermal-blast effects are the most important. Methodology for computing thermal and thermal-blast effects is summarized and references are given to provide the omitted details.

DD FORM 1 JAN 73 1473 EDITION OF 1 NOV 65 IS OBSOLETE
S/N 0102-014-6601

UNCLASSIFIED
SECURITY CLASSIFICATION OF THIS PAGE (When Data Entered)

The methods given were all used to compute effects in simple structural elements which are taken to be components of larger structures or systems. Graphs for thermal effects are presented which allow estimates of the resulting peak temperatures but no corresponding result exists for stresses due to thermal-blast effects. Instead, examples are given to illustrate general principles and computer programs are referenced for the solving of specific problems.

This report emphasizes the thermal and thermal-blast effects of nuclear weapons on aluminum structural elements. Aluminum elements are particularly sensitive to thermal weakening hence changes in mechanical strength of aluminum due to rapid heating are given in detail. Although reference is made to ship systems, the methods and results presented are general and can be used to compute effects on any structure in a nuclear weapon environment.

NSWC/WOL/TR 75-134 26 March 1976

A SUMMARY OF METHODS FOR COMPUTING THE DEGRADATION OF STRUCTURAL ELEMENTS DUE TO THE THERMAL AND THERMAL-BLAST EFFECT OF NUCLEAR WEAPONS

This report represents part of a continuing effort to find techniques to protect shipboard elements from the combined thermal radiation and airblast of a nuclear weapon explosion. The summary of these techniques given herein is derived from past research performed at the Naval Surface Weapons Center as well as similar research from other government organizations and from industry. Equations and graphs are presented which allow stresses to be computed or temperatures to be easily found for some simple structural elements.

This work is sponsored by the Defense Nuclear Agency under Subtask V99QAXND015 - Work Unit 03.

LEMMUEL L. HILL
By direction

CONTENTS

ILLUSTRATIONS

ILLUSTRATIONS (cont.)

TABLES

I. INTRODUCTION

This report presents the results of a literature survey whose purpose was to review, condense, and present in a useable form the state of the art information on nuclear weapon thermal radiation effects. All thermal radiation effects are emphasized herein; all nuclear weapon phenomena which are damaging to shipboard systems or personnel are considered. Thermal radiation effects on personnel; i.e., skin burn and eye damage, are not considered in depth. It is assumed that adequate warning of an imminent nuclear attack will be available for crew members to take cover. Thermal radiation effects on optical systems have not been considered because present combat vessels do not rely heavily on such equipment. However, more extensive utilization of such systems is anticipated in the future. Optical systems may be extremely vulnerable because they can be degraded at large ship to weapon distances; hence, they should be considered in susceptibility studies on future combat systems. Damage phenomena independent of thermal effects such as nuclear radiation, nuclear fallout, or electromagnetic pulse are considered only to show where these might dominate and thereby preclude the consideration of thermal radiation effects. Nuclear weapon blast phenomena will be covered in detail because these can couple with thermal effects to drastically effect the damage done to a system. The response of specific military systems is not considered in the interest of keeping this report general. Only the unclassified literature has been summarized in order to produce an easily useable report available to a wide audience. The blast-thermal response of some military systems such as radar antennas has been reported in the classified literature. Instead, the response of simple elements which might be vulnerable components of a larger system is given in detail. Also, this report will emphasize the response of aluminum alloy elements. Aluminum alloys are commonly used in shipboard structures and are very susceptible to thermal and blast effects of a nuclear weapon due to their low thermal tolerance and relatively low mechanical strength. This report is intended to summarize existing knowledge into a reference that will provide a quick and reasonably accurate estimate as to the vulnerability of a given system in nuclear warfare. Additional material required for an in-depth analysis will be referenced as appropriate.

The combat effectiveness of the surface fleet would be enhanced by providing it protection against the effects of nuclear weapon explosions. Although a surface ship cannot at present defend against a well targeted direct attack, it could be made capable of withstanding the effects of an attack on another, perhaps higher value, target ship in its vicinity. Furthermore, it may not be necessary to redesign ships to withstand all of the effects of nearby nuclear explosions. The combat capability of many ships would be improved

by hardening vulnerable ships systems such as radar antennas or exposed weapon systems. The survivability of a vulnerable system is a complex problem because a nuclear weapon causes several damaging phenomena within a short period of time. A sensible approach to hardening is to provide protection against the dominant and practically-protectable effects up to a level where other, more difficult to protect against, effects begin to govern system response. It will be shown that thermal and blast, or a combination of these effects, are still damaging to aluminum structures at weapon to ship ranges where initial nuclear radiations are no longer hazardous to personnel. Thus, protection against thermal-blast and perhaps electromagnetic pulse effects must be considered for those ranges where radiation levels are no longer detrimental to crew survival. The concept of providing protection to ships for specified weapon to ship ranges and for pertinent weapon phenomena up to the necessary level only is termed "balanced hardening".

II. SYMBOLS

a - coefficient of linear thermal expansion

al - width of plate (dimension in x-coordinate direction)

A - absorptance

Ac - cross-section area

bl - length of plate (dimension in y-coordinate direction)

B - longest length dimension of plate or beam

C - constant (see equation (33))

Cd - drag coefficient

Co - speed of sound in undisturbed sea level atmosphere

Cp - specific heat at constant pressure

d - dynamic pressure of nuclear weapon explosion

dmax - peak dynamic pressure

D - structural rigidity $[EL^3/(12 \cdot (1 - u))]$

DS - slant distance from a nuclear weapon burst

E - elastic (Young's) modulus

Emax - maximum field strength of nuclear weapon electric field

Et - total nuclear weapon energy which appears as prompt thermal radiation

F - force developed in thermal expansion against edge restraint

Fx - in-plane tension force per unit width in a constrained plate

Fy - in-plane tension force per unit length in a constrained plate

G - distance variable for nuclear weapon burst of W kt. weapon yield

Gl - distance variable for nuclear weapon burst of 1 kt. weapon yield

GR - ground range from a nuclear weapon burst

h - heat transfer coefficient for convective cooling

H - nuclear weapon thermal irradiance

HMAX - maximum thermal irradiance

HOB - height of burst of nuclear weapon relative to sea level

HT - height of burst of nuclear weapon above ground level

I - moment of inertia

Io - initial gamma radiation dose per unit area from a 1 kt. nuclear weapon burst

k - thermal conductivity

Kb - buckling coefficient for a rectangular flat plate

K - constant (see equation (32))

L - thickness of structural element

Mmax - maximum field strength of nuclear weapon magnetic field

Mt - thermal moment in plate or beam

Ncr - buckling load for plates

No - initial neutron dose per unit area from a 1 kt. nuclear weapon burst

Nt - thermal reaction force in plate or beam

P - pressure pulse received from a nuclear weapon burst

Pa - atmospheric pressure as a function of altitude

Pcr - buckling load for the beam column

Pd - fundamental period of vibration

PDUR - positive phase duration for nuclear weapon pressure pulse

Pmax - peak overpressure

PmaxA - peak overpressure as a function of altitude

Pn - Prandtl number

Po - atmospheric pressure in undisturbed air at sea level

Pr - peak reflected pressure for blast wave at normal incidence

Ps - stagnation pressure

q - heat transfer rate per unit area

QT - radiant exposure

r - radius of circular cylinders

R - radius of nuclear weapon fireball

Re - Reynolds number

RF - radius of nuclear weapon fireball flattened by interaction with ground

S - smaller dimension of 1/2 width or 1/2 length of a flat plate

t - time

t1 - time variable for a 1 kt. nuclear weapon burst

t2 - time for nuclear weapon blast wave to traverse thickness of flat plate

tb - time for pressure back of plate to rise to stagnation pressure

Tmax - time at which maximum irradiance of nuclear weapon thermal pulse occurs

tt - time variable for W kt. nuclear weapon burst

ts - time for initial reflections of blast wave to dissipate

tsm - time for maximum thermal moment to be developed in plates or beams

tx - optical thickness

T - temperature

Ta - atmospheric temperature as a function of altitude

Tc - atmospheric transmission factor for nuclear weapon thermal radiation

Ti - initial temperature

To - atmospheric temperature in undisturbed air at sea level

Ts - surface temperature

U - shock front velocity of nuclear weapon blast wave

v - velocity

V - peak wind velocity of nuclear weapon blast wave

Vis - visibility of atmosphere

w - displacement

W - weapon yield

x - coordinate in x direction

y - coordinate in y direction

z - coordinate in z (thickness) direction

α - thermal diffusivity $(K/\rho \cdot Cp)$

β - parameter equal to $\sqrt{F/E \cdot I}$

ϵ - emissivity

η - generalized coordinate (see equation (B-17))

γ - viscosity

μ - Poisson's ratio

ω - angular frequency of vibration

ω_{ss} - fourier transformed angular frequency

ρ - density

σ - Stephan-Boltzmann constant

σ_p - principal stress

σ_x -- stress in x direction

σ_y - stress in y direction

τ_{xy} - shear stress

Subscripts

p - pressure

th - thermal

III. NUCLEAR WEAPON EFFECTS

The principal damaging phenomena of a nuclear weapon can be divided into three broad categories; namely, radioactivity, thermal and blast, and electromagnetic. Although effects of all three categories can occur simultaneously, they can be differentiated by the ship to weapon distance where their effect is dominant. Thus, radioactivity is likely to be the dominant concern at short distances and electromagnetic effects at great distances. It is at intermediate ranges where damage to structures caused by thermal and blast effects is important. Each of the three categories of weapon phenomena will be discussed in this section and the ship to weapon distances where their effects dominate will be given.

Radioactivity from a nuclear weapon explosion consists of gamma rays, neutrons, beta, and alpha particles emitted in the nuclear reaction or by secondary nuclear processes which are caused by energetic particles of the reaction or by the fission product decay of radioactive particles. Thus, these nuclear processes causing radiation are occurring long after the original nuclear explosion. For convenience, the nuclear radiations produced are divided into initial and residual radiations. Initial nuclear radiations are arbitrarily defined as those which appear within the first minute of a nuclear explosion. Residual radiations occurring after the first minute are due to the decay of fission products or radioactive weapon materials. In fusion weapons these are also due to the reaction of high speed neutrons with weapon materials or the surrounding atmosphere. Residual radiations are divided into early fallout which reaches the ground within 24 hours and delayed fallout which arrives in small quantities over several weeks or months. The radioactivity of fission products and other effected material is continually reduced in intensity by radioactive decay; hence, the radiation levels of delayed fallout are too low to present an immediate danger to health. Early fallout may produce hazardous radiations consisting mainly of relatively large particles. However, these rapidly decay; hence, radioactivity decreases rapidly with time after explosion. Also, these particles can be washed away on ships equipped with washdown systems. It will be assumed herein that residual radiations represent only a minor threat that can be coped with by ships in a nuclear warfare environment.

The initial nuclear radiations present an immediate danger to personnel within relatively short distances of a nuclear weapon explosion. Of the radioactive particles initially released, the alpha and beta particles have ranges too short to reach personnel in numbers large enough to be harmful. But the gamma rays and neutrons can travel considerable distances through air and both cause harmful effects on living organisms. Although the initial gamma rays and neutrons represent only about 3 percent of the total explosive energy or weapon yield, they are the most harmful and difficult to protect against weapon effect for short ship to weapon burst point ranges. For example, a shield which would reduce the intensity of gamma rays to 1/10 their initial value would require approximately 15 inches of

aluminum, 18 inches of concrete, or over 3 feet of water. Furthermore, the best shield for gamma ray attenuation may not be effective for neutron flux attenuation, hence either two shields or a compromise material such as concrete must be used.

The previous discussion showed that it is difficult to provide nuclear radiation protection on ships where weight is an important consideration. However, the distance from weapon burst to ship where radiation effects are harmful to personnel must be known so that the ship can be protected from other weapon effects beyond this range. The determination of initial radiation received at a point is given by semi-empirical laws which account for the attenuation of gamma rays and neutrons when they pass through the atmosphere. The dosage unit of received gamma ray radiation is the roentgen. By definition one roentgen is the quantity of gamma radiation which causes the formation of 2.08×10^9 ion pairs per cubic centimeter of dry air at standard temperature (0^oC) and pressure (one atmosphere). The semi-empirical law for initial gamma ray dosage is the following where Io is the exposure in roentgens at distance D in yards from a one kiloton nuclear weapon explosion[1].

$$Io = \frac{3.2 \times 10^9}{D^2} \; e^{-D/360} \qquad (1)$$

This equation shows that the quantity of gamma radiation decreases with distance according to the inverse square law. This is due to the spread of radiation over larger and larger areas as distance is increased from its source. The exponential factor accounts for radiation attenuation due to absorption and scattering in the atmosphere. The average density of the air between the weapon burst point and target in this formulation was 0.9 that of normal sea-level density. A scaling factor applied to equation (1) to account for weapon yields larger than one kiloton has been derived from weapon test data. This factor is reproduced in Figure 1 which is taken from the literature on nuclear weapons[2]. The scaling factor for gamma dosage increases more rapidly than weapon yield because of the sustained low density air resulting from the passage of the weapon shock wave. The lowered density results in less attenuation by absorption and scattering, hence an enhancement of gamma radiation occurs for large weapon yields which have stronger shock waves. Equation (1) and Figure 1 do not give an exact prediction for received gamma radiation dose due to variations in the nuclear explosive processes caused by differences in weapon design. The prediction is accurate within a factor of two for

---

[1] S. Glasstone, Ed., "Effects of Nuclear Weapons", U.S. Atomic Energy Commission, revised edition, reprinted February 1962.

[2] Ibid, p. 378

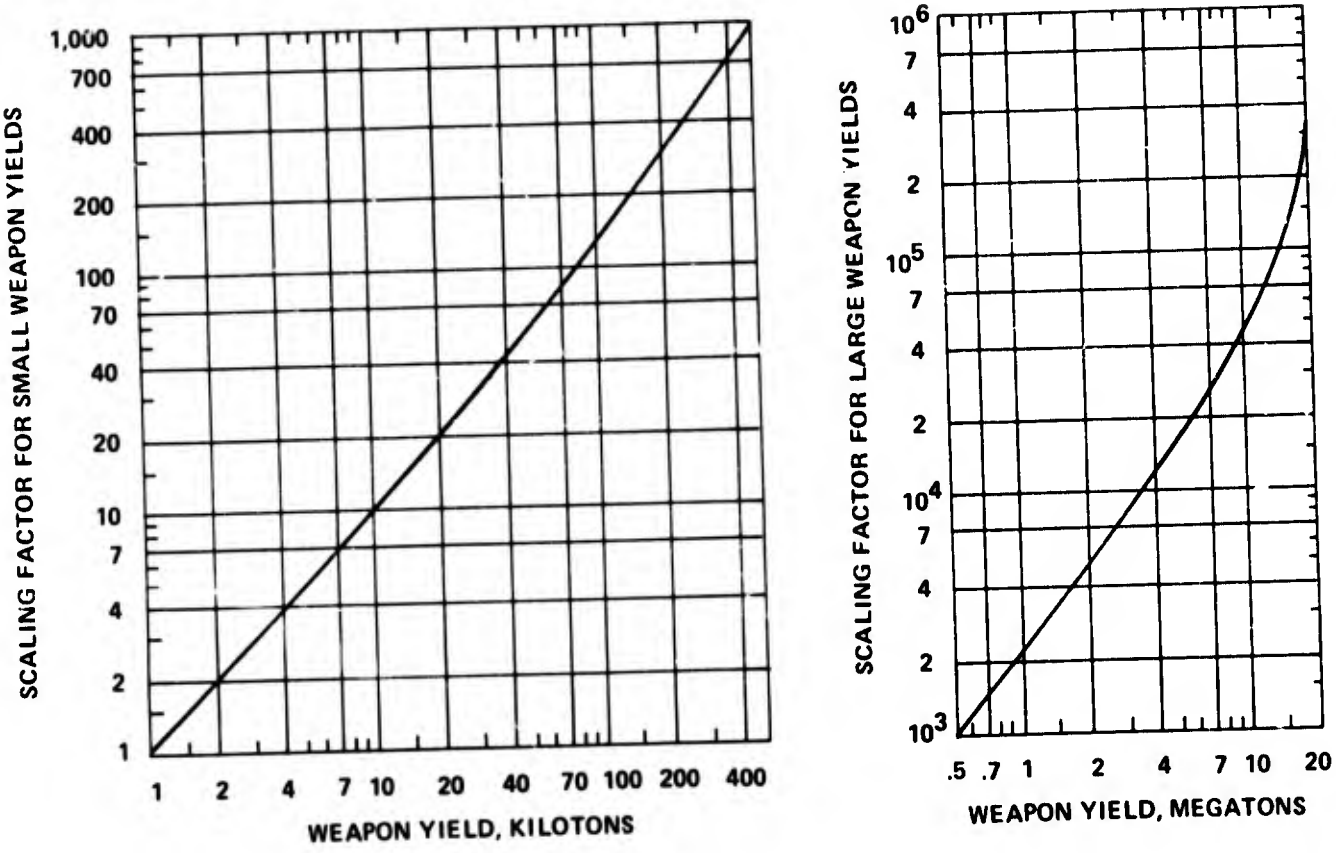

FIG. 1 SCALING FACTOR FOR INITIAL GAMMA-RADIATION DOSE, SMALL AND LARGE WEAPON YIELDS.

weapon yields below 100 kilotons but only within a factor of five for 500 kilotons and 10 for yields above 1 megaton. Also, this analysis is based on data for air bursts. In surface bursts, the presense of dust and debris produced by the explosion causes an additional attenuation of gamma radiation. It is generally assumed that the initial gamma radiation dose from a surface burst will be two-thirds of that predicted for an air burst. The semi- empirical law for initial neutron dosage is the following, where No is the

is the total neutron exposure in neutrons/centimeter^2 at distance D from a 1 kiloton nuclear weapon explosion.

$$No = \frac{8.6 \times 10^{18}}{D^2} e^{-D/210} \quad (2)$$

A scaling factor to account for larger weapon yields is to simply multiply equation (2) by the weapon yield, W. Thus, for a weapon yield of W kilotons,

$$No = \frac{8.6 \times 10^{18}}{D^2} \cdot W \cdot e^{-D/210} \quad (3)$$

Equation (3) also yields only an approximate result for received neutron dose due to differences in weapon design. Also, the number of neutrons emitted in a nuclear explosion depends on whether the weapon is a fission or fusion type weapon. Equation (3) represents a compromise between fission and fusion weapons and this also causes it to yield only approximate results.

The initial radiation laws described above, although approximate, are adequate for estimating the range where radiation is likely to be harmful. Both of these laws must be converted to amount of radiation absorbed in the tissues of exposed personnel. The unit of absorbed radiation is the rad. One rad is the amount of absorbed radiation that results in the liberation of 100 ergs of energy per gram of absorbing material. Also, about 88 ergs of energy are liberated in one gram of air exposed to one roentgen of gamma radiation. It is generally assumed that an exposure of one roentgen gamma radiation will result in an absorbed dose of one rad in biological tissue. For other than gamma radiation, the absorbed dose in rads may produce more or less damage in tissue depending on the type of radiation. The relative biological effectiveness of nuclear radiations is defined as the ratio of the absorbed dose in rads of gamma radiation which produces a given biological effect to the absorbed dose in rads of another type of radiation that causes the same effect. The biological damage done by weapon neutrons is similar to that done by weapon gamma rays, hence the relative biological effectiveness of weapon neutrons is unity. However, the relative biological effectiveness for neutrons can be much greater than one for a specific biological effect such as the formation of eye cataracts. The delivered dosage for neutron radiation, given in neutrons per square centimeter, must be converted to an absorbed dose expressed in rads. This was accomplished by considering a typical spectrum of neutron energies from a fission type weapon and assuming that the neutron delivers all its energy to the body tissue upon colliding with an atomic nucleus of this tissue. (For neutrons with energies greater than 200 electron volts.) The following conversion factor was found.[3]

[3] Ibid, p. 581

$$1 \frac{\text{neutron}}{\text{centimeter}^2} = 1.8 \cdot 10^{-9} \text{ rad} \quad (4)$$

Equation (4) allows the absorbed doses for neutron and gamma radiation to be summed to yield the absorbed dose for initial radiation as a function of distance, D, from the nuclear weapon burst point. However, common practice is to express absorbed radiation results in rems, the dose unit of biological effectiveness. The rem which stands for roentgen equivalent mammal is the product of the relative biological effectiveness and the absorbed dose in rads. Thus, expressing absorbed radiation in rems accounts for the differences in the effectiveness of different types of radiation when absorbed by personnel. The initial nuclear radiations consist principally of gamma rays and neutrons which both have a relative biological effectiveness of one. Hence, for these, the absorbed dose in rems is equal to the absorbed dose in rads. The laws given herein for absorbed dose of initial radiation were used to calculate the absorbed radiation, in rems, for personnel located at various ranges from a nuclear weapon burst point. These calculations are summarized in Figure 2.

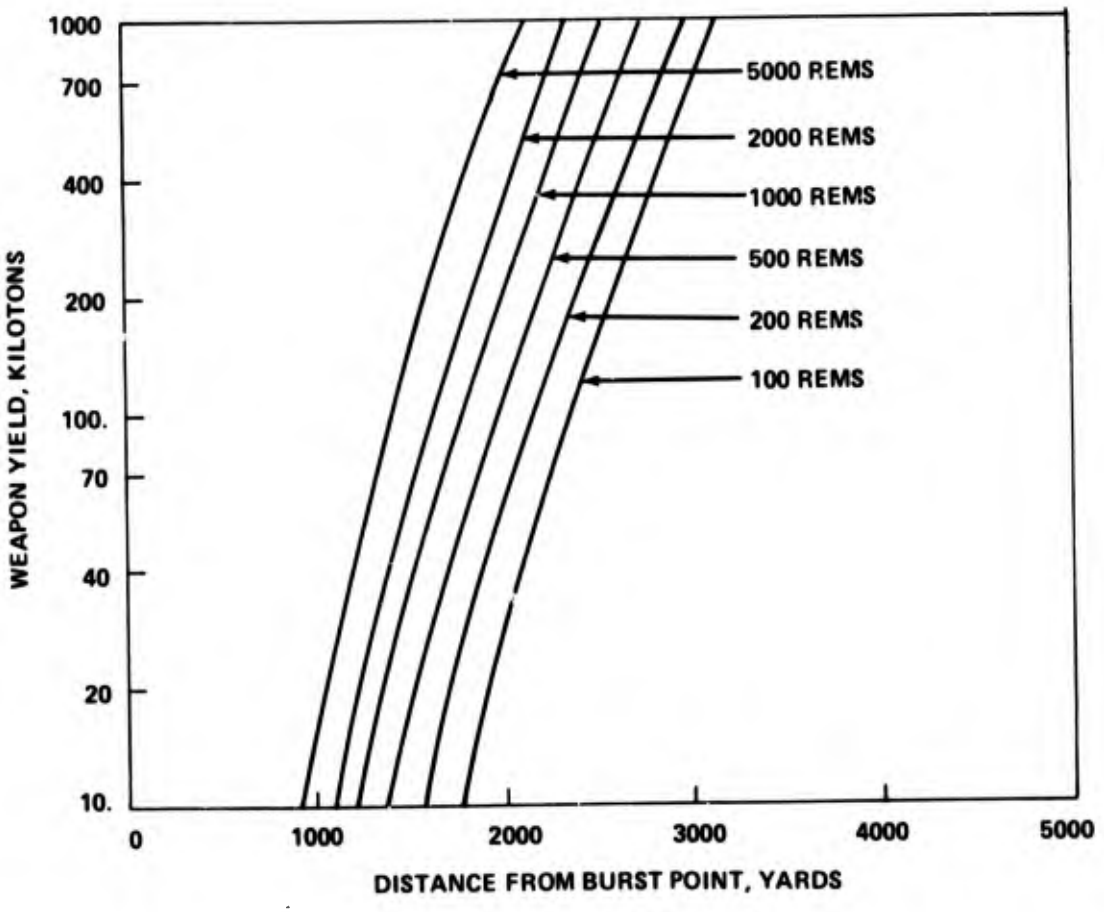

FIG. 2 ABSORBED RADIATION DOSE FOR INITIAL NUCLEAR RADIATION

Figure 2 shows that the absorbed flux of gamma rays and neutrons are rapidly attenuated by distance from the burst point. Thus, the initial radiation dose decreases from a devastating value of 5,000 rems to a relatively safe value of 100 rems in about 1,000 yards for any weapon yield between 10 and 1000 kilotons. In fact, the initial radiation dose decreasesby about a factor of two for every 100 yards increase in distance for the initial radiation doses given in Figure 2. Thus, the fact that the analysis leading to Figure 2 may contain relatively large errors is not important in determining safe ranges for initial radiation. A comparison of the exponential terms for scattering and absorption shows that neutrons are attenuated much more readily than gamma rays, that is their "relaxation length", 210 yards, is much less than that of gamma rays, 360 yards. The relaxation length is the distance in which attenuation by a factor of 1/e occurs. The contribution of neutrons to the total absorbed dose is relatively less as distance from the burst point increases. Neutron flux predominates for ranges less than 1,000 yards but is only about 10 percent of the total at 2,000 yards and is negligible beyond about 3,000 yards.

Information on the clinical effects of a rapidly received radiation dose has been gathered from a few laboratory accidents and from observations made on Japanese victims of nuclear warfare at the close of World War II. This information is summarized in Table 1.[4]

TABLE 1 - CLINICAL EFFECTS OF A RAPIDLY RECEIVED RADIATION DOSE

Dose	Time to Illness	Characteristic Illness	Therapy	Convalescent Period	Incidence of Death	Time to Death
0-100 Rems	-	-	Reassurance	None	None	-
100-200 Rems	3 hrs.	White Blood Cell Loss	Clinical Surveillance	Several Weeks	None	-
200-600 Rems	2 hrs.	Severe Loss of White Blood Cells	Blood Transfusion Anti-Biotics	1-12 Months	0-80%	2 Months
600-1000 Rems	1 hr.	Hemorrhage and Infection	Consider Bone Marrow Transplant	Years	80-100%	2 Months
1000-5000 Rems	1/2 hr.	Diarrhea, Fever Electrolyte Imbalance	Maintenance of Electrolyte Balance	Years	90-100%	2 Weeks
Over 5000 Rems	-	Convulsions, Tremor, Lethargy	Sedatives	Years	~100%	2 Days

[4] Ibid, p. 591

The information in Table 1 is considered to be reliable for humans up to 200 rems only. From 200-600 rems experiments performed on animals were used to support some observations of human reaction. Above 600 rems data on humans is rare and all significant conclusions must be made from animal reactions. It is thought that immediate incapacitation and future likely death will result for radiation doses of 1,000 rems or greater. For doses of 100 rems or less the response is subclinical. That is, most individuals experience no illness although some long lasting changes may have occurred in the blood. For doses between 100 and 200 rems, an individual would feel only slight immediate discomfort; i.e., nausea or slight vomiting, followed by mild symptoms two weeks later; i.e., loss of appetite and eventual total recovery. For doses greater than 200 rems the radiation effects become increasingly serious and incapacitation is likely. When recovery is possible an extended convalescence is usually required. Therefore, in this report, a dose of 200 rems will be taken as the limit to which personnel can be exposed without taking casualties or without effecting the mission of a ship in a nuclear warfare environment. It should be remembered that radiation effects are somewhat cumulative so that personnel receiving radiation in one engagement will not be able to stand a full 200 rems in a second encounter.

Initial nuclear radiation can also damage electronic equipment. For example, integrated circuits are impaired by neutron doses of about 5×10^{13} neutrons/cm^2 and these fail at doses of 10^{15} neutrons/cm^2. Semi conductors are vulnerable to the ionizing effects caused by initial gamma rays. However, the damage to electronic equipment is likely to be significant only at very close ranges where initial radiation effects on personnel are of the most concern.

Thermal radiation and air blast are the nuclear weapon effects which physically threaten ships systems for ranges greater than those shown in Figure 2 for 200 rems of initial radiation. First, thermal radiation and then air blast weapon output will be given for the intermediate ranges where they are the most important weapon effect. Thermal radiation from a nuclear weapon explosion results from the very high temperatures, tens of millions of degrees, caused by the rapid release of energy in the nuclear reaction. These high temperatures cause electromagnetic radiation of short wavelength (x-rays) to be emitted and these heat the surrounding air to high temperatures; i.e., several thousand degrees. The radiation is readily absorbed within a few feet by the surrounding air thereby creating the fireball. The fireball then emits relatively long wavelength radiation in the ultraviolet, visible, and near infrared spectral region which is not readily absorbed by the atmosphere. Since this radiation travels at the speed of light, 3×10^8 m/sec, its effects begin to be felt immediately after the formation of the fireball. The fireball remains at high temperature and emits visible radiation for about one minute (1 megaton weapon yield) although by then the energy flux has decreased to a negligible value. The physical reaction of the fireball with its environment causes its radiant energy to be emitted in two distinct pulses. The initial increase in emitted radiant energy is due to the increase in size of the early stages of expansion of the incandescent shock front. A first maximum results when the enhancement of radiant

energy due to increasing area of the source is just offset by the temperature decrease of the hot gases due to expansion. The radiant power measured at a distance will increase again due to a decrease in opacity of the shock heated air surrounding the fireball. A second maximum results when the enhancement of power due to decreasing opacity is just offset by the radiative cooling of the hot gases which constitute the fireball. After the second maximum, the radiative power slowly decreases as the fireball is slowly cooled by radiation. This sequence of events occurs only for air bursts in the lower atmosphere; i.e., below 100,000 feet altitude. Above 100,000 feet there is only a single peak of thermal radiance. The first pulse duration is only about one percent that of the second pulse and it contains less than one percent of the total emitted thermal energy. Hence, the first pulse does not contribute to nuclear weapon thermal damage except for temporary or perhaps permanent damage to the eyes of individuals who happen to be looking in the direction of the explosion. It has been found that the prompt thermal radiation emitted in a nuclear weapon explosion plotted against time after the explosion can be scaled with weapon size to yield a universal relationship of scaled irradiance versus scaled time. Irradiance is scaled by the maximum second pulse irradiance and time by the time at which the maximum irradiance occurs. The second pulse of scaled irradiance versus scaled time is shown in Figure 3. The first pulse was omitted due to its lack of contribution to structural damage and it will not be considered further.

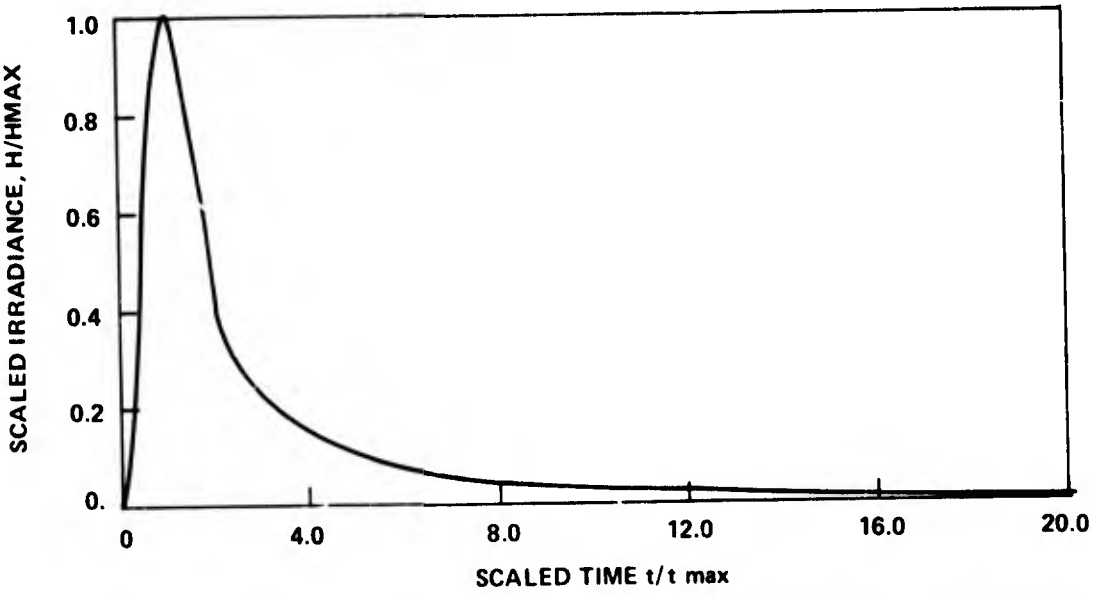

FIG. 3 UNIVERSAL IRRADIANCE RELATIONSHIP FOR NUCLEAR WEAPON THERMAL PULSE

The relationship between time to maximum irradiance and weapon yield also depends to a lesser extent on height of burst above sea level. Equation (5) relates this time in seconds to weapon yield in megatons (1 megaton = 1×10^6 tons TNT) and height of burst in miles.

$$Tmax = 0.82 \cdot W^{0.42} \cdot e^{-.09 \cdot HOB} \qquad (5)$$

This equation is valid for air bursts in the lower atmosphere; i.e., below altitudes of 100,000 feet. The thermal characteristics of a nuclear burst are altered if the fully developed fireball radius intersects the surface. The fully developed fireball radius in miles is given by equation (6) where weapon yield is also in megatons and height of burst is in miles[5]

$$R = 0.41\ W^{0.35} \cdot e^{.0465 \cdot HOB} \qquad (6)$$

A surface burst has occurred if the radius given by equation (6) is less than the height of burst. In this case, the time to maximum irradiance is modified as given by equation (7)[6]

$$Tmax = 0.82 \quad (2 - \frac{HOB}{RF}) \cdot W^{0.35} \cdot e^{-.09 \cdot HOB} \qquad (7)$$

where RF is the flattened fireball radius given by equation (8)[7]

$$RF = 2.44\ (.53 - .12\ \frac{HOB}{R}) \cdot R \qquad (8)$$

The time to maximum irradiance is important in determining the length of time that irradiance will be received. For example, approximately 90 percent of the total received irradiance has arrived by 20 times the value of Tmax.

The maximum irradiance can be related to the radiant exposure by integrating the irradiance versus time relationship expressed in Figure 3. The result of this integration is:

$$HMAX = \frac{QT}{2.57 \cdot Tmax} \qquad (9)$$

5. C. Colvin and S. Martin, "Computer Program for Estimating Free-Field Thermal Radiation Characteristics," URS Corp. Report URS 683-1, Dec. 1967
6. Colvin and Martin, Op. Cit.
7. Colvin and Martin, Op. Cit.

The important quantity in determining thermal damage from a nuclear weapon explosion is usually the total heat energy or radiant exposure, QT, received at a distance, DS, from the burst point. The radiant exposure decreases with distance from the burst point according to the inverse square law due to the spread of energy over larger and larger areas. A certain percentage of the released energy will be absorbed or scattered by the atmosphere. This quantity is given by an atmospheric transmission factor, Tc, which is discussed later. Thus, the radiant exposure in terms of the heat energy liberated, Et, is the following.

$$QT = \frac{Et \cdot Tc}{4\pi \cdot DS^2} \qquad (10)$$

For an ordinary air burst, approximately 30-50 percent of the total weapon energy yield appears as prompt thermal radiation emitted from the fireball. This percentage is somewhat lower for a surface burst. In this report, the total energy appearing as prompt thermal radiation, Et, is assumed to be 0.4 times the total weapon yield, W, for an air burst in the lower atmosphere. Equation (10) can be recast to yield the radiant exposure, QT, in units of cal/cm^2 given weapon yield W in kilotons and distance DS in miles. This is accomplished using the conversion that 1 kiloton equivalent TNT explosive energy equals 10^{12} calories heat energy. The result is,

$$QT = \frac{1.229 \cdot W \cdot Tc}{DS^2} \qquad (11)$$

The utilization of equation (11) depends on the evaluation of the transmission, Tc. This factor is governed by the following variables: (1) state of the atmosphere, (2) presence or absence of clouds, (3) albedo of the surface between burst and target, and (4) height of burst above ground. The transmission factor is a complicated function of the above variables and it has not been accurately determined how each variable or combination of variables will effect the transmission of thermal radiation. Instead, guidelines will be given to judge how each factor considered separately might effect the overall atmospheric transmission. The state of the atmosphere is indicated by the visibility, VIS, in miles. The guidelines for judging visibility are as follows[8].

Atmospheric State	Very Clear	Clear	Light Haze	Medium Haze	Heavy Haze	Thin Fog	Light Fog	Heavier Fog
VIS (miles)	30	12	6	3	2	1.2	0.6	< 0.5

8. Colvin and Martin, Op. Cit.

The presence of clouds are accounted for by giving a multiplication factor for transmission, Tc, depending on the degree of cloud presence. Thermal radiation must pass through the clouds for these factors to be valid; therefore, they are more likely to apply to aircraft flying above the burst point than to ships sailing on the sea. The factors are as follows.[9]

Cloud Presence	Clear	Light Haze	Medium Haze	Heavy Haze	Light Cloud	Medium Cloud	Heavy Cloud
Factor	1.0	0.7	0.5	0.4	0.3	0.2	0.1

The albedo factor is applied to cloud presence factor only as follows. If the surface between burst and target has high reflectance, the albedo factor is 1.5 times the cloud presence factor. If the surface has low reflectance, the albedo factor is unity. The visibility and the height of burst above the surface are used in the scattering and absorption model for thermal radiation. This model consists of two cases. These are (1) transmission along the surface when both the fireball and the target are immersed in a nearly uniform scattering layer, (2) transmission from a fireball which is above the scattering layer. The height of the scattering layer is arbitrarily taken to be 1/4 mile above the surface. For case (1) the transmission is given by the following equation.

$$Tc = e^{-2 \cdot DS/VIS}\left(1 + 1.4 \frac{DS}{VIS}\right) \qquad (12)$$

For case (2) the path from fireball to target is divided into two lengths, D1 and D2. D1 is the slant distance inside the scattering layer and D2 is the slant distance above the scattering layer (DS = D1 + D2). The transmission for path length D1 is given by equation (12) with DS replaced by D1. The transmission for path length D2 is given in terms of the optical thickness for scattering, tx, as follows.

$$Tc = e^{-tx \cdot D2/HT} \qquad (13)$$

In equation (13) HT is the distance above the surface to burst in miles. The dimensionless optical thickness, tx, is a function of altitude above surface to burst. The following values were derived.[10]

HT (mi.)	0.25	0.35	0.50	0.70	1.0	1.5	2.0	3.0
tx	.0310	.0425	.0570	.0717	.0890	.1073	.1179	.1294

5.0	10.0	∞
.1403	.1520	.1570

[9] Colvin and Martin, Op. Cit.

[10] L. Elterman, "Atmospheric Attenuation Model, 1964, In the Ultraviolet, Visible, and Infrared Regions for Altitudes to 50 km", Environmental Research Papers, No. 46, AFCRL 64-740, Sep 1964.

The transmission for case (2) is the product of the individual transmissions given by equation (12) for distance D1 and by equation (13) for distance D2.

Equations (11), (12), and (13) were used to compute the maximum radiant exposure received from a nuclear weapon burst of given yield as a function of distance along the surface from the burst point projection on the surface; i.e., the ground range. The maximum possible radiant exposure is delivered to a target when the fully developed fireball just intersects the surface. Thus, equation (6) for fireball radius is used to calculate the height of burst as a function of weapon yield. The result of these calculations for weapon yields between 10 and 1,000 kilotons is given in Figure 4.

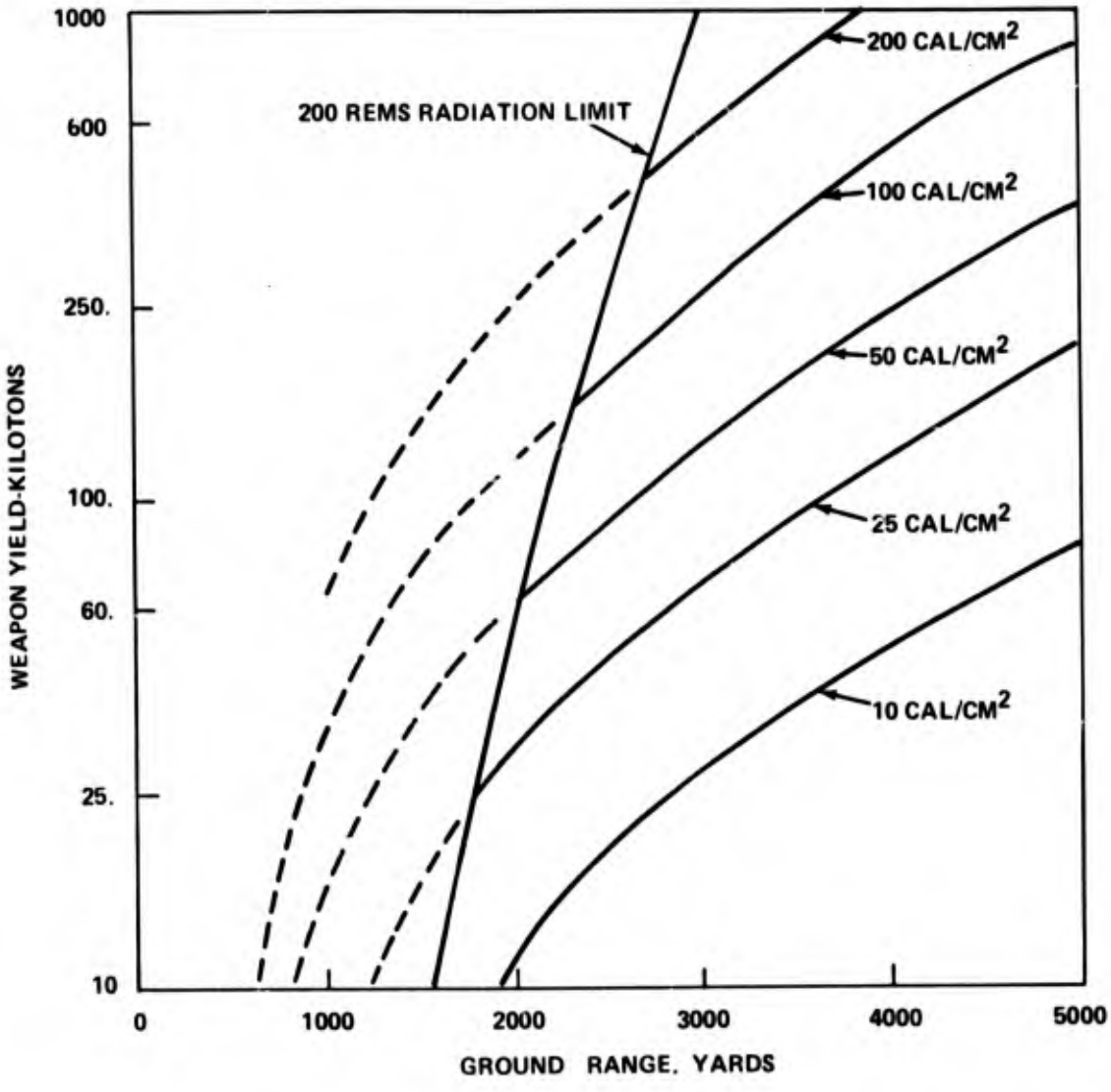

FIG. 4 MAXIMUM RADIANT EXPOSURE AS FUNCTION OF GROUND RANGE FROM A NUCLEAR BURST

The radiant exposures shown in Figure 4 are for ideal conditions; i.e., visibility of 12 miles, no intervening clouds but low surface albedo. Thus, these radiant exposures are maximum values for 12 mile visibility and low surface albedo conditions. Also shown in Figure 4 is the distance where 200 rems of initial radiation would be absorbed by personnel. This boundary represents the limit where nuclear radiation effects would begin to predominate and present the greater hazard to the ship mission. Even relatively small amounts of thermal radiation can be detrimental to a ship's mission. For example, 5 cal/cm^2 from a short thermal pulse (low weapon yield) can cause disabling skin burns on exposed personnel. Clothing material may ignite for short pulses yielding 10-12 cal/cm^2 (dark colors) and rubber or plastic materials may burn or melt in the 10-20 cal/cm^2 range. Thus, critically important elements such as the radomes of radar antennas may be damaged at relatively low thermal irradiance levels. Higher radiant exposure levels can weaken or even melt aluminum structures. The temperatures resulting from exposing aluminum structural elements to nuclear weapon thermal radiation will be given in subsequent sections of this report.

The blast wave from a nuclear weapon explosion is caused by the expansion of the intensely hot gases existing at extremely high pressures within the fireball. This high pressure wave develops within a fraction of a second after the nuclear reaction, rapidly expands and "breaks away" from the fireball, and then travels outward at high velocity. The maximum pressure occurs at the shock front and is termed the peak overpressure. This pressure drops with distance due to the spreading of the blast wave from the point of explosion. The shock front velocity and the particle velocity (peak wind velocity) behind the shock also drop with distance since these are driven by the overpressure. The pressure immediately behind the blast wave decays from the peak overpressure in a regular manner. After a short time when the blast wave has traveled away from the fireball, the pressure behind the shock drops to below that of the surrounding atmosphere. Thus, the passage of a nuclear weapon blast wave consists of a positive overpressure phase followed by a negative pressure phase where a partial vacuum is produced and air is sucked in rather than blown away. Although the negative phase is somewhat longer than the positive phase, its peak values are much lower hence it is of much less importance in causing damage. The important parameters in causing blast wave damage are the peak overpressure, the dynamic pressure, and the duration of the positive overpressure and dynamic pressure phases. If a structure is narrow in the direction of blast wave travel, it will usually fail by overpressure induced stresses exceeding the yield or ultimate strength of the material or it will fail by buckling. In this case, the peak reflected pressure which is generally several times the peak overpressure will govern the failure or endurance of the structure. However, there is the possibility that the dynamic response of large thin structures will depend upon the pressure pulse shape hence the positive overpressure duration becomes important. The blast damage to simple structures will be discussed in a later section of this report. If a structure is wide in the direction of the blast wave, the blast damage may depend upon the strength and duration of the dynamic pressure pulse. This will cause a diffraction load to be put on the structure

when the front surface is at higher pressure than the back surface. A drag loading will result due to the drag force of winds on the front and side surfaces.

The magnitude of the peak overpressure depends on whether the blast wave is in a regular reflection or Mach reflection region. These regions are caused by the reflection of the wave at the earth's surface. The reflected wave travels through air that has been heated and compressed by the incident wave, hence it travels faster than the reflected wave. A regular reflection region is one in which there are two distinct waves; i.e., two distinct shocks will be felt, an incident shock followed by a less intense reflected shock. A Mach region results when the reflected wave catches and merges with the incident wave. The point where the incident wave, reflected wave, and fused wave meet is called the triple point and the fused wave below the triple point is called the Mach stem. Since the Mach stem is nearly vertical, the transient winds are nearly parallel to the ground in the Mach reflection region. This is the region a ship in nuclear warfare is likely to be in because Mach fusion occurs rather quickly; i.e., at a surface distance approximately equal to the height of burst for moderate burst heights.

The shock front velocity, the particle velocity, and the dynamic pressure behind the shock can all be related to the peak overpressure by use of the Rankine-Hugoniot equations[11].

These relationships are based on the conservation of mass, momentum, and energy across a shock front and provide simple formulas when the shock front is nearly vertical; i.e., in a Mach reflection region. The following equations apply to a Mach reflection region (or to a contact surface burst which produces a single wave).

1. Shock front velocity, U

$$U = Co \sqrt{1 + \frac{6\ Pmax}{7\ Po}} \tag{14}$$

2. Particle (Peak Wind) Velocity, V

$$V = \frac{5\ Co^2}{7\ U} \frac{Pmax}{Po} \tag{15}$$

3. Peak dynamic pressure, dmax

$$dmax = \frac{2.5\ Pmax^2}{7\ Po + Pmax} \tag{16}$$

---

[11] A. H. Shapiro, "Compressible Fluid Flow", Ronald Press, New York, Vol. 1, 1953

In equations (14)-(16) Co is the sound speed and Po is the atmospheric pressure in the undisturbed air ahead of the shock. If the blast wave strikes a flat surface at normal incidence, the peak reflected pressure is related to the peak overpressure by the following relationship.

$$Pr = 2 \cdot Pmax \left(\frac{7Po + 4Pmax}{7Po + Pmax} \right) \qquad (17)$$

Equation (17) shows that the peak reflected pressure for normal incidence varies from two to eight times the peak overpressure depending on the shock strength. At other than normal incidence, the ratio of reflected pressure to overpressure is less. This ratio is given as a function of incidence angle[12]. In equations (14)-(17) the ratio of specific heats for air is taken to be 1.4. This is an adequate value for undisturbed air if its temperature is not extreme.

The previous discussion indicated that peak overpressure is important in determining blast damage. Therefore, its variation with weapon yield, height of burst, and ground range from the nuclear burst point will be given herein. Theoretically, a given pressure will occur at a distance from an explosion that is proportional to the cube root of the weapon yield. The cube root scaling law has been found to hold in nuclear weapon tests for yields up to the megaton range. This allows the nuclear weapon test data to be given for a one kiloton equivalent TNT explosion and cube root scaling can be used to get peak overpressures for larger weapon yields. The peak overpressure versus height of burst and ground range are given for a one kiloton weapon yield. The following cube root scaling law is used to convert distances for a W kiloton weapon to data given for one kiloton.

$$G = G_1 \cdot W^{1/3} \qquad (18)$$

Note that G can be either the height of burst or the ground range for a W kiloton burst and G_1 is the corresponding distance for one kiloton. Figure 5 presents the curves of peak overpressure versus scaled height of burst and scaled ground range.

[12]Glasstone, Op. Cit., p. 147

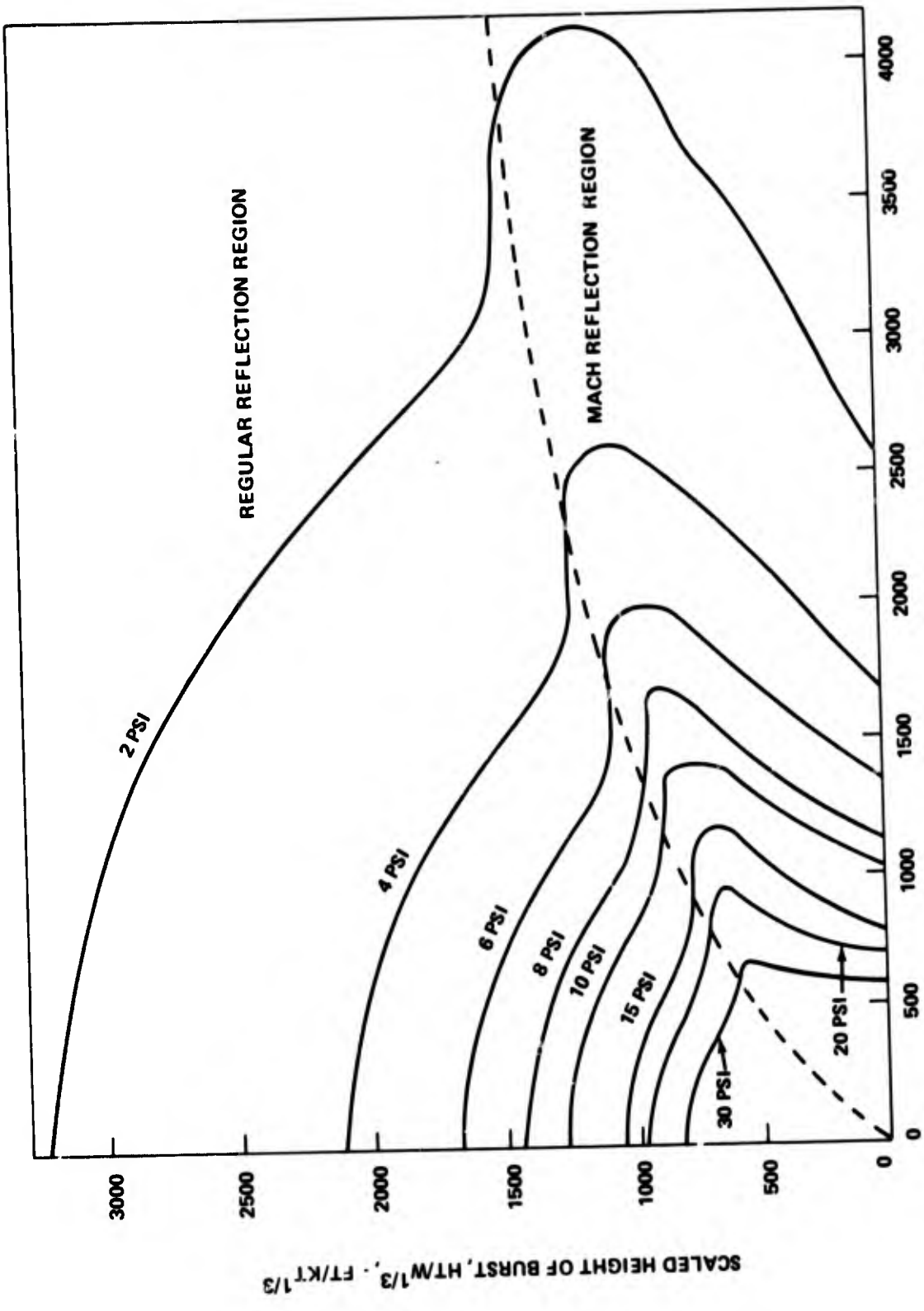

FIG. 5 PEAK OVERPRESSURE ON GROUND, SCALED FOR NUCLEAR BURST OF ANY WEAPON YIELD

The curves for overpressure plotted in Figure 5 are for near-ideal conditions; i.e., they are based on nuclear test data which was free of thermal or mechanical interactions with the ground. The mach-reflection region is based entirely on experimental data while the regular reflection region is based on step-shock reflection theory. Non-ideal surfaces are those that absorb thermal radiation and consequently produce a hot layer of air above it before the blast wave arrives. This layer which may contain smoke, dust, particles, etc. interacts with the undisturbed air and effects the reflection of the blast wave with the ground. Under suitable conditions, an auxiliary blast wave called a precursor forms and moves ahead of the main wave for a limited distance. The precursor and the thermal layer can cause severe modifications to the blast wave characteristics. However, the sea surface is considered to be near-ideal; therefore, the non-ideal complications will not be considered further in this report. Peak overpressure relationships for non-ideal surfaces are given in the nuclear weapon effects literature.[13]

The peak overpressure curves given in Figure 5 can be used with the Rankine-Hugoniot relationships and with equation (17) to compute shock velocity, peak wind speed, maximum dynamic pressure, and peak reflected pressure. There are three additional quantities which are important in assessing blast damage. These are the duration of the positive overpressure and dynamic pressure phases and the arrival time of the blast wave. All of these variables depend upon the distance from the nuclear weapon burst and the height of burst above the surface. The positive phase durations for both the overpressure and the dynamic pressure are shown in Figure 6.

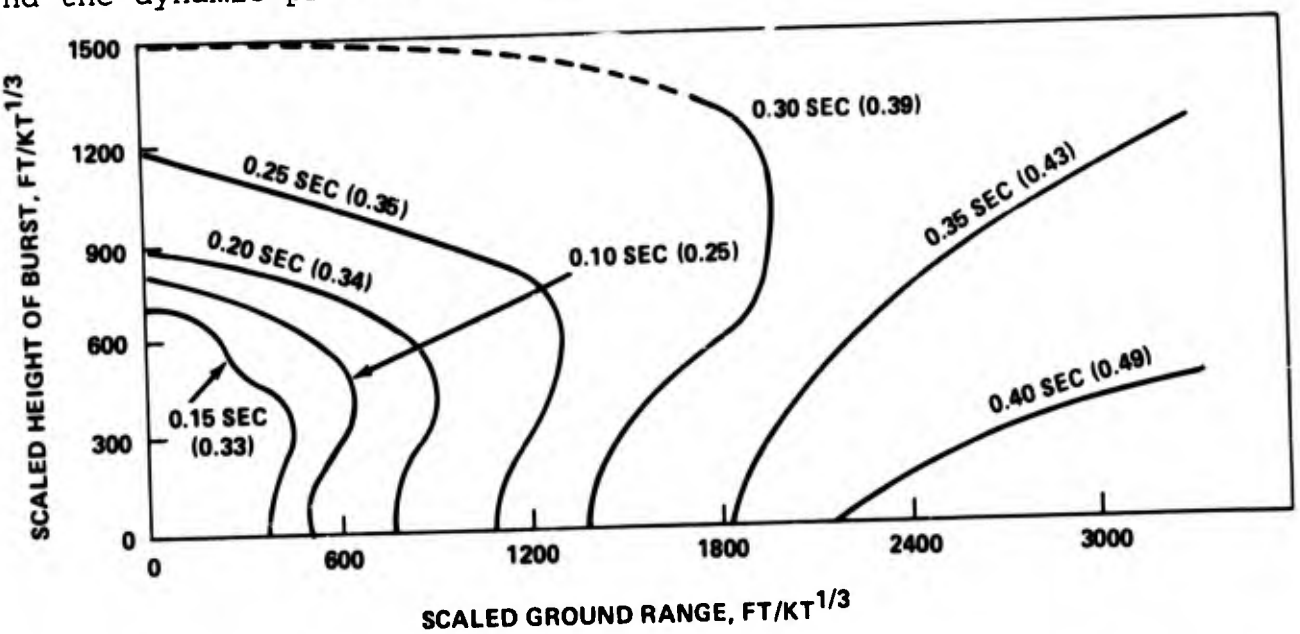

FIG. 6 POSITIVE PHASE DURATION OF OVERPRESSURE AND DYNAMIC PRESSURE (IN PARENTHESES), SCALED FOR ANY WEAPON YIELD

[13] Colvin and Martin, Op Cit.

Figure 6 shows positive phase durations for both overpressure and dynamic pressure in terms of the scaled height of burst and scaled ground range. Thus, equation (18) is used to determine the scaled quantities, G1, in terms of the actual distances, G, corresponding to the given weapon yield, W. The durations shown in Figure 6 must also be cube root scaled for weapon yields larger than one kiloton. That is, if t1 represents the duration from Figure 6 for a one-kiloton nuclear burst, the positive phase duration for a weapon yield of W kilotons is

$$t = t_1 \cdot W^{1/3} \tag{19}$$

The positive phase durations increase as the blast wave moves outward from the burst point. The positive phase duration for overpressure will be used in a later section to assess the nuclear blast wave damage in structural elements. The blast wave arrival time is shown in Figure 7.

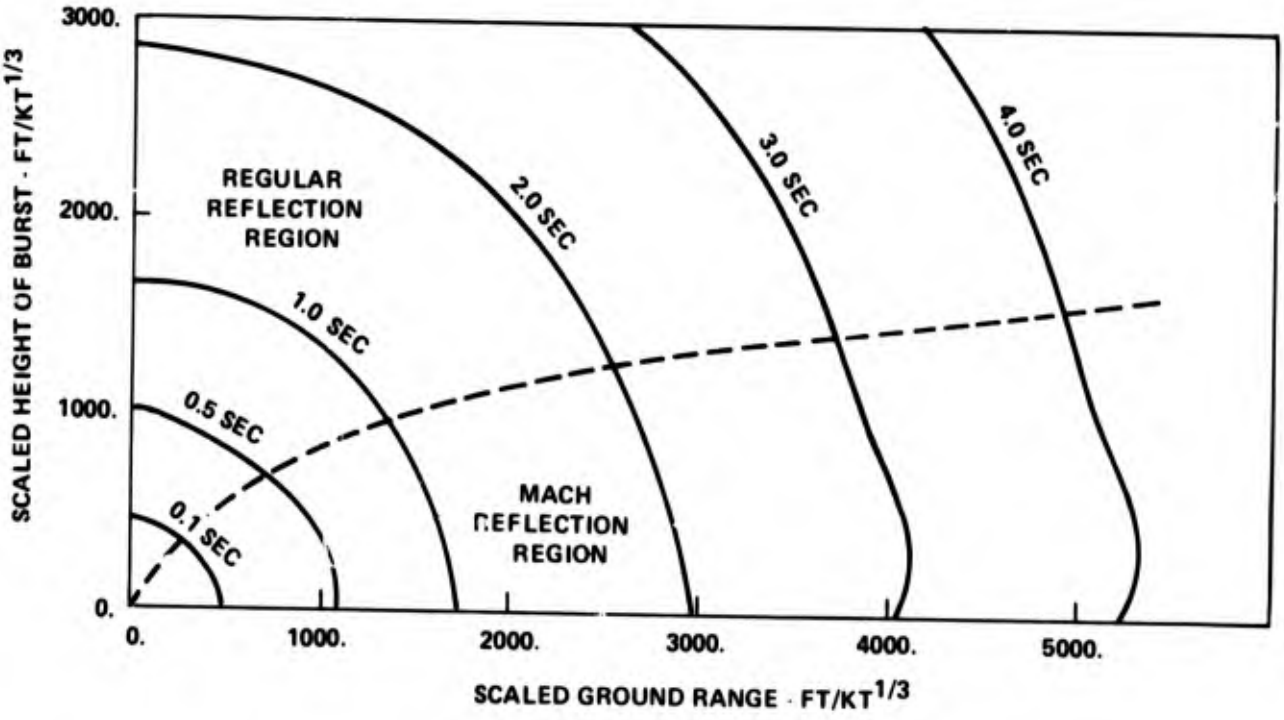

FIG. 7 BLAST ARRIVAL TIME, SCALED FOR NUCLEAR BURST OF ANY WEAPON YIELD

Figure 7 shows the blast arrival time in terms of the scaled height of burst and scaled ground range. Equation (18) must be utilized to calculate the scaled quantities G1 in terms of actual quantities G which correspond to the weapon yield, W. The blast arrival time must also be cube root scaled for weapon yields greater than one kiloton as given by equation (19). Here t1 from Figure 7 represents the blast arrival time for a one kiloton weapon yield and t the time for W kilotons.

The decay of overpressure with time at a given location is necessary in determining the pressure loading on a given structure. If the peak overpressure is about 5 psi, the decay of overpressure with time is given accurately by a simple exponential as follows.

$$P(t) = Pmax \left(1 - \frac{t}{PDUR}\right) e^{-t/PDUR} \qquad (20)$$

where PDUR is the positive phase duration for overpressure. Equation (20) is a good approximation for peak overpressures between 2 and 10 psi. A good approximation for peak overpressures between 10 and 50 psi results by substituting -2t/PDUR in the exponential term only. The decay of overpressure with time is accurately known[14]. The decay of dynamic pressure with time can also be represented by an exponential function. The following equation accurately represents the dynamic pressure for a peak overpressure of 5 psi.

$$d(t) = dmax \cdot \left(1 - \frac{t}{PDUR}\right)^2 e^{-1.5\ t/PDUR} \qquad (21)$$

Equation (21) is also a good approximation for peak overpressures between 2 and 8 psi. A good approximation for dynamic pressure decay between 10 and 20 psi peak overpressure results by substituting -3 • t/PDUR in the exponential term. The decay of dynamic pressure with time is also accurately known.

The cube root scaling laws given by equations (18) and (19) allow the peak overpressure, the positive phase durations of overpressure and dynamic pressure, and the blast arrival time to be scaled from data given for a one kiloton explosion. However, these relationships are strictly valid only for blast waves in a homogeneous atmosphere at standard sea level conditions. (Temperature of 288°K and pressure of 14.7 psi.) The scaling laws hold approximately up to about 5,000 feet altitude after which a correction must be made to account for changes in pressure and temperature with altitude. The following changes must be applied to the curves given in Figures 5, 6, and 7 if the nuclear burst occurs at an altitude greater than 5,000 feet. (1) The distance, G, for a W kiloton burst.

---

[14]Glasstone, Op. Cit., p. 125

$$G = G1 \cdot W^{1/3} \cdot \left(\frac{Po}{Pa}\right)^{1/3} \qquad (22)$$

where Pa is the atmospheric pressure at altitude and Po is the standard sea level atmospheric pressure (14.7 psi). (2) The peak overpressure, Pmax, from Figure 5 becomes

$$PmaxA = Pmax \cdot \left(\frac{Pa}{Po}\right) \qquad (23)$$

where PmaxA is the peak overpressure at altitude. (3) The blast arrival time, from Figure 6, or positive phase duration, from Figure 7 becomes

$$tt = t1 \cdot W^{1/3} \left(\frac{Po}{Pa}\right)^{1/3} \left(\frac{To}{Ta}\right)^{1/2} \qquad (24)$$

Here, Ta is the atmospheric temperature at altitude and To is the standard sea level temperature ($288^{o}K$).

The electromagnetic pulse emitted by a nuclear weapon burst causes damage to sensitive electronic equipment. These effects are not of prime concern at close-in ranges where radiation or thermal and blast effects may be more damaging. However, they can cause troublesome damage at ranges far beyond the ranges associated with radiation, blast or thermal effects. The electromagnetic pulse is a high intensity burst of radio-frequency energy produced by the electric charge and current distribution in the vicinity of a nuclear burst. The pulse is produced by electrons which are stripped from the surrounding air molecules by interactions of initial gamma radiations and the atmosphere. These electrons move outward leaving slower moving positive ions behind. This causes a current to flow which produces an associated radial electric field. Furthermore, when the electrons are driven back under the influence of the radial electric field, a second pulse of current is created but this is rapidly terminated by the recombination of electrons with positive ions. An external electromagnetic pulse is emitted provided an asymmetry of the electron distribution and motion exists. If the explosion were perfectly symmetrical in a uniform atmosphere, the ionizing effects would be equal in all directions, would compensate each other, and there would be no electromagnetic signal. The above mechanism of electromagnetic pulse generation is called the "Compton-electron model" and it is believed to be the primary mechanism for generating an electromagnetic pulse in the atmosphere where a density gradient exists. Asymmetries of the electron distribution arise when electron production is favored in one direction. Thus, nuclear explosions near the earth's surface favor electron production above the burst and explosions high in the atmosphere favor electron production below the burst where the higher air density provides more air molecules for interactions with gamma rays. Asymmetry effects can also be designed into the weapon by controlling the amount and direction of primary gamma ray radiation.

Three transient effects are caused by the generation of the electromagnetic pulse in a nuclear explosion. These are (1) a pulse of ground current that flows radially from the burst point, (2) an electric field, and (3) a magnetic field that propagates away from the current source. The electric and magnetic fields are emitted from the instantaneous pulse of current in a preferred direction much like that which occurs from an "electric dipole" of classical electromagnetic theory. The strength of the electric and magnetic fields developed depend upon the degree of electron distribution asymmetry and the size of the ionized region. Although it is difficult to relate field strength to weapon size, the following conservative estimates were made for maximum strengths.[15]

$$Emax = 10^5 \frac{\text{volts}}{\text{meter}} \tag{25}$$

$$Mmax = 100 \frac{\text{Amp.}}{\text{meter}} \tag{26}$$

The pulse duration (at the half-peak points) is typically 50 - 200 nanoseconds. The duration generally increases with distance from the burst while the maximum field strength values given above decrease with distance.

A somewhat different mechanism, the field displacement mechanism, causes the generation of radio frequency signals when a nuclear explosion occurs at extremely high altitudes where Compton electrons are not produced in significant numbers. This mechanism is believed to be responsible for the very long distance propagation of an electromagnetic pulse when a nuclear weapon is exploded above the atmosphere. Here, the hot weapon debris forms a highly ionized plasma which expands rapidly. This plasma tends to exclude the earth's magnetic field from its interior hence it causes a violent distortion of the earth's magnetic field. The distorted field interacts with charged particles in the expanding plasma and with the surrounding ionized gases to create a disturbance propagating a "hydromagnetic wave." The hydromagnetic wave retains its characteristics over long distances (hundreds of miles) at high altitudes. An EMP is generated when the wave interacts with the lower, more dense, atmosphere.

The power or energy flux of any electromagnetic wave, including the nuclear EMP, is the vector cross product of the electric and magnetic field vectors. If a nuclear weapon is detonated close to the earth's surface, the power of its EMP attenuates as R^{-4} where R is the radial distance from the burst point. The magnitude of the field strength for both the electric and the magnetic field will attenuate as R^{-2}. However, for detonations above the atmosphere, the power of the EMP attenuates inversely as the square of the distance, i.e. as

[15] L. W. Ricketts, "Fundamentals of Nuclear Hardening of Electronic Equipment", John Wiley and Sons, Inc., New York, 1972.

R^{-2}. Here, the electric and magnetic field strengths will attenuate as R^{-1} hence the EMP is propagated much further in the high altitude explosions.

The direct influence of EMP on a ship is via antennas which are designed to extract energy from incident EM waves. Often the EMP contains significantly more energy than the electronic equipments connected to these antennas are designed to handle. Consequently, component damage, or system operational upset may occur. A cure for this problem is to keep the EMP energy out of the equipment by using surge arresters near the antenna, by providing attenuation, diversion, and circumvention techniques to the equipments themselves, and by disconnecting antennas at their base terminals when not in use.

A more subtle threat is the indirect penetration of EMP. Ships are usually thought to be impervious to EMP because the multiplicity of steel hulls, decks, and bulkheads are thought to provide a series of attenuating shields through which EMP energy must pass to reach the interior compartments. However, these metal structural elements are penetrated in places by cables, ducts, pipes, hatches, etc. All of these can serve to collect and to conduct EMP energy into the ship's interior where it manifests itself as voltage or current surges at the terminating components or subsystems. Hardening against these penetrations requires keeping the collected energy on the exterior of the ship generally by enclosing exterior cables in conductor raceway, by good grounding of the outermost cable braid at points of penetrations, by full peripheral grounding at the point of penetrations of pipes, air ducts, and waveguides, and by using electrically conducting gasketing around hatches and doors in the weatherdecks and bulkheads.

EMP presents a problem to a ship if the energy in the incident pulse causes degradation or loss of critical electronic functions of that ship. There are two types of system degradation that can result from an electrical transient, namely (1) permanent damage, and (2) transient upset. Transient upset refers to temporary impairment caused by the electrical transient. Usually the energy level for transient upset is much lower than that required for permanent damage. The trend toward miniaturization has increased the susceptibility for permanent damage.

Devices which may be susceptible to permanent damage caused by electrical transients include high frequency transistors, integrated circuits, electroexplosive devices, etc. Devices, or systems which may be susceptible to transient upset include digital processing systems, memory units, control systems for guidance, etc. Potentially dangerous situations may also occur in the presence of explosive fuel vapors if an arc should happen to form. An example is that of rocket fuels containing premixed oxidizers.

The effects of EMP on a system depend not only upon the energy collected by the system, but also upon the nature of the circuits and components in the system. Widespread use of digital electronic equipment makes consideration of transient upset more important. With

digital equipment, a transient may cause the device to jump to a new state which is totally unrelated to the initial state, and from which it may never return of its own accord after the transient has subsided.

Additional information on the protection of electronic equipment from the EMP is given in a reference.[16]

IV. THERMAL EFFECTS ON STRUCTURAL ELEMENTS

The thermal radiation pulse of a nuclear weapon explosion travels ahead of its blast wave and heats any exposed ship structure or system in its path. The resulting temperature rise from this heating can cause serious problems in temperature sensitive materials. That is, rubber or plastic materials used on or to protect radar antennas or the clothing of exposed personnel will char or fail at relatively low levels of thermal flux. However, it is the aluminum structures on a ship which may be the most threatened by thermal radiation. The thermal threat to aluminum is due to the fact that aluminum alloys rapidly lose strength after a temperature of approximately 200°C has been reached. The loss in strength could cause a load bearing element in a structure to fail. If the element does not immediately fail, it may fail when the blast loading arrives due to its weakened state. Also, there is the possibility that high temperatures may induce thermal stresses in structural elements and these alone will cause or contribute to failure.

The calculation of the temperature rise in structures due to the nuclear weapon thermal pulse can be a complicated procedure. The heat flow in a body is governed by the partial differential equation for heat conduction with associated boundary conditions to allow for heating by the thermal pulse and cooling by convection, radiation, and conduction at its surfaces or boundaries. For general problems, these equations cannot be solved in closed form; hence, a numerical solution depending on the usage of a digital computer is necessary. Some very large heat transfer computer programs have been written which allow rather general boundary conditions. An example of these is the TRUMP program.[17] The main difficulty in using one of these general programs is the amount of effort required to define the boundary conditions in their input data for a specific problem. This effort can be reduced by writing a computer routine which contains the necessary information for the boundary conditions of a specific problem or class of problems. This was done to calculate the temperature histories in solid or hollow, rotating or stationary, up to three-dimensional bodies with circular or rectangular cross sections. The computer routine also inputs the universal irradiance for the nuclear weapon thermal pulse

---

16 Ricketts, Op. Cit.

17 A. L. Edwards, "TRUMP: A Computer Program for Transient and Steady-State Temperature Distribution in Multidimensional Systems", Lawrence Radiation Laboratory UCRL-14754, Rev II, 1 July 1969.

which was given in Figure 3. It permits heat losses by radiation or convection at the exposed surfaces or losses by conduction through heat sinks at its unexposed boundaries. The TRUMP program is used as a subroutine to compute temperatures, but the large amount of input data preparation is reduced to as few as seven cards. This new computer program was named TRIN and a report was written describing it in detail.[18]

In many cases it is not necessary to compute the temperature rise in complex structures to determine if a thermal problem exists. Here, a most susceptible element of the structure can be isolated and thermal calculations made for it. Thus, a three-dimensional geometry with complex boundary conditions can be replaced with simpler calculations made in one or two dimensions. Individual computer programs have been written for several of these simple structural elements. Each of these will solve the heat conduction equation numerically for heating given by the nuclear weapon thermal pulse. These programs will be described briefly in turn. First is the one dimensional program for flat plates.[19] This program computes the temperature history through the plate due to the nuclear weapon thermal pulse and allows heat removal by convection or radiation to occur at either surface. The plate program was used to present the temperature histories of plates in easy to read chart form. A dimensional analysis of the heat conduction equation and boundary conditions was made to find the dimensionless temperature, time, convective cooling, and material property parameters that describe the plates thermal behavior. Charts of dimensionless temperature versus dimensionless time were derived for a wide range of values of a dimensionless parameter. Additional charts were also given for both thermally thin and thermally thick plates for a wide range of convective cooling conditions. These charts and the dimensional analysis leading to their development are given in the literature.[20] A computer program was written to compute the temperature distribution histories in two-dimensional hollow or solid stationary cylinders.[21] This program computes the temperature distribution history throughout the circular cross section due to the

---

18 D. M. Dancer and D. M. Wilson, "TRIN: Computer Program to Calculate Temperature Distributions in Circular and Rectangular Sections Exposed to Thermal Radiation from Nuclear Weapon Explosions", NOLTR 72-117, 12 May 1972.

19 M. L. Cohen, J. E. Koch, and R. J. Heilferty, "A Numerical Technique to Determine the Thermal Histories of Two-Dimensional Solids Exposed to the Thermal Pulse of a Nuclear Weapon", Naval Applied Science Laboratory Project 940-105, Progress Report 5, 2 Jan 1968.

20 P. Bergman, R. Heilferty, and N. Griff, "Temperature Response Charts for Opaque Plates Exposed to the Thermal Radiation Pulse from a Nuclear Detonation", Naval Applied Science Laboratory, Lab Project 940-105, Progress Report 10, July 1969.

21 R. Kaufmann and R. J. Heilferty, "Equations and Computer Program to Calculate the Temperature Distribution and History in a Cylinder Subject to Thermal Radiation from a Nuclear Weapon", Naval Applied Science Laboratory, Lab Project 940-105, Progress Report 8, Jul 68.

nuclear weapon thermal pulse and allows heat removal by convection or radiation to occur at either surface. The cylinder program was also used to prepare charts of temperature history for cylinders exposed to a nuclear weapon thermal pulse. A dimensionless analysis of the governing heat conduction equation and boundary conditions yielded the dimensionless parameters that describe the thermal behavior. Finally, the charts of dimensionless temperature versus dimensionless time were presented for a wide range of values of other dimensionless variables. Since this is a two-dimensional problem, it was necessary to repeat the charts for different angular positions on the cylinder and for different ratios of inner to outer radius. In fact, 90 figures were required to adequately describe the dimensionless temperature histories in the circular cylinders. These figures and the dimensional analysis leading to their development are given in the literature.[22] Computer programs were also written to compute the temperature distribution histories in T-beams[23] and Box-beams (unpublished) subject to nuclear weapon thermal radiation. Dimensional analysis and temperature history charts were not prepared for these structural elements. However, a series of simple computer programs were written to quickly compute the temperature histories in circular cylinders, flat plates, circular cylinders rotating at 6 rpm (a rate typical of certain search radars) and thermally thin elements. These programs are simplified by containing the dimensionless temperature histories previously derived and they merely interpolate between these to solve a given problem. These four programs are described in a report.[24]

Most of the above mentioned computer programs provide for convection and radiation heat losses. However, it will be shown that these losses are small in comparison with the weapon pulse heating for shipboard applications. The equations allowing these effects to be calculated and an estimate of the losses in Naval situations will be given. Thermal radiation losses per unit area are proportional to the fourth power of the surface temperature. Radiation losses are given by[25]

$$q = \sigma \cdot \epsilon \cdot Ts^4 \qquad (27)$$

---

22 D. M. Wilson, "The Distribution and History of Temperature in Circular Cylinders Exposed to the Thermal Radiation Pulse of a Nuclear Detonation", NOLTR 71-61, June 1971.

23 R. Kaufmann and R. J. Heilferty, "Equations and Computer Programs to Calculate the Temperature Distribution and History in a Tee Beam Subject to Thermal Radiation from a Nuclear Weapon", Naval Applied Science Lab., Lab Proj. 940-105, Progress Rpt. 6, Feb 68.

24 D. M. Wilson, "A Method of Efficiently Calculating the Temperature Distribution History in Structural Elements Exposed to the Thermal Radiation Pulse of a Nuclear Weapon Explosion", NOLTR 72-177, 10 Aug 1972.

25 F. Kreith, "Principles of Heat Transfer", International Textbook Company, Scranton, PA, Second Edition, April 1965.

where σ is the Stephan-Boltzmann constant and ϵ is the emissivity of the surface. The maximum radiation loss per unit area for an emissivity of unity is small compared to the heat supplied by the nuclear thermal pulse (see Figure 4 for maximum values of radiant exposure). For example, radiation losses amount to only 0.1 cal/cm^2 sec at 300°C and about 0.75 cal/cm^{2}sec at 600°C. Heat removal by convection is also likely to be negligible in a sea environment. Convection losses are given by[26]

$$q = h(Ts - To) \tag{28}$$

where h is the convective cooling coefficient. The evaluation of h will depend on whether the boundary layer flowing over the structure is laminar or turbulent. This is determined by the numerical value of the local Reynolds Number, Re, where

$$Re = \frac{v \rho L}{\gamma} \tag{29}$$

A boundary layer flow over a flat plate will become turbulent for a Renolds number of approximately 320,000.[27] The average convective coefficient for a plate in laminar flow is[28]

$$\bar{h} = \frac{0.664 \cdot K \cdot Re^{1/2} \cdot Pn^{1/3}}{L} \tag{30}$$

and for the turbulent flow region[29]

$$\bar{h} = \frac{.036 \cdot K \cdot Re^{4/5} \cdot Pn^{1/3}}{L} \tag{31}$$

In equations (30) and (31), K is the thermal conductivity of the boundary layer (air) and Pn is its Prandtl number. A 50 knot wind blowing across a flat plate will develop a turbulent boundary layer about 8 inches from its leading edge. Equation (31) predicts a turbulent heat transfer coefficient of about .0025 cal/sec cm^2°C for a plate one foot wide in turbulent flow. Thus, the rate at which heat is removed in turbulent flow is only about 0.75 cal/sec cm^2 at 300°C and 1.50 cal/sec cm^2 at 600°C. The corresponding values for laminar flow are approximately one-half as much. These rates of heat removal are small in comparison with the much higher heating rates required to threaten the integrity of aluminum structures.

---

26 F. Kreith, "Principles of Heat Transfer", International Textbook Co., Scranton, PA, Second Edition, Apr 1965.

27 H. Schlichting, "Boundary Layer Theory", Pergamon Press, New York, First English Edition, 1955, p. 32.

28 Kreith, Op. Cit.

29 Kreith, Op. Cit.

A great deal of effort has been expended on the calculation of temperatures on structural elements subjected to the thermal pulse of a nuclear weapon explosion. The complete thermal history of flat plates or cylinders can be read off charts or easily computed from the simple computer programs previously described. However, the large mass of existing temperatures data can be used to isolate the maximum temperature that a flat plate or a circular cylindrical structural element will experience. The maximum temperature will indicate whether the given weapon is likely to cause weakening or failure of the element by heating. It can also be used to indicate whether elements made of rubber, cloth, plastic, etc. will ignite or char in a given nuclear warfare environment. Methods will be given for easily finding the maximum temperature for either a flat or cylindrical element. First, for the plate it was found that the dimensionless temperature, $(T - Ti)/A \cdot HMAX \cdot L/k$ is a function of a dimensionless variable, $\alpha \cdot Tmax/L^2$ if the convective and radiative losses are neglected. If equation (9) is used to eliminate the maximum irradiance, the following relationship can be derived for the temperature rise.

$$(T - Ti) = \frac{0.39 \cdot K}{\alpha \cdot Tmax/L^2} \frac{A \cdot QT}{\rho \cdot Cp \cdot L} \qquad (32)$$

In equation (32) K is the proportionality factor between the dimensionless temperature and the dimensionless time and it is given by charts in a previous reference.[30] The values of K for the maximum temperature rise can be found from the charts as a function of the dimensionless parameter, $\alpha\ Tmax/L^2$. Thus, the maximum temperature rise in flat plates is proportional to the parameter, $A\ QT/\rho\ Cp\ L$, for a given value of $\alpha\ Tmax/L^2$. This relationship for maximum temperature is given in Figure 8. The relationship between maximum temperature rise and the heating parameter, $A\ QT/\rho\ Cp\ L$ is unchanged for values of $\alpha\ Tmax/L^2$ greater than 0.20. This occurs because the plate is thermally thin for the nuclear thermal pulse and the given combination of material properties, α, heating pulse length, Tmax, and plate thickness, L. Thus, the weapon heating acts to increase the plate temperature uniformly without a temperature gradient front to rear. The resulting temperature is that given by a heat balance equating heat absorbed by the plate to its increase in heat energy as indicated by its temperature. Note that for these thin plates without heat losses, the temperature will continue to rise as long as any heat is received. If the plate is not thermally thin, the maximum temperature occurs before all of the heat is received. In fact, the time at which maximum temperature is reached approaches the time to maximum irradiance, Tmax, as the values of $\alpha\ Tmax/L^2$ decrease; i.e., as the plate becomes thermally-thick.

A similar analysis can be made to determine the maximum temperature rise in a circular cylinder. Here, it was found that the dimensionless temperature, $(T - Ti)/A\ HMAX\ Ro\ k$ is a function of the dimensionless variable, $\alpha\ Tmax/Ro^2$, the inner to outer radius ratio,

---

[30] Cohen, et. al., Op. Cit.

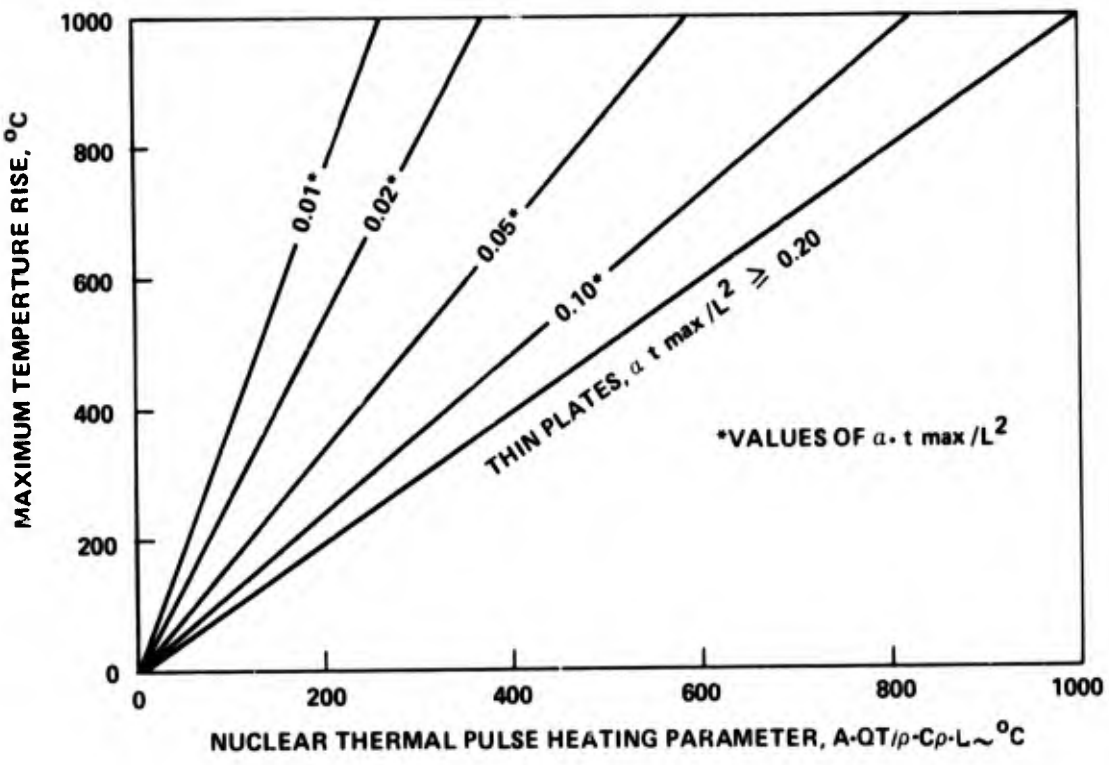

FIG. 8 MAXIMUM TEMPERATURE RISE IN FLAT PLATES SUBJECTED TO THE NUCLEAR THERMAL PULSE.

Ri/Ro, and the angular location on the cylinder. This will be the case only if the convective and radiation losses are neglected. Proceeding in the same manner as was done for a plate, equation (9) is used to eliminate the maximum irradiance, and the following relationship is derived for temperature rise

$$(T - Ti) = \frac{0.39 \cdot C}{\alpha\ Tmax/Ro^2} \left(1 - \frac{Ri}{Ro}\right) \frac{A \cdot QT}{Cp\ \Delta r} \qquad (33)$$

In equation (33) C is the proportionality factor between the dimensionless temperature and dimensionless time and is given by charts.[31] The value of C for the maximum temperature rise can be found from these charts as a function of the parameter, $\alpha\ Tmax/Ro^2$, and the dimensionless inner radius ratio, Ri/Ro. The angular location does not enter into this determination since the maximum temperature always occurs at the most forward point on the cylinder which is normal to the incoming radiation. Thus, the maximum temperature rise is proportional to the parameter, $A\ QT/\rho\ Cp\ \Delta r$ for a given value of the inner radius ratio and given values of the parameter $\alpha\ Tmax/Ro^2$. This relationship is shown in Figures 9 - 12 for four inner radius ratios; i.e., Ri/Ro - 0.9, 0.8, 0.6, and 0.0.

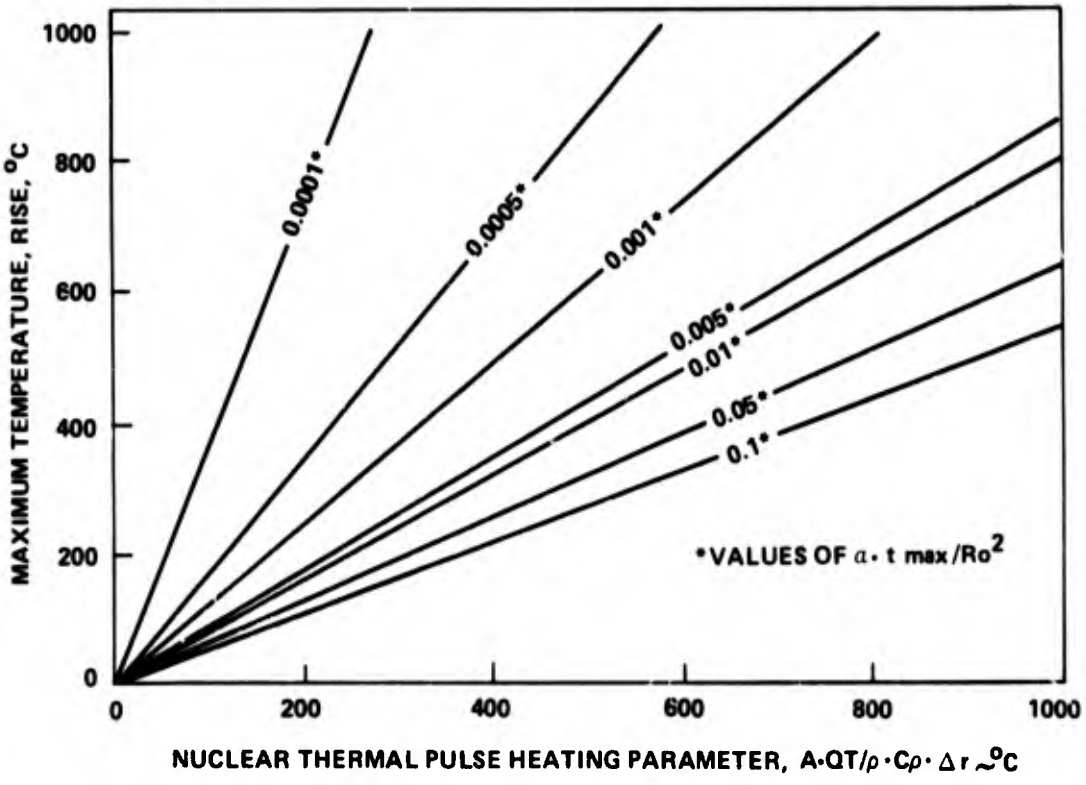

FIG.9 MAXIMUM TEMPERATURE RISE IN CIRCULAR CYLINDERS, Ri/Ro = 0.9

31 D. M. Wilson, "The Distribution and History of Temperature in Circular Cylinders Exposed to the Thermal Radiation Pulse of a Nuclear Detonation", NOLTR 71-61, Jun 1971.

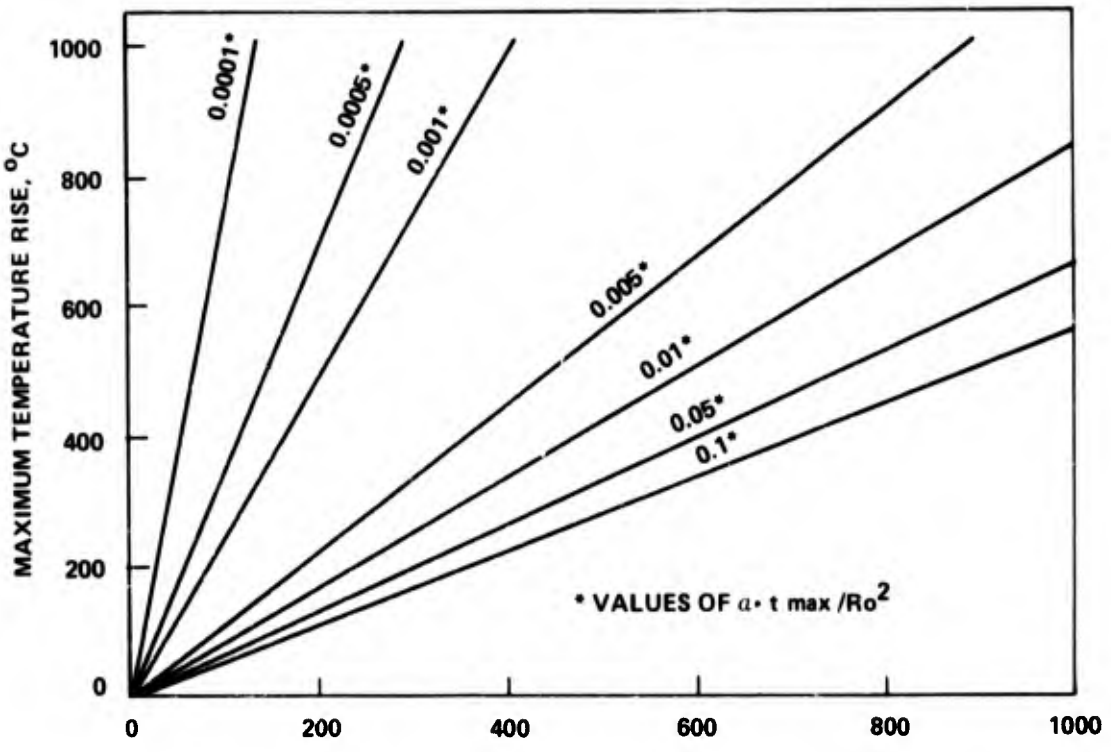

FIG.10 MAXIMUM TEMPERATURE RISE IN CIRCULAR CYLINDERS, Ri/Ro = 0.8

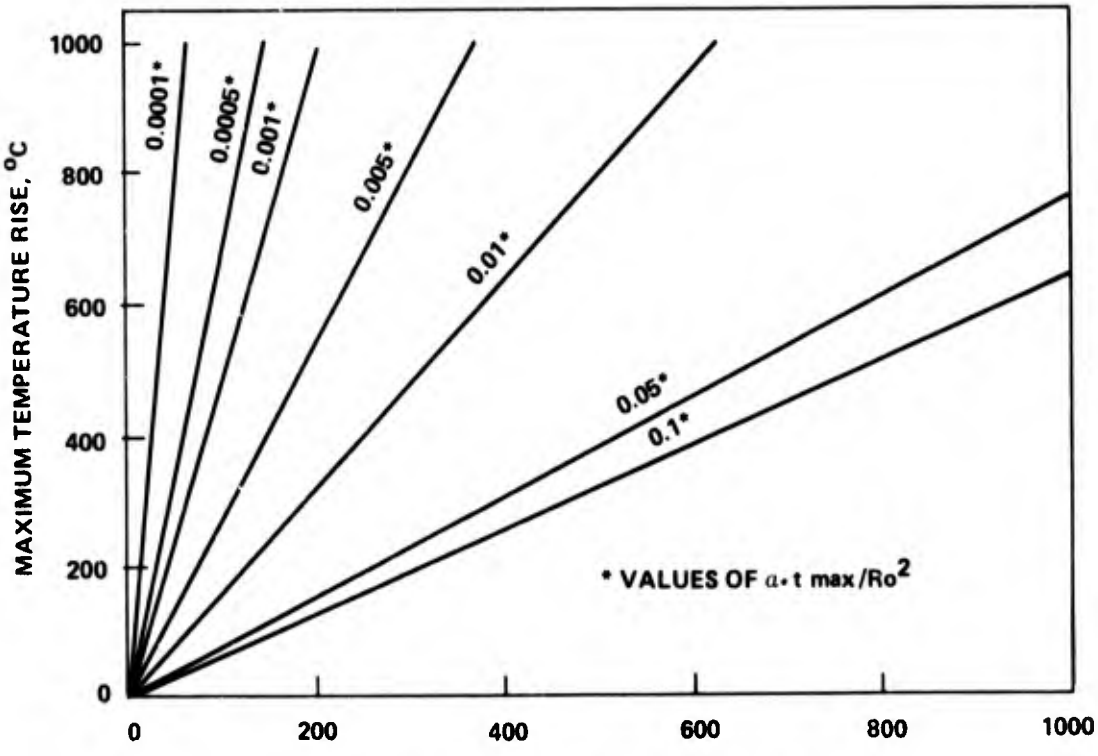

FIG. 11 MAXIMUM TEMPERATURE RISE IN CIRCULAR CYLINDERS, Ri/Ro=0.6

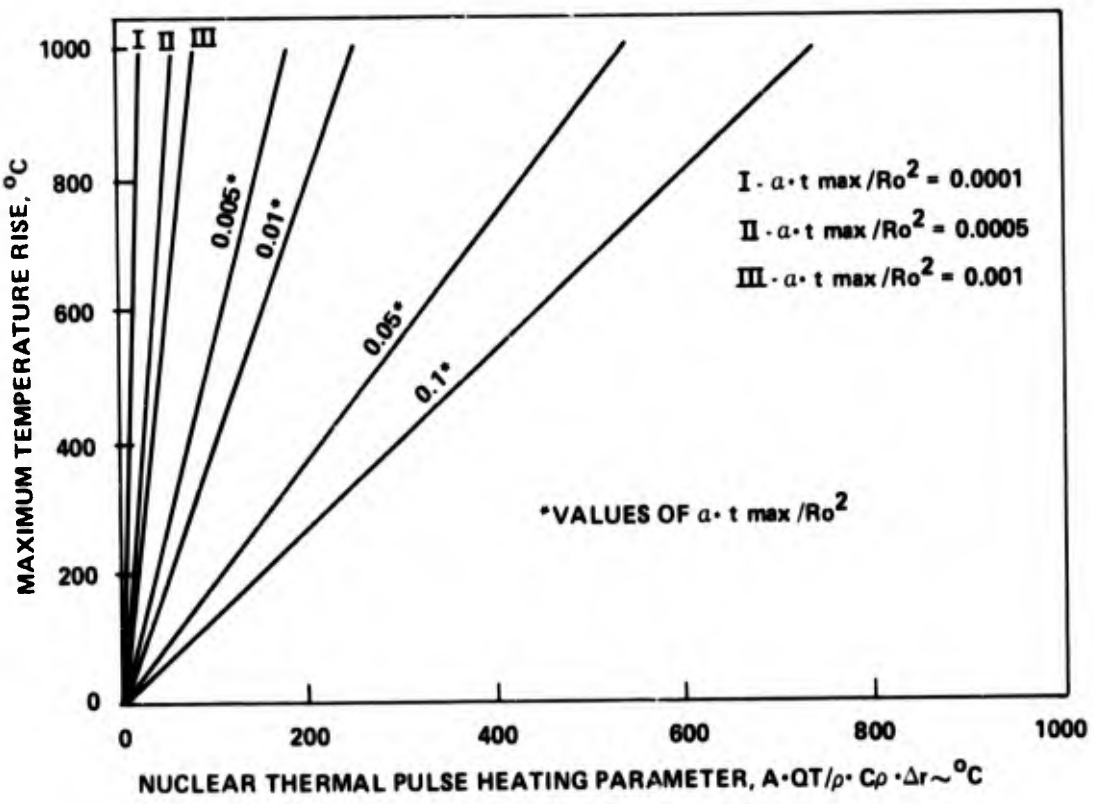

FIG.12 MAXIMUM TEMPERATURE RISE IN CIRCULAR CYLINDERS, Ri/Ro = 0.0

In contrast with the flat plate correlation, the thermally-thin region for circular cylinders is very restricted in allowable values of time and the parameter $\alpha \cdot Tmax/Ro^2$. (See reference 32 for a specification of allowable values.) This occurs because in regions where the cylinders are physically thin, heat may be transferred by angular conduction; i.e., conduction around the circumference, and the temperature rise cannot be found from a heat energy balance. The maximum temperature rise can be found for a wide range of conditions by referring to Figures 9 - 12. Rules for interpolating or extrapolating these data can be found in reference 33.

The high temperature induced by the nuclear weapon thermal radiation pulse can produce two detrimental effects in aluminum structures by itself irrespective of any damage caused by the weapon's airblast. These are (1) a drop in mechanical strength due to high temperatures, which may cause failure of structural elements which are carrying loads or will result in a weakened state that may fail at blast arrival; (2) the development of thermal stresses which in special cases may be large enough to cause failure before blast arrival. How the strength of an aluminum alloy changes upon heating is a complicated subject because it depends upon changes in the alloy's micro-structure. Furthermore, these changes in microstructure are also dependent on time at temperature in addition to the absolute temperature. A discussion of how microstructural changes effect the mechanical strength of aluminum upon rapid heating is given in Appendix A. The following rules are developed from the discussion in Appendix A to predict the decrease in yield strength of aluminum for the rapid heating given by the nuclear weapon thermal pulse. These will be used for all stress comparisons made in this report. If time spent at elevated temperature is less than a few seconds (the exact time depending on the temperature), the decrease in yield strength with increased temperature is proportional to the shear modulus decrease with temperature. Shear modulus as a function of temperature does not depend on time at temperature and is well known for most aluminum alloys. This relationship is given in Appendix A for 6061-T6 aluminum. If more than a few seconds is spent at elevated temperature, the yield strength decreases faster with temperature and experimental data must be consulted. Representative data is given in Appendix A for some aluminum alloys and specific short times at temperature.

Thermal stresses will develop in structures that have relatively large temperature gradients from the front to rear surfaces. In general, it will require a thick structure to develop the large thermal gradients necessary for large thermal stresses. This is in contrast to blast stresses which are the largest in thin elements. A sample calculation will be given below to show that under proper conditions thermal stresses can be damaging in themselves. For

---

32 Wilson, NOLTR 71-61, Op. Cit.
33 Wilson, NOLTR 72-177, Op. Cit.

example, consider a 6061-T6 aluminum plate that is 0.5 inches thick and is simply supported. This plate will be in a nuclear warfare environment producing the maximum radiant exposures shown in Figure 4 as a function of weapon yield and ground range. The time to maximum irradiance as given by equation (5) is 0.118 seconds for a 10 kiloton yield and 0.790 seconds for 1,000 kilotons. The use of room temperature thermophysical properties for 6061-T6 aluminum[34] allows the dimensionless parameter $\alpha \cdot T_{max}/L^2$ to be computed. Thus, $\alpha \cdot T_{max}/L^2$ is approximately .05 for the 10 kiloton case and 0.29 for 1,000 kilotons. The dimensionless temperature histories for temperature through the plate can be easily found from the charts[35] or the simplified computer program previously discussed.[36] These temperature histories are given below in Figure 13 for both weapon yields.

Figure 13 shows that the 10 kiloton yield has a much larger dimensionless temperature gradient through the plate than does the 1,000 kiloton yield. This is misleading in that the maximum temperature gradient in the 1,000 kiloton case is much larger because the radiant exposure, QT, is much larger (see Figure 4). The thermal stresses for a 0.5 inch thick aluminum simply supported plate were computed using the temperature histories of Figure 13. The equations used to determine the thermal stresses will be given later. The result of these calculations are given in Figure 14 where thermal stress is plotted against ground range from the nuclear burst point.

The yield strength curves shown in Figure 14 were computed from the data of Appendix A and the rules stated above. That is, the maximum temperature gradient occurs at times of 0.165 seconds; 0.400 second and 1.00 second for the weapon yields of 10,100 and 1,000 kilotons, respectively. Thus, the length of time spent at elevated temperature is relatively short, and the yield strength should decrease with temperature as the shear modulus decreases with temperature. A room temperature yield strength of 40,000 psi for 6061-T6 aluminum was taken from reference[37] and the variation of yield strength with temperature was derived from Figure A-5. The temperature for yield strength determination was found by averaging the average temperature in the top 1/4 inch and the average temperature in the bottom 1/4 inch. Figure 14 shows that for certain conditions of weapon yield and ground range the thermal stress in the plate exceeds the yield stress thereby causing a permanent deformation or a failure of the plate. It should be noted the thermal stresses computed here are internal stresses due to uneven thermal expansion caused by the temperature gradient through the plate. Thermal stress due to thermal expansion against constrained ends will be discussed later. However, a few facts about thermal stress due to temperature gradients become clear from this example. These are (1) it takes a great deal

34 T. Lyman, Editor, "Metals Handbook", American Society for Metals, Vol I, 8th Edition, 1961.
35 Cohen, et. al., Op. Cit.
36 Wilson, NOLTR 72-177, Op. Cit.
37 Lyman, Op. Cit., p. 946.

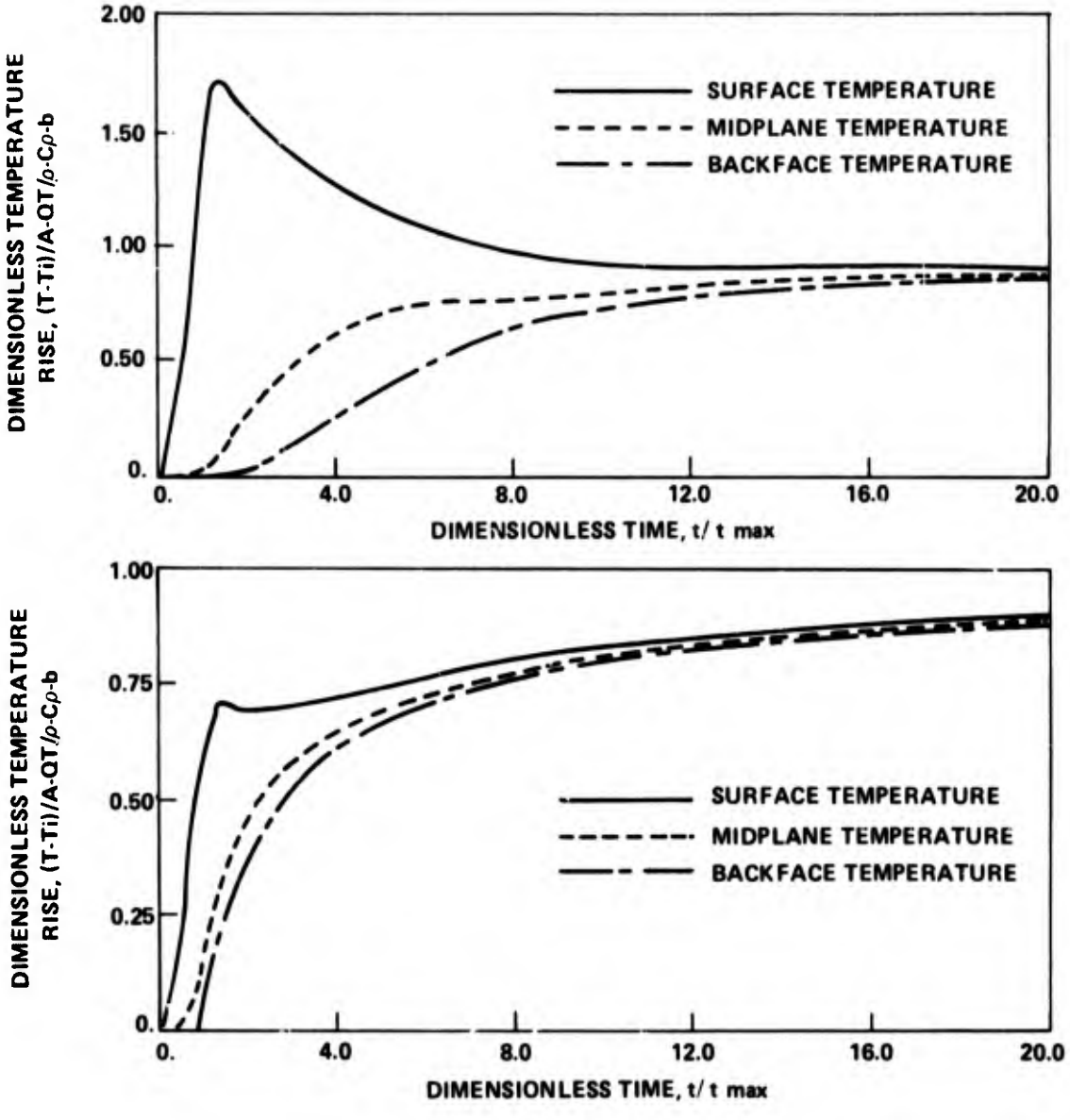

FIG. 13 DIMENSIONLESS TEMPERATURE HISTORIES IN 0.5 INCH ALUMINUM PLATES AND WEAPON YIELD OF 10 KILOTONS (TOP) AND 1000 KILOTONS (BOTTOM).

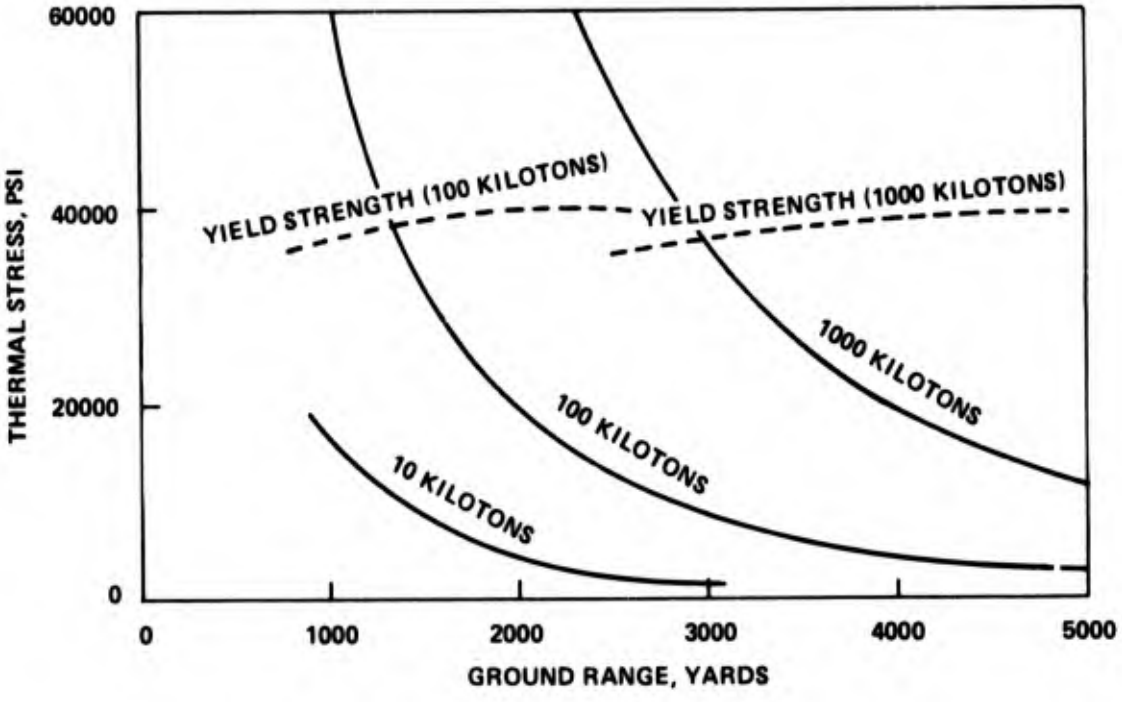

FIG. 14 THERMAL STRESS IN 0.5 INCH THICK SIMPLY-SUPPORTED PLATES

of heat acting on a thick element to produce large enough thermal gradients to cause significant thermal stresses. (Compare Figure 14 and Figure 4 to determine radiant exposure levels.) (2) Large thermal gradients and associated thermal stresses occur early in the pulse heating; i.e., near the time of maximum irradiance (see Figure 13). Thus, the occurrence of large thermal stresses will not influence the development of blast stresses which generally occur much later (see Figure 7 for blast arrival times). When the blast wave arrives, the thermal stresses will have decayed to a small value because the thermal gradients are generally small. This behavior is exemplified in Figure 13.

V. BLAST-THERMAL EFFECTS ON STRUCTURAL ELEMENTS

The airblast parameters which determine the amount of blast damage induced in a target were discussed in an earlier section of this report. Blast damage is caused by the interaction of the blast wave with its target. It is convenient to consider two types of target structures; namely, diffraction structures and drag structures, depending on how these targets interact with the blast wave. In a diffraction type structure, the principal loading is due to the

differential in pressure between the front and rear surfaces of a structure. In a drag type structure, the prinicpal loading is drag due to the dynamic pressure of the winds accompanying the blast wave. The diffraction loading is usually larger in magnitude, but the drag loading is usually active for a much longer time. The loading history on a simple structure subject to the airblast of a nuclear weapon explosion will be given and the relative importance of diffraction and drag loading indicated.

When an airblast wave encounters the front face of a structure, a reflection of the pressure wave occurs which causes its pressure to be magnified to several times the peak overpressure of the incident wave front. (See equation (17) for the peak reflected pressure of a wave at normal incidence.) As the incident wave engulfs the target, the reflected overpressure on the front face drops rapidly to the overpressure produced by the blast wave without reflection plus an added drag force due to the dynamic pressure of the wind. The overpressure without reflection is referred to as the "side-on" overpressure and this added to the drag force due to dynamic pressure is equal to the stagnation pressure, Ps, on the plate; i.e.,

$$Ps = P(t) + Cd \cdot d(t) \tag{34}$$

where Cd the drag coefficient for air flow normal to a plate is equal to unity. The overpressure, P, and the dynamic pressure, d, decay exponentially with time as given by equations (20) and (21). Hence, the stagnation pressure, Ps, also decays in an exponential manner with time. The time when the reflected pressure decays to the stagnation pressure has been measured in laboratory experiments on flat plates with blast waves at normal incidence. The following formula is found to give a good approximation of the time for initial reflections to dissipate[38].

$$ts = \frac{3s}{U} \tag{35}$$

where S is the smaller of the 1/2 width or 1/2 length of the plate and U is the shock front velocity. It is common practice to assume that the reflected pressure decays linearly from its maximum value, Pr, to the value of the stagnation pressure, Ps, at time, ts. After time ts, the initial reflections have been dissipated and the front face loading decay is given by equation (34). The above pressure history describes the loading on an enclosed flat surface; i.e., a surface where the blast wave does not influence the pressure field behind the plate. If the plate forms one wall of a free standing structure, the blast wave can envelope the structure and influence the pressure field behind it thereby altering its net loading. The back pressure loading is assumed to begin at a time t2 which is the time required for the shock wave to travel from the front face to the back face; i.e.,

$$t2 = \frac{L}{U}$$

---

[38]Glasstone, Op. Cit., p. 183

where L is the thickness of the plate. The back pressure loading is assumed to increase linearly from zero at time t2 to the back stagnation pressure which results when the blast wave completely engulfs the structure. Back stagnation pressure is given by equation (34) with the stipulation that the time origin is at t2 relative to time for the front face loading. Also, the drag coefficient, Cd, for the back (or sides) of a rectangular structure is 0.4. Laboratory experiments have also been performed to determine the time for the back pressure to reach its stagnation value. This is for flat plates[39].

$$tb = \frac{4S}{U}$$

The net loading on an unenclosed structure such as a beam or a plate with exposed sides can be found by subtracting the back face loading from the front face loading (net diffraction load only). This is shown schematically in Figure 15.

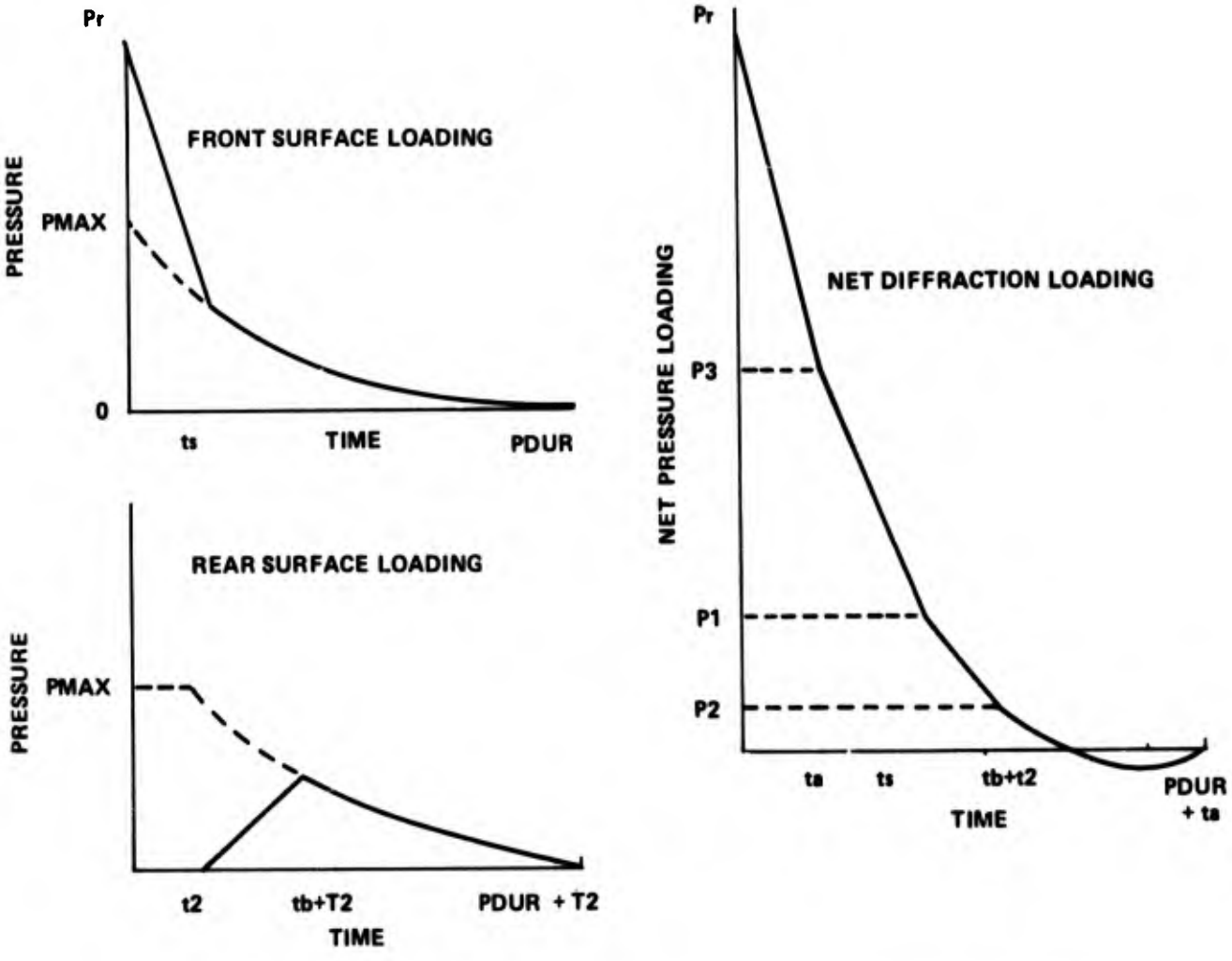

FIG. 15 DIFFRACTION LOADING ON A FLAT PLATE DUE TO NUCLEAR WEAPON AIRBLAST

[39]Glasstone, Op. Cit., p. 184

This Figure shows schematically the front face loading, the rear face loading, and the resulting net loading on a flat structure interacting with a blast wave at normal incidence for relatively narrow plates or beams. The time t2 for the shock front to negotiate the depth dimension is negligible. With this simplification, the net pressures given in Figure 15 are given by the following equations.

$$\begin{aligned} P3 &= Pr \\ P1 &= P(ts) + d(ts) - 0.75\ P(tb) - 0.3\ d(tb) \\ P2 &= 0.6 \cdot d(tb) \end{aligned} \tag{38}$$

The loading shown in Figure 15 is the loading for an enclosed structure (front surface loading only) or an open structure (net diffraction loading). This type of loading is characterized by an almost instantaneous rise in pressure to the maximum reflected pressure, Pr, followed by a rapid decrease to much lower pressures. The times ts and tb are usually small compared to the positive overpressure duration, PDUR; hence, the pressure loading approximates that of a suddenly applied pressure pulse. If the period of vibration of a structural element is also much less than the overpressure duration, it will respond to the initial pressure pulse. That is, the peak stresses developed in the structure are proportional to the reflected pressure and are independent of the later pressure history. The response of structural elements to diffraction loading will be discussed in detail later. The drag loading on the sides of a structure behaves similarly to the rear surface loading shown in Figure 15. Although drag loading begins immediately after the blast wave arrives at the front face, the sides are not fully loaded until the wave travels the distance L equal to the thickness of the plate. This requires a delay time equal to L/U. After the delay time, the drag loading curve is given by equation (34) with Cd equal to 0.4. Drag loads may be important on slender objects such as poles or on large wide objects such as buildings which may be susceptible to the relatively long duration load. Drag loading is generally small for the narrow structural elements that are discussed later in this report.

Methods have been developed to compute the stresses in simple elements which have been exposed to the blast and heating effects of a nuclear weapon explosion. The simple elements considered are rectangular and circular plates and beams of constant cross sectional area. The plates are simply supported while three types of edge support are allowed for the beam; namely, a simple support, a cantilever support, and both ends clamped. Beams and rectangular plates with their ends constrained against axial motion were also analyzed. The methods of analysis and the resulting equations for stress and displacement are given in Appendix B. Results generated from computer programs based on these equations will be considered.

The methods of computing stress and displacements for structural elements in a nuclear weapon environment generally consider the

thermal and pressure pulses simultaneously. That is, computations are made while the element is heated before, during, and after the arrival of the blast wave. The radiant exposure may be given by Figure 4 which shows the maximum possible total irradiance in terms of ground range from the blast. However, the weapon height of burst may be chosen to maximize the distance to which a particular peak overpressure will extend. The existence of burst heights which maximize extent of peak overpressure is indicated by the "knees" of the peak overpressure curves shown in Figure 5. The total radiant exposure for the heights of burst that maximize peak overpressure is given in Figure 16.

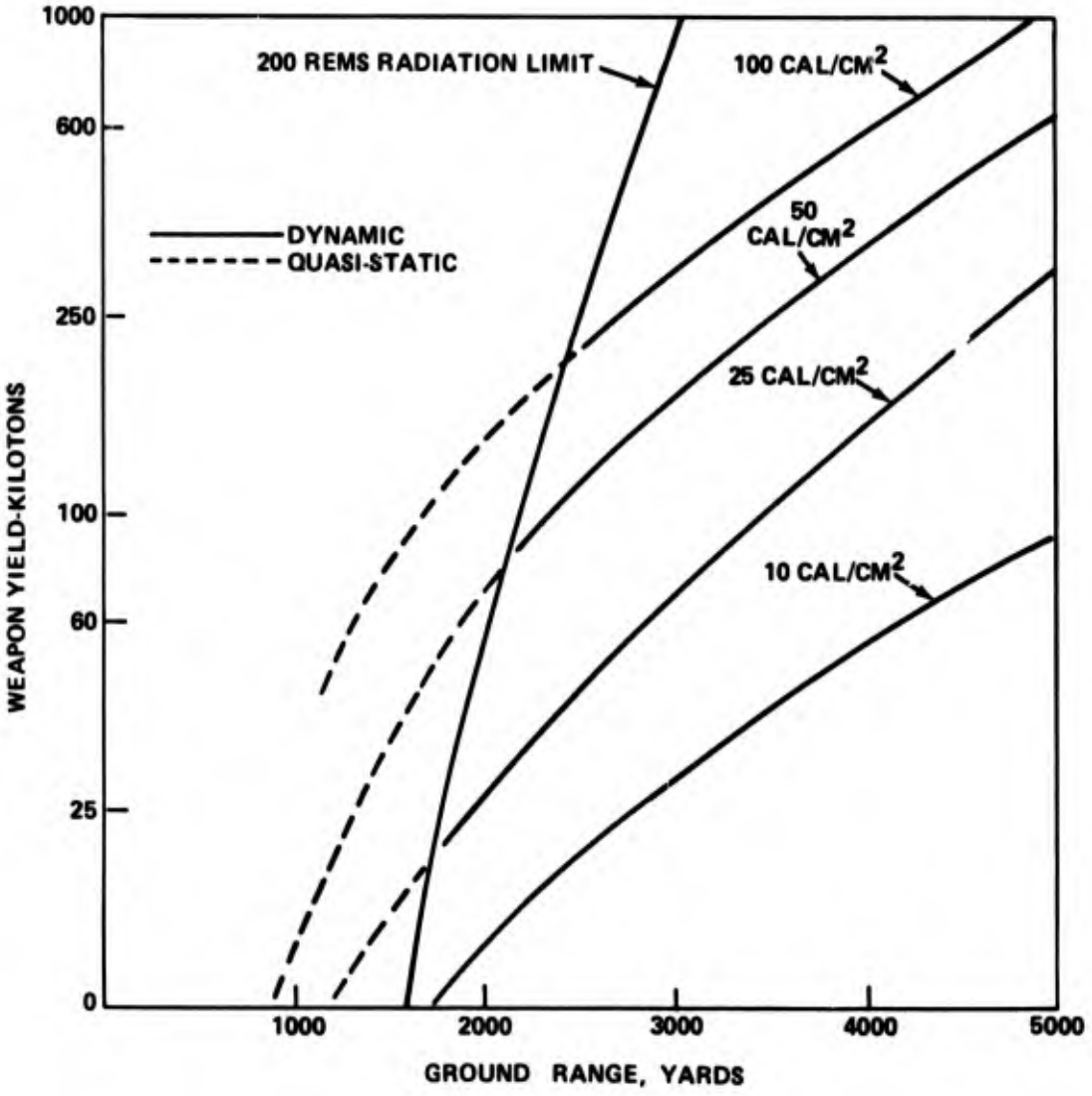

FIG. 16 NUCLEAR WEAPON RADIANT EXPOSURE WHEN EXTENT OF PEAK OVERPRESSURES ARE MAXIMIZED.

Figure 16 was derived by computing curves of constant total radiant exposure versus ground range for heights of burst that optimize the range of several peak overpressures. Points on these curves correspond to different heights of burst but have the virtue that each point corresponds to an optimized ground range for some value of peak overpressure. Thus, the radiant exposures shown in Figure 16 are representative of weapons whose heights of burst maximize peak overpressure range than are the maximum possible exposures shown in Figure 4.

The radiant exposures from Figure 16 and the peak overpressures from Figure 5 are used with the methods presented in Appendix B to illustrate some of the features of the blast-thermal problem. In these illustrations, the height of burst will be chosen to maximize the range of peak overpressures. The following table shows the resulting ground ranges of a function of peak overpressure for three weapon yields.

TABLE 2 - GROUND RANGE WHEN EXTENT OF PEAK OVERPRESSURE IS MAXIMIZED.

Peak Over-Pressure	2 psi	4 psi	6 psi	8 psi	10 psi	15psi	20 psi	30 psi
GR-Yards (10 kt)	3,000	1,870	1,440	1,230	1,040	850	680	480
GR-Yards (100 kt)	6,460	4,030	3,100	2,650	2,250	1,840	1,460	1,030
GR-Yards (1,000 kt)	13,920	8,680	6,680	5,720	4,810	3,970	3,150	2,230

The first illustration of blast thermal effects considers a 1/4 inch thick by 12.0 inch square aluminum plate which is simply supported. The thermal radiation pulse shown in Figure 3 and the pressure pulse for front surface loading shown in Figure 15 were used with the analysis of Appendix B to compute the stress history. Computations were made for both a dynamic and a quasi-static analysis to determine if the more complicated dynamic analysis is necessary. The peak stresses developed in the 6061-T6 aluminum plate for ground ranges given by the preceding table are shown in Figure 17. Figure 16 can be used to estimate the radiant exposures received on the plate in Figure 17. The curves shown in Figure 17 prove that the quasi-static analysis greatly underestimates the peak stress developed in the plate. However, these calculations showed that only the blast loading behaves dynamically, and the thermal portion of the stresses shown in Figure 17 can more easily be obtained from a quasi-static analysis. The room temperature yield strength of 6061-aluminum alloy was previously given as 40,000 psi. The peak stresses shown in Figure 17 occur at blast arrival times between 2 and 10 seconds after weapon burst. Since more than a few seconds are spent at elevated temperatures, the yield strength decreases faster with temperature than that predicted by the shear modulus decrease method. Hence, experimental data, such as that shown in Figure (A-2) or (A-6), must be consulted for guidance in predicting yield strength. The results given by

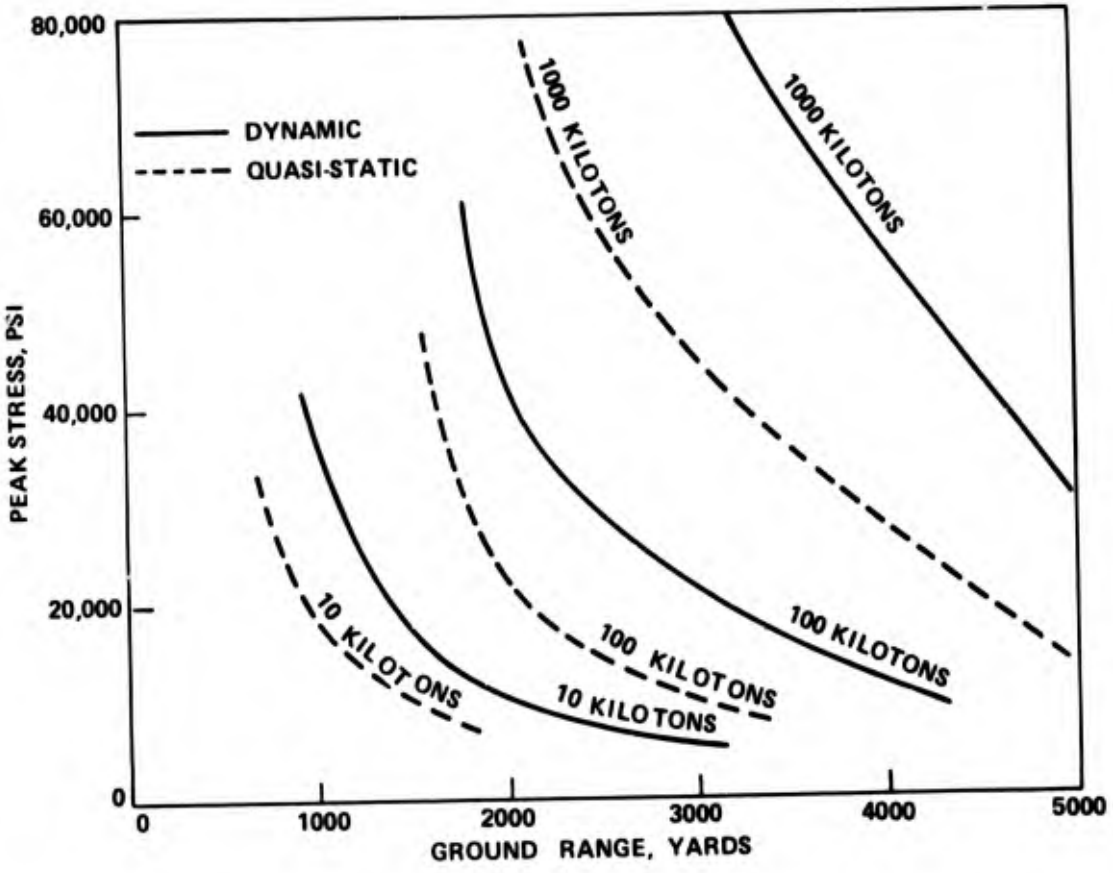

FIG. 17 DYNAMIC AND QUASI-STATIC STRESSES IN A 1/4" PLATE SUBJECT TO NUCLEAR WEAPON ENVIRONMENTS.

Figure 17 are quite general. That is, plates of this size and thickness have relatively high natural frequencies hence exhibit dynamic behavior. For example, the fundamental frequency for this plate, as given by equation (B-11), is 2,080 cycles/second.

A second example will be given to illustrate the relative importance of blast and thermal stresses. It was previously shown that thermal stresses can be large in thick members if large thermal gradients are developed. The present example is a 1/4-inch thick by 12.0-inch long narrow clamped beam constructed of 6061-T6 aluminum alloy. Computations were made using the dynamic analysis to find the peak thermal stresses due to the thermal pulse acting alone, and to compare this to the corresponding blast-thermal stresses. Nuclear weapon peak overpressures and radiant exposure as a function of ground range were the same as those used in the first example. However, the pressure pulse for this beam is taken to be that for net diffraction loading shown in Figure 15. The results of these calculations are shown in figure 18.

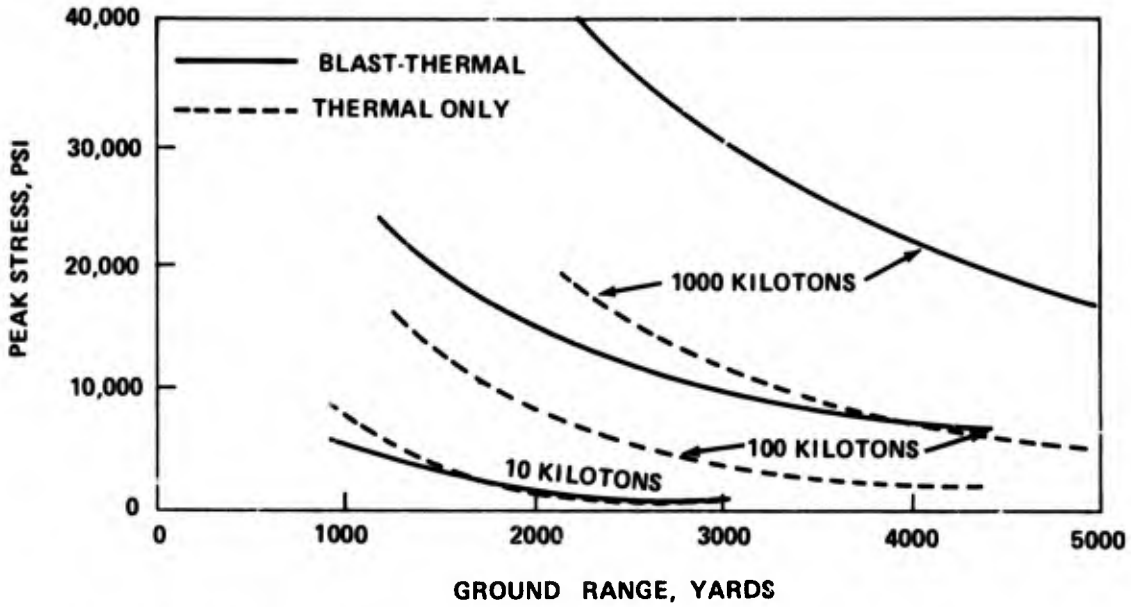

FIG. 18 BLAST-THERMAL AND THERMAL ALONE STRESS IN A 1/4" BEAM SUBJECT TO NUCLEAR WEAPON ENVIRONMENTS.

Figure 18 shows that the blast-thermal stresses are much larger than the thermal stresses due to the heating alone. The blast thermal stresses shown are almost entirely due to the action of the pressure pulse. This is true because the peak blast-thermal stresses occur at the blast arrival time and here the thermal gradients are greatly reduced from their peak values. The peak thermal stresses shown here for the relatively thin beam occur near the time of maximum irradiance and even then are in general much lower than the peak blast-thermal stresses. Since the peak stresses occur at blast arrival, the aluminum beams must spend several seconds at relatively high temperatures. Hence, Figure A-2 or A-6 must be used to estimate the decrease in yield strength with temperature for this example.

The analysis and resulting computer programs presented in Appendix B have been used in a parametric study which computed the stress and displacement in beams and plates exposed to nuclear weapon environments. Twelve loading conditions consisting of weapon yields of 10,100 and 1,000 kilotons and peak overpressures of 3, 5, 7 and 10 psi were chosen. Heights of burst to maximize radiant exposure where used hence the maximum total irradiances shown in Figure 4 were realized. A variation of yield strength with temperature for 6061-T6 aluminum alloy was chosen to represent the decrease in strength for time at temperature greater than a few seconds. Plates and beams of nine different sizes were considered. Simply supported square plates of length 1/4, 1/2 and 1.0 meters and thicknesses of 1/8, 1/4 and 3/8 inches were analyzed for the twelve loading conditions. Similar circular plates of diameters equal to the square plate length were

also considered. Stress and displacement calculations were also made for simply-supported, cantilever and clamped beams. Beams were 1/4, 1/2 and 1.0 meters long and 3/8, 1/2 and 5/8 inches thick. The computed peak thermal and peak blast-thermal stress for each of the above structural elements is presented in the references[40] as a function of peak overpressure.

In addition to showing the conditions under which the aluminum structural elements would yield, several general conclusions were drawn from the parametric study.[41] The principal results are the following:

1. The stress due to pressure loading in both plates and beams is approximately proportional to B^2/L^2.

2. The displacements due to pressure loading in both plates and beams is approximately proportional to B^4/L^3.

3. The magnitude of the weapon yield has no significant effect on the stresses and displacements due to pressure loading. This result is due to sharply peaked nature of the nuclear weapon pressure pulse and the dynamic nature of the response of the structural elements selected for this study.

4. The displacements and stresses in simply supported circular and square plates are virtually identical when the diameter of the circular plate equals the length of the square plate.

5. The stresses and displacements due to the thermal pulse acting alone are accurately described by the quasi-static analysis in all cases. A further study was made to determine when a dynamic analysis is required for thermal loading from nuclear weapon explosions. These results are given below.

6. The calculation of stresses and displacements due to the pressure pulse requires dynamic analysis in all cases. However, a method based on an equivalent pressure concept was developed to relate dynamic calculations of stress and displacement to the more easily obtained quasi-static values. This method is discussed in detail in the literature.[42]

The determination of whether a target responds quasi-statically or dynamically to the thermal pulse alone is important in estimating the influence of thermal effects in the blast-thermal response of structures. That is, much labor can be saved if thermal effects are quasi-static and simple calculations will indicate if thermal stresses will cause failure or if thermal stresses are negligible at blast arrival.

---

40 Koch, J. E., "Parametric Study of Stresses and Displacements in Certain Structural Elements When Exposed to the Thermal and Blast Effects of a Nuclear Event", N. Eastern Res. Associates,No.RR-NA-12 1 June 1973

41 Ibid

42 Koch, N. Eastern Research Associates No. RR-NA-12, Op. Cit.

If thermal effects are dynamic, thermal vibrations would cause thermal stresses and displacements to be propagated in time from when the maximum temperature gradients occur to the time of blast arrival. Then, thermal stress might be a significant portion of the total blast-thermal effect when combined with blast-induced stress. The importance of dynamic thermal effects was found by computing the dynamic magnification of displacement and stress in plates and beams. The dynamic magnification is the ratio of displacement or stress computed by a dynamic analysis to the corresponding value given by a quasi-static analysis. The dynamic magnification was found to depend on the variable, 0.5 Pd/tsm. Here, Pd is the fundamental period of vibration, $Pd = \frac{2\pi}{W_{11}}$, where W_{11} is the fundamental frequency of vibration given by equation (B-11) or (B-32). tsm is the time at which the maximum value of the thermal moment, Mt, occurs. The dynamic magnification for displacement in both plates and beams is given in the references[43,44] and is shown in Figure 19.

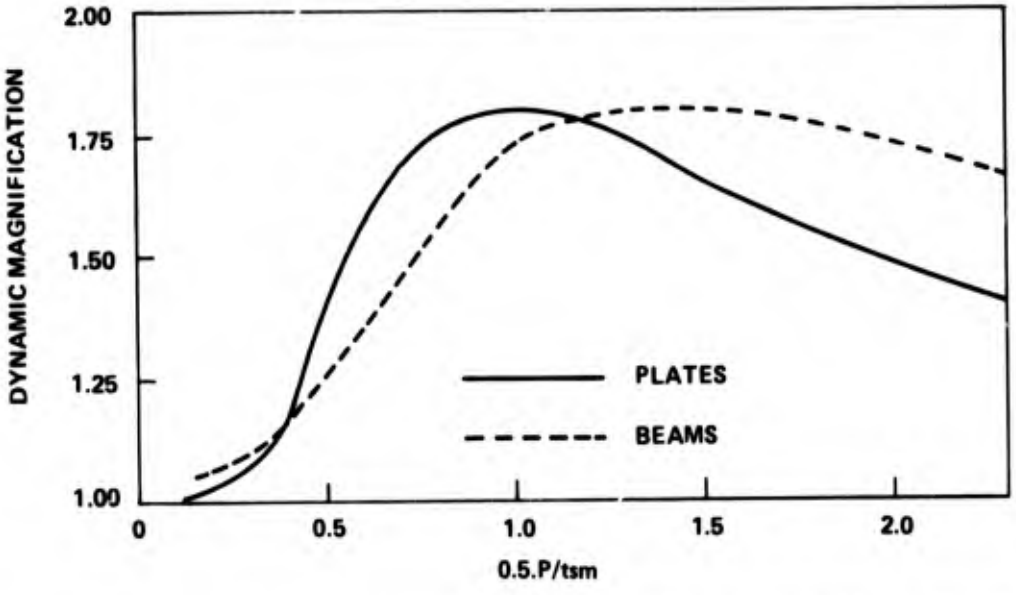

FIG. 19 DYNAMIC MAGNIFICATION OF DISPLACEMENT IN PLATES AND BEAMS

43 Koch, North Eastern Research Associates No. RR-NA-12, Op. Cit.

44 Koch, J.E., "Equations, Computer Programs and Computations of Displacements and Stresses in Beams Having Temperature Dependent Material Properties When Exposed to the Thermal and Blast Effects of a Nuclear Event," North Eastern Research Associates No.RR-NA-13 15 June 1973

It was found that the values of 0.5 Pd/tsm for the 12 loading conditions and geometries of the parametric study were 0.3 or less. Thus, dynamic magnification of displacement is about 5 percent or less and the thermal response of the structural elements considered is quasi-static. However, dynamic magnifications as high as 1.7 were reported for circular plates[45] and these large displacements are propagated in time after their initial occurrence. The dynamic magnification for stress in beams is similar to that for displacement and is given in the references[46].

The effect of allowing elastic properties to vary with temperature was included in the parametric study of structural elements. In this consideration, the Young's Modulus and the coefficient of expansion were allowed to vary with temperature for 6061-T6 aluminum alloy. The dynamic and quasi-static analyses for beams were repeated to derive equations which included variable elastic properties. Calculations were repeated for beams subject to the 12 loading conditions previously given. The details of this study are reported in the references.[47] Here, it was found that stress computations were not appreciably different from the corresponding constant property values. The displacements were found to be up to 9 percent higher than those given by the corresponding constant property calculations. Hence, it was concluded that it is not important to include variations in elastic properties for the weapon conditions and structural elements considered in these studies.

The previous study considered elements which were not constrained against movement in an axial direction, hence inplane thermal forces are not developed. Another study was made which allowed an initial force to represent inplane thermal loads on simply supported or clamped rectangular plates. A dynamic analysis for this problem is described in Appendix B and reported in the references.[48] Calculations were performed to determine the influence of plate geometry, material, initial loading conditions and loading time on the response to a nuclear weapon pressure pulse. Results were obtained by varying one factor at a time in a standard problem. The standard problem

---

45 Koch, J. E., and Cohen, M. L., "Response of a Simply Supported Circular Plate Exposed to Thermal and Pressure Loading", The Shock and Vibration Bulletin, Part 2, pg 171-180, Jan 1972.

46 Koch, J/E., "Parametric Study of Stresses and Displacements in Certain Structural Elements When Exposed to the Thermal and Blast Effects of a Nuclear Event," North Eastern Research Associates No. RR-NA-12, June 1973.

47 Koch, North Eastern Research Associates No. RR-NA-12, op.cit.

48 Cost, T.L., Griffin, J.R., and Pettey, R.H., "Analysis and Design of Thermally and Mechanically Prestressed Flat Plates Subjected to Transverse Blast Loads", U.S. Army Missile Command Technical Report RL-72-18, May 1973.

consists of an 8.0 inch square aluminum plate, fully clamped and subject to a nuclear weapon pressure pulse. This pressure pulse is described by equation (2) and has a peak overpressure of 10 psi and a positive phase duration of 1.0 second. Principal results of this parametric study are the following:

1. The maximum stress and displacement in plates increases more rapidly with plate width and decreases more rapidly with plate thickness than would be predicted by a linear law. This results due to changes in plate stiffness as evident from changes in the fundamental frequency of vibration as width and thickness changes.

2. Material property effects, given by changes in Young's Modulus and density are also non-linear. However, the changes in stress or displacement are less than that observed by making proportional changes in width or thickness.

3. Prestressing the plate causes a dramatic decrease in maximum stress and displacement as prestressing is increased until very low values of maximum stress and displacement are realized. This result is true for both equal and unequal biaxial tension on the plate.

4. A thermal preload causes a compressive inplane stress which increases rapidly as the initial temperature increment is increased. This effect, which can lead to buckling of the plate, is discussed in Appendix B.

5. The simply supported plate with its end constrained against axial movement exhibits higher maximum stress and displacement than a corresponding clamped plate.

6. The maximum stress and displacement is independent of loading time (positive phase duration) for loading times greater than 0.1 seconds. This relatively low value of critical loading time is due to the relatively high value of fundamental frequency, 300 cycles/sec., of the standard problem.

A second study also described the behavior of plates having a hinged boundary condition. A hinged boundary is a simply supported plate with its ends constrained against axial motion. In this study, the axial force can either be due to thermal expansion or an axial force history can be supplied. The given axial force history can act in addition to blast-thermal effects supplied by a nuclear weapon. The analysis for this case is given in Appendix B and reported in the literature.[49]

[49] Koch, J.E., "Equations and Computer Program to Compute Stresses and Displacements in a Constrained or an Unconstrained Beam-Column When Exposed to the Thermal and Blast Effects of a Nuclear Event," North Eastern Research Associates No. RR-NA-14, 30 Jun 73.

VI. METHODS FOR THERMAL PROTECTION

This report has pointed out the potential damage to ship systems which have been exposed to the pressure and thermal pulses of a nuclear weapon explosion. Thermal effects have been shown to be damaging in themselves and can also enhance pressure damage by causing materials to be in a weakened state at blast arrival. Hence, in many cases of protecting systems or their elements, it may be necessary to first consider the thermal protection requirements. Three basic methods of providing thermal protection against a nuclear weapon environment will be considered. These are, thickening or substitution of materials to provide additional heat sinks, application of water to carry away the excessive heat and coatings which reflect heat or provide insulation.

One of the most obvious methods of preventing high temperatures in an element being heated is simply to make it thicker or replace its material with material of better thermal properties. The methods discussed in the section, Thermal Effects on Structural Elements, can be used to determine the amount of thickening or new material required to reduce temperatures to safe levels. Figure 8 showed the maximum temperature rise in flat plates exposed to the nuclear weapon thermal pulse. If the plate is thermally-thin after thickening, Figure 8 shows that the maximum temperature is directly proportional to the thickness. If the plate is not thermally thin, a less than proportional benefit is gained by thickening. The maximum temperature rise in circular cylinders exposed to the nuclear weapon thermal pulse is given in Figures 9 - 12. These figures show that a temperature rise reduction greater than proportional to a thickness increase can be realized in many cases if the cylinders are sufficiently thick, i.e., if the values of $\alpha \cdot t_{max}/R_o^2$ are low enough. This occurs because of enhancement of the heat sink effect caused by the unexposed rear of the cylinders. The reduction in maximum temperature for cylinders or plates by thickening is easily found from Figures 8 - 12. Hence, these figures can be used to design new structural elements which will withstand the thermal effects of a nuclear weapon explosion. Thickening also increases the resistance to blast damage. The new thickness in an element can be a compromise between that required to reduce maximum temperatures and that required to increase mechanical strength.

Thickening of structures may cause an unacceptable cost or weight penalty hence other thermal protection methods should be considered. An experimental study was conducted to determine the effectiveness of using water to remove the heat absorbed from nuclear weapon thermal radiation. Heat transfer rates were measured for water flowing down or sprayed onto a flat plate. In the water flow experiments, the plate was simultaneously heated by igniting a sheet of rocket propellant placed behind the plate. The experimental set-up and resulting heat transfer rates are given in

the references.[50] It was assumed that a system could be activated to allow water to be flowed or sprayed onto a plate which is simultaneously heated by the nuclear weapon's thermal pulse. Calculations based on the previously derived heat transfer rates were made to determine the effectiveness of water cooling aluminum plates of thicknesses between 1/8" and 1/4". The total irradiances shown in Figure 16 were used with an absorptance of 0.8. These calculations showed that flow cooling was ineffective at ranges corresponding to peak overpressures greater than 8 psi. Spray cooling was found to be effective at ranges corresponding to peak overpressures of 8 and 10 psi but was ineffective at 15 psi. The reason that water cooling becomes ineffective is due to the behavior of water on a hot surface. Water goes through several stages from convective cooling to nucleate boiling to fully developed film boiling as the plate temperature increases. Therefore, if the maximum irradiance of the thermal radiation pulse is large enough, it will overwhelm the cooling effect of the water and allow the plate temperature to increase rapidly. That is, when the plate temperature exceeds the maximum allowed value for nucleate boiling, film boiling will begin. Film boiling is very inefficient in removing heat because a vapor layer forms and insulates the plate from the water. The important parameter in determining if water cooling can be overwhelmed is the maximum nucleate boiling heat transfer rate. This was observed to be 10 - 15 $cal/sec\text{-}cm^2$ for flow cooling and 50 - 60 $cal/sec\text{-}cm^2$ for spray cooling. Indications are that these maximums are not very sensitive to increased flow rates. Therefore, nuclear weapon thermal pulses which have peak irradiances greater than these observed maximums are capable of overwhelming the cooling effect of the water. Hence, it was concluded that water cooling alone could be used to provide thermal protection up to 8 psi only. For higher peak overpressures, it should be used in conjunction with other thermal protective measures.

The third and perhaps best method for saving weight and cost is thermal protection by use of coatings. Coatings can provide thermal protection by reflecting away much of the incoming irradiance, by absorbing it and subsequently releasing energy through chemical changes, or by simply insulating the element. All of these effects can be observed by measuring an effective absorptance of the coating system. An experimental study was initiated to measure the effective absorptance of paint systems presently used by the Navy and on some candidates to provide additional thermal protection. These tests consist of coating thin aluminum buttons and exposing these to a thermal radiation pulse produced by a carbon arc source. The carbon arc is designed to produce the irradiance history of a nuclear weapon

---

[50] Wilson, D.M., Katz, B.S., and Demske, D., "The Use of Water Cooling for Protection Against Thermal Radiation From A Nuclear Weapon Detonation," NOLTR 74-59, April 1974.

thermal pulse.[51] Temperature histories were recorded by thermocouples attached to the back face of the buttons and a simultaneous measurement of the incident heat transfer rate was made using a thin film radiometer. The effective absorbtance as a function of temperature was defined from the following energy balance on the thermally-thin specimens

$$A_{eff} = \frac{\rho \cdot Cp \cdot L}{q} \left(\frac{dT}{dt_h} - \frac{dT}{dt_c} \right) \tag{39}$$

In equation (39), the subscript, "h" corresponds to the temperature derivative during the heating cycle while "c" corresponds to this derivative at the same temperature in the cooling cycle. The derivative measured under natural cooling conditions is used to subtract out the heat losses that occur by convection, radiation and conduction while the sample is being heated.

The effective absorbtance for the paint systems tested are given in Table 3. These absorptances are preliminary results only.

PRIMARY COATING	DESIGNATION	THICKNESS	UNDERCOATING	THICKNESS	$\bar{A}_{eff}$	Tmax
Haze Gray #27	TT-E-490	.003"-.004"	Mil-C-15328 Mil-C-15930	.0015"	0.65	120°C
IR near Black	-	.003"-.004"	Mil-C-15328 Mil-C-15730	.0015"	0.75	125°C
Insignia White	C-832864	.004"	2 Coats Primer	.002"	0.35	150°C
White	C-81773	.005"	1 Coat Primer	.001"	0.35	200°C
Haze Gray over Intumescent White	IT-E-490 over CCL-728-921	.002" over .012"	MIL C-5541 MIL C-15328	.0015"	0.50	150°C
Teflon	Green	.004"	None	-	0.70	450°C

TABLE 3. AVERAGE ABSORPTANCES FOR SEVERAL COATING SYSTEMS

[51] Griff, N. and Heilferty, R.J., "Image Furnace for Low Yield Nuclear Weapons Effects Simulation," Naval Applied Science Laboratory, LP940-105, Progress Report 2, 14 Jul 1966.

Table 3 lists the observed absorptances averaged over the temperature interval from room temperature to temperature Tmax given in the table. For temperatures above Tmax, large changes in absorptance were observed which probably result from burning or chemical changes in the paint. The absorptances given in Table 3 show that the paint systems, Navy gray and IR black, highly absorb thermal radiation. The two white coatings have much lower absorptances hence their use would provide significant thermal protection. The Intumescent Coating (coating #5) provides thermal protection by absorbing additional energy at temperatures greater than the 150°C given in the table. Green Teflon did not have a low effective absorptance but can stand a much higher temperature without degrading. It is planned to make a detailed analysis of the data gathered in this coating study and publish it in the future.

VII. SUMMARY

This report was written to review, unify and condense the existing large body of work on the effects of thermal radiation alone and thermal radiation as it influences nuclear weapon air blast response. Other nuclear weapon phenomena such as nuclear radiation and electromagnetic pulse were treated lightly in order to show the distances from a nuclear burst where each phenomena is dominant. Thus, the total received thermal radiation and the peak overpressures were given in terms of ground range and weapon yield in Figures 4, 5 and 16 for the ranges where thermal and blast effects are likely to be the most damaging influences on ship survivability or performance of mission. The approach to summarizing existing information has been to review the methods of computing temperatures or stresses in simple structural elements. Only general results or examples to illustrate specific points were presented but references are given to obtain specific information. Some Navy systems have been analyzed but these have not been included in order to keep this report general and unclassified.

The results in this report can be used to give a first estimate of the possible effects of nuclear weapon thermal and blast on a military structure. In doing this, the thermal effects are easily estimated by finding the maximum temperature in structural elements from Figures 8 - 12. Blast thermal effects may be estimated by use of the examples and observations given herein or in the references or it may be necessary to exercise one of the reported computer programs. Also, the results of Appendix A can be used to estimate the mechanical strength of aluminum alloys which have been rapidly heated by the thermal pulse.

This report has been primarily concerned with methods of computing the thermal and blast effects of nuclear weapons on structural components. The calculations have shown that these effects are potentially damaging to ships' systems at relatively large distances from a nuclear weapon burst. Experimental measurements have also

been made to indicate the damage caused by blast or thermal effects. A listing of facilities for thermal simulators is reported in the references.[52] Also reported is a similar listing for blast and shock simulators.[53] Recently, efforts have been made to measure combined thermal-blast effects and one facility for these measurements is reported.[54] To date, very few measurements of combined thermal-blast effects have been made. Also lacking is information on methods of providing thermal protection for critical elements of a ship's system. A particularly promising area where additional information is needed is the characteristic of coatings which can be applied to these elements to provide efficient thermal protection.

A late addition to this survey is the report of the Mathematical Methodology Workshop, Panel N-2 of the Defense Nuclear Agency sponsored Technical Cooperation Program. (TTCP Panel N-2 Report N2:TR 3-72 issued 1 Oct. 1975). This report is a technical summary of computational methods for the determination of nuclear blast, shock, and thermal phenomena and describes many computer programs available for the prediction of these nuclear weapon effects.

---

52 Loop, J.D., Nebert, D.L., and Quigley, E.F., "Characteristics of High Intensity Facilities for Nuclear Thermal Effects Analysis of Tactical Systems," BRL MR2083, Dec 1970.

53 "The Technical Cooperation Program, Panel N-2 Nuclear Blast and Shock Simulators", DOD Nuclear Information and Analysis Center Report N2:TR 2-72, 28 Dec 72.

54 Katz,B.S., and Connor, J.G.,Jr., "Development of the NOL Thermal Blast Simulator", NOL TR 72-183, 19 Jul 72.

Appendix A

MECHANICAL PROPERTIES OF ALUMINUM ALLOYS AFTER RAPID HEATING

The mechanical properties of aluminum alloys which determine their strength and fracture characteristics are dependent upon the microstructure of the matrix of crystals which comprise their structure. The microstructure is sensitive to changes in temperature. In fact, elevated temperatures are used to induce microstructural changes that allow alloys of greater mechanical strength to be produced. Hence, it should not be surprising that the rapid heating of aluminum alloy structures by a nuclear weapon's thermal pulse could destroy beneficial microstructures and lower the alloy's strength before the blast wave has time to arrive. The residual values of strength at blast arrival are hard to predict due to a lack of experimental data on this phenomenon. Also, it is difficult to extend existing data because the microstructural changes that occur depend on time at temperature and other factors such as temperature level and strain rate at which the structure is deformed. This section will discuss how these factors cause microstructural changes and will present some data on aluminum alloy strength after rapid or slow heating. An attempt will be made to predict the strength properties of several aluminum alloys which have been heated by the thermal pulse of a nuclear weapon explosion.

The dislocation theory of plastic deformation explains the yielding of metals under load. A dislocation is an imperfection in the space lattice of atoms forming the crystals of a structure. For example, the lattice could contain an extra plane of atoms above a certain line in the matrix (an edge dislocation). These dislocations are very mobile. The critical shear stress required to move a dislocation would be several orders of magnitude less than that required to overcome the lattice binding force. The movement of dislocations causes a slip process which results in the movement of entire planes of atoms. But the slip process of individual crystals is not sufficient to explain yielding in a polycrystalline substance. Here, the existence of grain boundaries influence the mechanical behavior of an aggregate of crystals which have all possible orientations. The grain boundaries are regions of misfit in the material, i.e., where crystals meet but do not allow room for other space lattices to develop. These regions are the plates where arrays of dislocations may terminate or originate. The random orientation of dislocations and grain boundaries contribute to the strength and ductility of polycrystalline materials. The widely varied orientation of crystals produces a homogeneous isotropic mass with characteristic grain boundaries. Therefore, experimental measurements can be made on a

representative sample with confidence that the results will apply to all structures made of the same material.

Higher mechanical strength is produced in aluminum alloys by three processes. These are, (1) solid solution strengthening, (2) responding to precipitation hardening, and (3) strain hardening by cold work. Each of these processes will be briefly discussed because their original effect can be modified by the heating and blast damage caused by a nearby nuclear weapon explosion. In the case of alloys hardened by heat treatment (precipitation hardening), the hardening effect tends to be reversed due to a subsequent large temperature rise in the alloy. However, the yield strength of these alloys will be raised relative to their handbook values by strain hardening due to the high strain rates induced by the blast wave. The handbook values are obtained by conventional testing at very low strain rates.

Solid solutions of alloys are formed when one element can be completely dissolved in a second element. That is, the atoms of the first element become part of the space lattice of the second element. Hardening may occur because the presence of these foreign atoms in a lattice structure modifies the movement of dislocations. Although the formation of a solid solution may in itself provide hardening, its importance for aluminum alloys lies in providing a product that can respond to precipitation hardening. Most commercially important aluminum alloys contain several alloying elements. These may form second phase zones for hardening or may be added for other properties such as corrosion resistance.

Precipitation hardening is the heat treatment applied to a solid solution of an alloy in order to increase its tensile strength or hardness. A solid solution of an alloy which exists at an elevated temperature is retained at room temperature by quenching the alloy. The solid solution is then supersaturated and there is a strong tendency for the alloying metal atoms to aggregate and coalesce into particles. The regions where this precipitate is nucleated is called the Guiner-Preston or GP zone and these particles grow to a size that is microscopically recognizable. However, although the hardening effect occurs while the particles are coalescing and growing, the maximum strength condition has been passed by the time that the particles are microscopically visible. The alloy is then said to be overaged. The reason that the alloy loses strength by overaging is based on the dislocation theory of plastic deformation. The precipitate acts as an obstruction to the motion of dislocations. But, as the precipitate coalesces into particles, there is less spacing between the larger particles and fewer obstructions to dislocation motion. Since the precipitation hardening process is controlled by the diffusion of atoms, it is time dependent. Furthermore, the ease with which atoms diffuse is temperature dependent hence the precipitation hardening treatment is dependent on time at temperature. A

detailed discussion of the precipitations hardening process is given in the references.[55]

The aging process should be negligible at room temperature for an alloy to be useful. The choice of an elevated temperature for aging represents a compromise between temperature level and time at temperature. Figure A-1 shows the room temperature yield strength attainable for aluminum alloy 6061 as a function of aging time and artificial aging temperature. The data in this figure was originally given in a reference.[56]

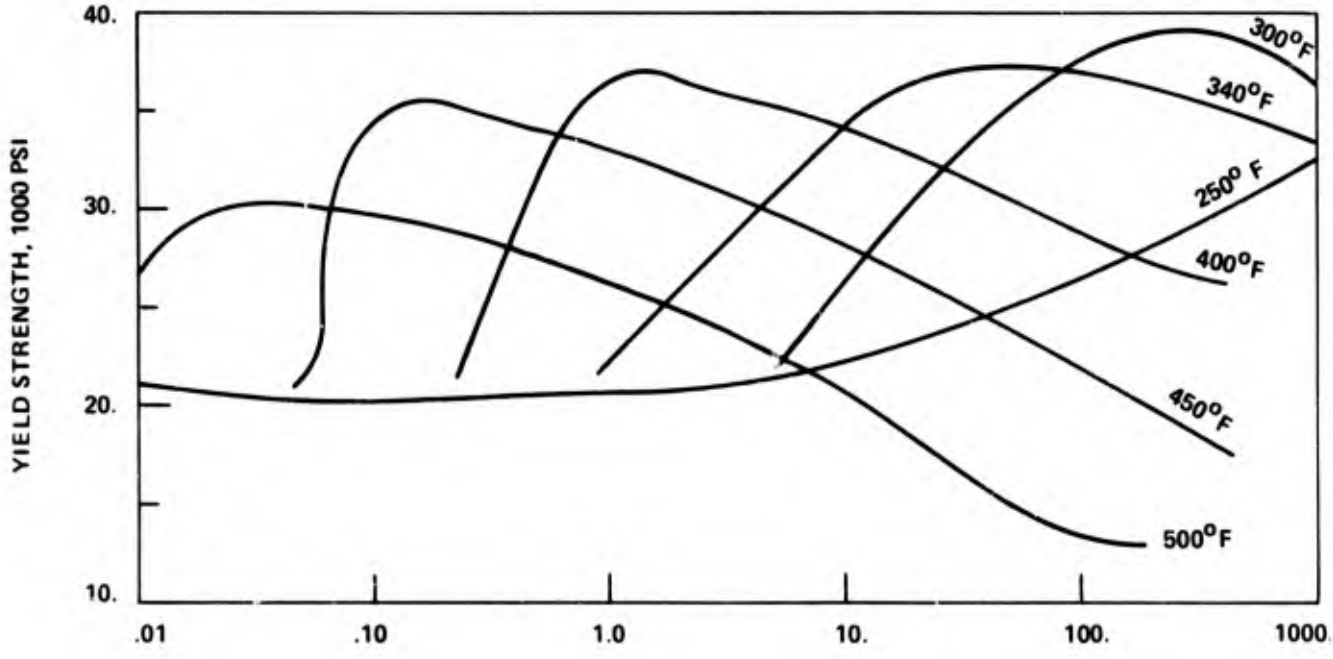

FIG. A-1 ARTIFICAL AGING TEMPERATURE AND TIME FOR ALUMINUM ALLOY 6061

In general, the alloy ages the most rapidly at the higher temperatures but the most practical temperatures for developing maximum yield strength lie between 300°F and 400°F. Thus the recommended precipitation heat treatment for 6061-T6 alloy (a high strength condition) is aging for 6 - 10 hours at 350°F. From the data shown in Figure A-1 it is clear that a subsequent heating of a structure composed of aluminum alloy 6061-T6 to 350°F for a sufficient time will cause it to have a lower room temperature yield strength due to overaging. If

55 Clark, D.S., and Varney, W.R., "Physical Metallurgy for Engineers", Van Nostrand Co., Princeton, NJ, Second Edition, 1962

56 Babcock, S.W., et al, "Subsequent Yield and High Heating Rate Properties of Two Aluminum Alloys", General Motors Corporation MSL 70-24, Sep 1970.

temperatures higher than 350°F are reached, the diffusion-controlled overaging process will occur much faster. When temperatures significantly above the artificial aging temperatures are reached, the loss in yield strength due to overaging can occur in seconds. Therefore, exposure of structures made of aluminum alloys to a nuclear weapons thermal pulse may cause a reduction in mechanical strength in the few seconds between the heating and the arrival of the weapon's blast wave. Experimental data on the mechanical strength of rapidly heated aluminum alloys will be presented and discussed later in this appendix.

Strain hardening of aluminum alloys is possible because their resistance to plastic deformation increases with increasing plastic strain. Strain hardening occurs when a suitable aluminum alloy is deformed past the proportional limit (plastically deformed), for example by rolling. A subsequent load on such an alloy will behave elastically up to the point of previous maximum plastic deformation. Hence the alloys proportional limit and its yield strength have been increased by the strain hardening. Strain hardening is done by cold working if the deformation is done at a temperature less than the recrystallization temperature of the alloy. However, if the deformations are applied at a temperature greater than the recrystallization temperature, little strain hardening occurs due to the recrystallization of the alloy microstructure. Although the minimum recrystallization process depends on the growing of a new grain structure which takes a large amount of time relative to the heating times of nuclear weapon thermal pulses. Therefore, a less than expected degradation of strength properties occurs in the relatively short time a structure remains at elevated temperature before blast arrival. Also, aluminum alloys may be hardened by the high strain rates caused by the blast wave. Experimental data on the mechanical strength of aluminum subjected to high temperature and high strain rates will be presented and discussed later.

The previous discussion indicated that the mechanical properties of aluminum alloys are critically dependent upon the microstructure of their constituent crystals and grain boundaries. Furthermore, the microstructure of aluminum alloys can be rapidly altered by the effects of temperature, time at temperature and strain rate. The thermal and blast characteristics of a nuclear weapon explosion can change the alloy's strength properties in the few seconds that the structure is heated and during the deformation caused by the blast wave. Thus, it is necessary to know how the nuclear weapon heating and induced strain rates effect mechanical strength before an assessment of damage to aluminum alloy structures in a nuclear warfare environment can be made. No experimental data on mechanical strength under these conditions exists. In fact, any data for short time at elevated temperature is scarce. Such data is available for only a few aluminum alloys and for a few strain rates. Representative experimental data will be presented to show how combinations of temperature, time at temperature and strain rate might influence the strength of aluminum alloys in a nuclear warfare environment.

An examination of experimental data shows that time at temperature has a large effect on the mechanical strength of an aluminum alloy heated to an elevated temperature. Figure A-2 shows the residual yield strength at elevated temperature as a function of temperature and time at temperature for aluminum alloy 2014-T6. The data plotted was taken from 3 different sources and are not all comparable due to different testing methods. Data for time at temperature from 1/2 hour to 1000 hours[57] was taken at a strain rate of approximately .0002 in/in/second. The data for a holding time of 10 seconds[58] was taken at a strain rate of .00005 in/in/second. The test conditions and strain rates of these tests are very similar hence the data can be directly compared. The remaining data[59] was found by continually heating a sample up to the test temperature at a constant rate instead of holding the sample at test temperature as was previously done. It was previously stated that time above the artificial aging temperature is important in causing detrimental microstructural changes in an aluminum alloy. If the artificial aging temperature is assumed to be 350°F for this alloy, it would take 6000, 600, 6 and .06 seconds for the alloy to go from 350°F to 500°F for the 4 temperature rise rates shown in Figure A-2. These times should be reduced somewhat in order to compare this data with previously referred to data[60,61] at 500°F because time spent held at 500°F is more effective in degrading strength than on equal time spent in going from 350°F to 500°F. Hence the data at 500°F for 10 second or 1/2 hour holding times can be compared favorably with the data for a temperature rise of .025° F/second. A further complication is that the data of one study[62] was taken at a strain rate of 10 in/in/sec. It will be shown later that this strain rate should be large enough to cause a slight strain hardening in an aluminum alloy. Figure A-2 shows that the data of this study[63] for temperature rates of .25°F/second or more does not agree with the data for samples held at temperature for 10 seconds. These higher temperature rise rates are equivalent to holding times of less than 10 seconds. The data shows that the strength degradation approaches a constant value as the time spent at elevated temperature becomes very small.

---

57 Voorhees, H.R., and Freeman, J.W., "Report on the Elevated-Temperature Properties of Aluminum and Magnesium Alloys," ASTM Special Tech. Pub. No. 291, Oct 1960.

58 Dotson, C.L., and Kattus, J.R., "Tensile Properties of Aircraft Structural Metals at Various Rates of Loading After Rapid Heating" WADC Tech. Rep. 55-199, August 1955.

59 Babcock, S.G., et al, Gen. Motors Corp. MSL 70-24, Op. Cit.

60 Voorhees, ASTM Special Tech. Pub. No. 291 Op. Cit.

61 Dotson, WADC Tech. Rep. 55-199 Op. Cit.

62 Babcock, Gen. Motors Corp. MSL 70-24 Op. Cit.

63 Ibid.

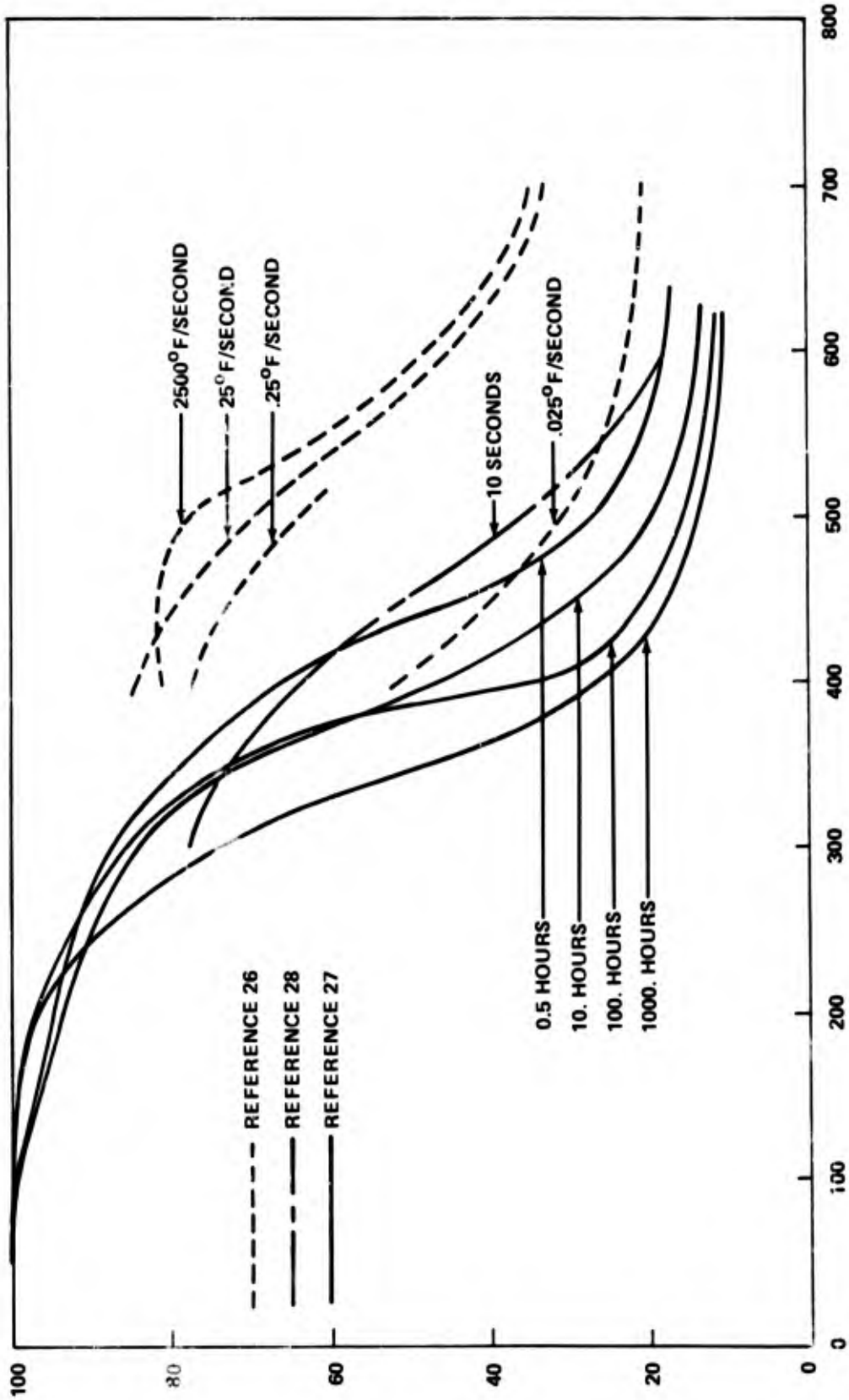

FIG. A-2 RESIDUAL YIELD STRENGTH OF ALUMINUM ALLOY 2014-T6 AFTER VARIOUS HEATING CONDITIONS

The mechanical strength data for two additional aluminum alloys, 2024-T3 and 7075-T6, is given in the references[64] for times at temperature of 10,100 and 1800 seconds, and strain rates between .00005 in/in/second and 1.0 in/in/second. Both of these alloys show the same trend of decreasing strength with increasing temperature and increasing time at temperature as that exhibited by the 2014-T6 aluminum in Figure A-2. However the 2024-T3 alloy does retain a larger percentage of its room temperature strength at elevated temperature. An explanation of this is that the T3 condition corresponds to an alloy which has only been solution treated and cold worked, but not artificially aged. Thus it is possible that the T3 condition can stand a degree of aging at elevated temperature before it begins to overage and lost strength.

A concerted effort has been made to study the effects of elevated temperature and time at temperature for aluminum alloy 6061-T6. Two test programs were conducted to extend the existing experimental data for holding times of 1/2 hour or greater to times in the microsecond range. Based on the results of these and other studies it was concluded[65] that three domains of time at temperature at elevated temperature exist. A different mechanism for governing mechanical strength behavior was postulated for each domain. The first domain is the very shortest time at temperature, i.e., time of the order of tens of microseconds obtained by pulse heating. The results of these experiments performed by the Sandia Corporation[66] are reproduced in Figure A-3. This figure shows yield strength measured at room temperature after the sample had been pulse heated to the temperatures shown. For microsecond times at temperature, pulse heating produced by electron beam energy deposition was used. This causes one-dimensional stress wave loading in the long slender rod test specimen. The rod heated in this manner cannot expand rapidly enough to prevent the propagation of stress relief waves. The resulting high strain rates cause permanent microstructural changes that reduce the mechanical strength of the alloy. The times at temperature in this first domain are too short to be of interest for nuclear weapon thermal radiation effects from an atmospheric explosion. A detailed explanation of the mechanisms reducing strength in this region is given in the reference[67].

The second time at temperature doman includes times ranging from several milliseconds to a few seconds. The results of experiments performed by the Physics International Company are

---

64 Dotson, WADC Tech. Rep. 55-199 Op. Cit.

65 Lipkin, J., Swearengen, J.C., and Karnes, C.H., "Mechanical Properties of 6061-T6 Aluminum After Very Rapid Heating," Sandia Lab. SC-RR-72 0030, Mar 1972

66 Ibid.

67 Ibid.

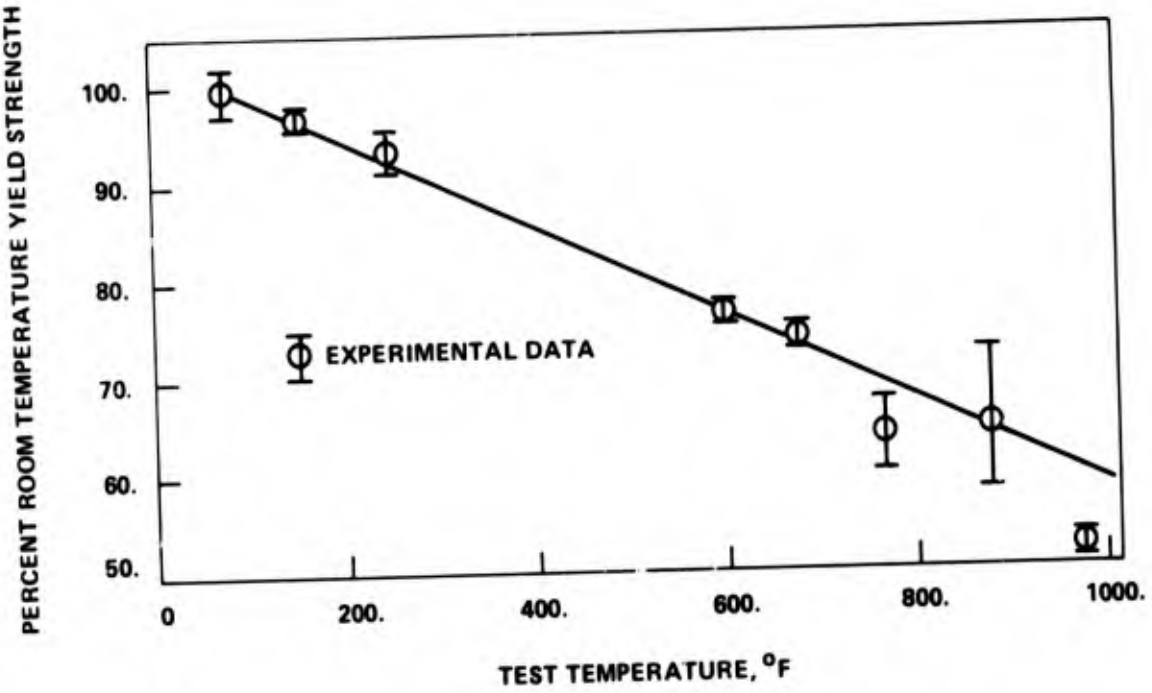

FIG. A-3 YIELD STRENGTH OF ALUMINUM ALLOY 6061-T6 AFTER MICROSECOND PULSE HEATING

reported[68] and are shown in Figure A-4 for time at temperature from 0.2 milliseconds to 10.0 milliseconds. The data lines shown in Figure A-4 are drawn through the experimental data points for each time at temperature. Although there is considerable scatter in the data the trend of decreasing strength with increasing time at temperature is very evident. The fact that the yield strength is not degraded as much as it is for much longer time at temperature (e.g. see Figure A-2) leads to the suspicion that a new mechanism is responsible for the reduction in strength. That is, it was suspected that microstructural changes by diffusion of atoms might not have time to occur in milliseconds of time. Instead, the smaller reduction in strength might be due only to the weakening of the crystal structure by temperature. Then, the reduction in yield strength should behave as the reduction in elastic modulus with temperature. The elastic modulus is known not to depend on time at temperature, i.e., it is a property of crystal structure alone. The suspicion was tested by measuring the elastic and shear moduli for time at temperature of 0.2, 1.0 and 10 milliseconds. These measurements showed that the elastic and shear moduli decrease with increases in temperature but no time at temperature effect was

[68] Stefansky,T., Triebes, K. and Shea,J., "Temperature-Induced Degradation of Mechanical Properties Following Instantaneous Heating," Air Force Weapons Lab. No. AFWL-TR-71-62.

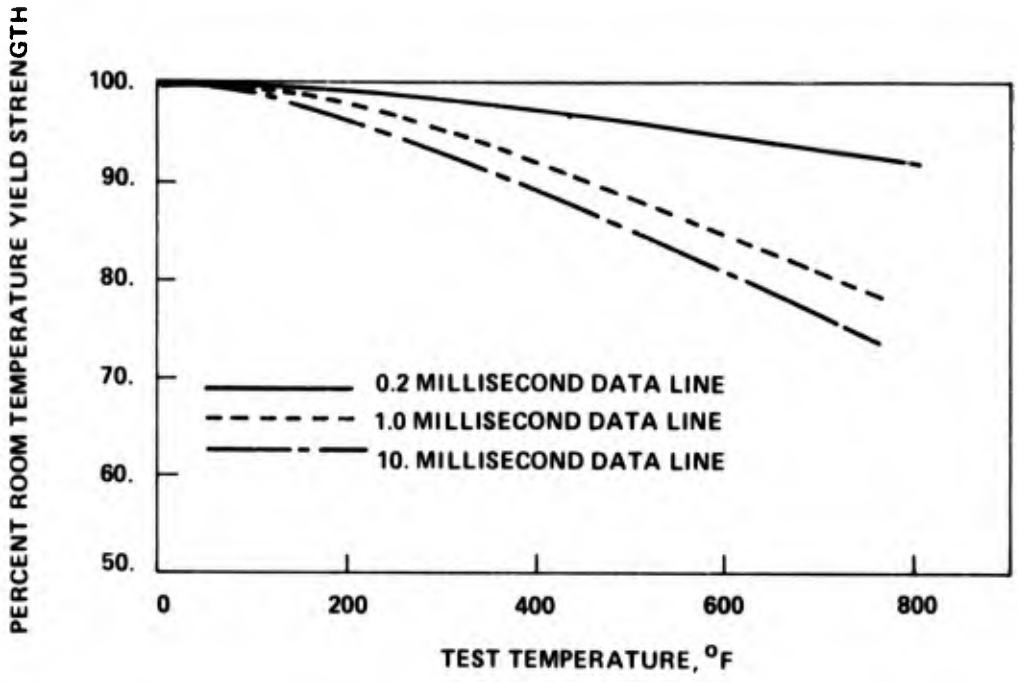

FIG. A-4 RESIDUAL YIELD STRENGTH OF ALUMINUM ALLOY 6061-T6 AFTER MILLISECOND PULSE HEATING

evident in the data. However, there was a discrepancy between these measurements made at Physics International and some of the handbook values for modulus as a function of temperature. Hence a subsequent measurement of elastic and shear moduli was made by the Sandia Corp. at time at temperature varying from several minutes to 3 hours. The results of these tests were reported[69] and are given in Figure A-5. The experiments resulting in the data shown in Figures A-4 and A-5 lead to the following 3 conclusions: (1) The measured values of elastic and shear modulus made independently by Sandia Corporation and by the Physics International Company are in good agreement; (2) The measured values of modulus are insensitive to time at temperature at elevated temperature; (3) The measured values of shear modulus correlate well with the measurements of yield strength made by Physics International for millisecond time at temperature (compare Figures A-4 and A-5). Since the shear modulus is not influenced by the growth and spacing of precipitates, but the yield strength is, it follows from the correlation of modulus and yield strength in domain two that microstructural changes have not had time to occur. This is the explanation for the relative insensitivity of yield strength on time at temperature in this domain. The reason that time at temperature in domaine one cause microstructural changes while those in domain two do not, lies in the thermal expansion of the material.

[69] Lipkin, Sandia Lab. SC-RR-72 0020 Op. Cit.

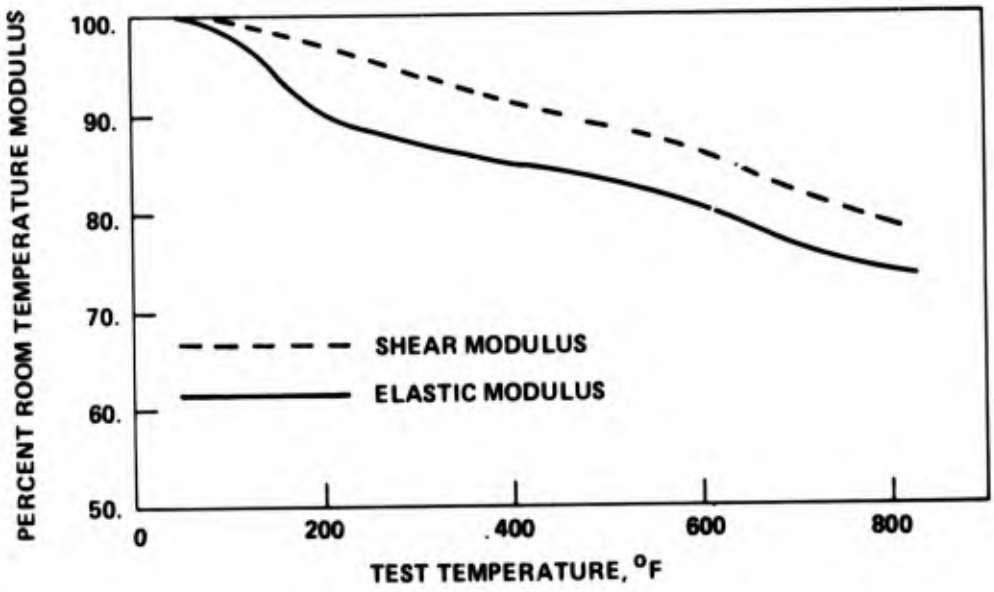

FIG. A-5 ELASTIC AND SHEAR MODULUS OF ALUMINUM ALLOY 6061-T6 AT ELEVATED TEMPERATURES

The samples pulse heated in times at temperature of domain one could not expand proportional to the expansion demanded by their rapid temperature rise hence a high rate of strain was induced in the alloy. In domain two, the heating is slow enough to permit expansion and no strain-induced microstructure changes occur.

The Sandia Corporation also conducted a series of tests to determine the maximum time at temperature that an elevated temperature point, 500°F, will be in domain two. This is the maximum time at 500°F before diffusion-controlled microstructural changes will begin. The tests consisted of immersing samples for various short times in a 500°F salt bath. These samples were subsequently tensile tested at room temperature. By extrapolating the data, it was concluded that the aluminum alloy 6061-T6 tested would not have lost any of its room temperature tensile strength for time at temperature less than 3 seconds. That is, if aluminum alloy 6061-T6 is held at 500°F for less than 3 seconds, no microstructural changes have time to occur and the alloy retains its original tensile strength upon returning to room temperature. Of course, the yield strength while the material is at 500°F is reduced proportional to the shear modulus shown in Figure A-5 since the alloy is in domain two.

Relatively high strain rates, approximately 500 in/in/second were reported for the tensile tests producing data in the second time at temperature domain. These rates are necessary because measurements

must be made very rapidly during the very short time at temperature. Data from these tests will apply to nuclear weapon blast damage because of expected high strain rates in structures loaded by the airblast pressure pulse.

The third time at temperature domain is that of all time greater than the few seconds terminating domain two. Standard tensile test results are available for many aluminum alloys and time at temperature of 1/2 hour to 1000 hours or more.[70] The results of such tests for aluminum alloy 2014-T6 were shown in Figure A-2. This data shows the characteristic decrease in strength of all aluminum alloys as time at temperature is increased at elevated temperatures. The mechanical strength in domain three is governed by the diffusion-controlled growth of precipitate particles. Hence, the aluminum alloys get progressively weaker as particles grow larger and dislocation movement becomes easier as time at temperature increases.

The tensile strength data shown in Figures A-2 and A-4 was taken at elevated temperatures immediately after the test specimens had been heated. A series of tests were conducted on three aluminum alloys to measure both the tensile strength at elevated temperature and the strength after the heated specimen return to room temperature. The test consisted of heating the alloy to a maximum temperature in approximately four seconds, allowing the samples to cool to room temperature, then repeating the thermal cycling up to 10 times. Ultimate tensile strength at elevated temperature was determined by preloading the test specimens with estimated failure loads. The results of these tests are reported in the references.[71] Data obtained for one aluminum alloy, 2024-T851, are shown in Figure A-6.

The specimens in these tests remained above the artificial aging temperature of approximately 350°F for 10 seconds or more during the heating cycle which lasted for 25 seconds or more. Hence, overaging and permanent microstructural changes are expected to occur. This is verified by noting the (permanent) loss in strength shown in Figure A-6 when measurements are made at room temperature. The large drop in strength when measurements are made at peak temperature shows that elevated temperature acts to weaken the crystal structure and thus reduce strength. This would be the only effect reducing strength if the alloy were in domain two but it combines with the effect of overaging to reduce strength for these alloys which are in domain three. These tests showed a similar result for the two other aluminum alloys tested, 2219-T851 and 7075-T7651.[72]

Aluminum alloys can be strain hardened by the application of a plastically deforming load and the increased strength due to strain

---

[70] Voorhees, ASTM Spec. Tech. Pub. No. 291, Op. Cit.

[71] Ferguson, R.R., "Effect of Nuclear Flash Heating on the Strength of Aluminum Alloys (B-1 Design)," North American Rockwell TFD-72-984 serial No. 28, Dec 1972.

[72] Ibid

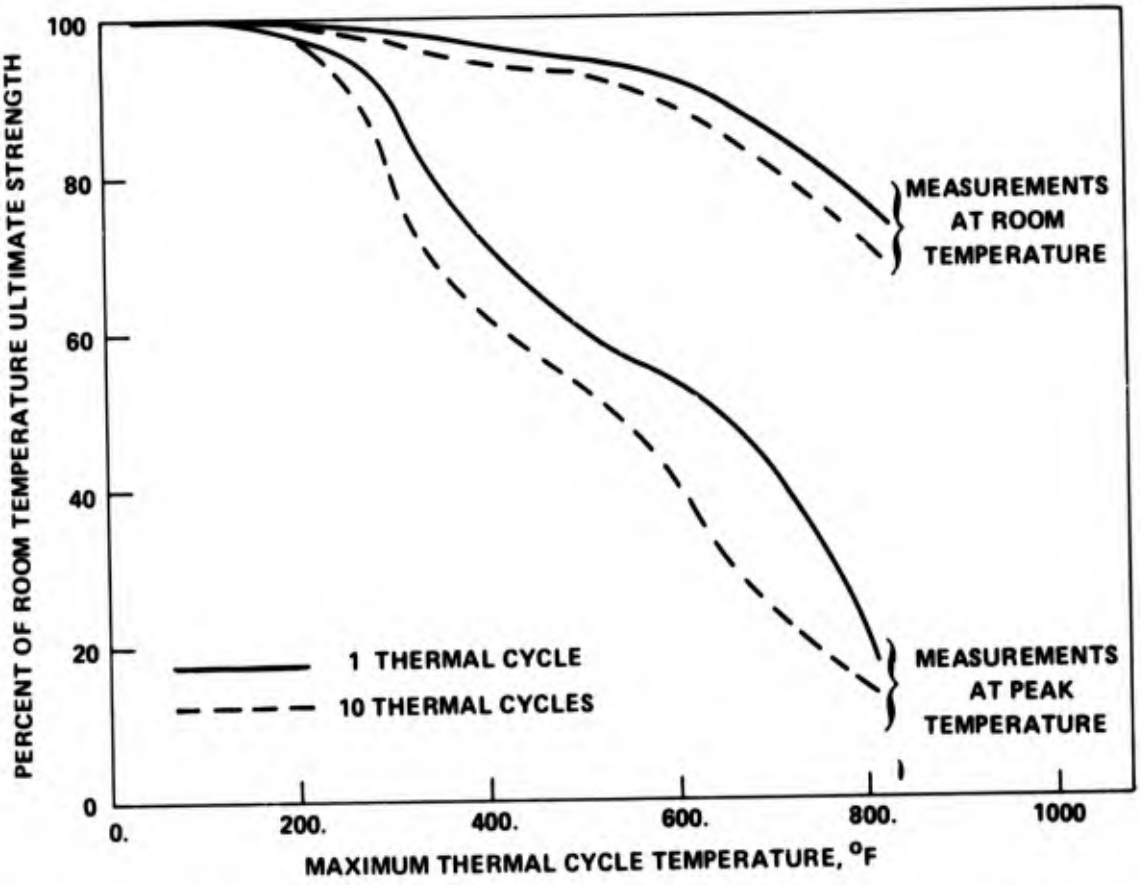

FIG. A-6 ULTIMATE STRENGTH OF ALUMINUM ALLOY 2024-T851 DURING AND AFTER CYCLIC HEATING

hardening depends on the strain rate at which the alloy is deformed. The results of a study to determine the ultimate tensile strength of aluminum alloy 6061-T6 for increasing strain rate are given in the references[73] and are shown in Figure A-7.

The data in Figure A-7 was normalized by the room temperature (75°F) ultimate strength (43,800 psi) at the lowest strain rate tested (1×10^{-5} in/in/second). The tensile tests of this study were made after holding the test specimens at test temperature for a period of five minutes. Hence, these data are for time at temperature domain three and weakening microstructural changes have occurred before testing. The data shows that strength is decreased by temperature and overaging effects but also strength is increased by strain hardening as the strain rate increases. Furthermore, the strain hardening strength increase is seen to approach a constant

[73] Hoge, K.G., "Influence of Strain Rate on Mechanical Properties of 6061-T6 Aluminum Under Uniaxial and Biaxial States of Stress," Experimental Mechanics, pg. 204-211, Apr 1966.

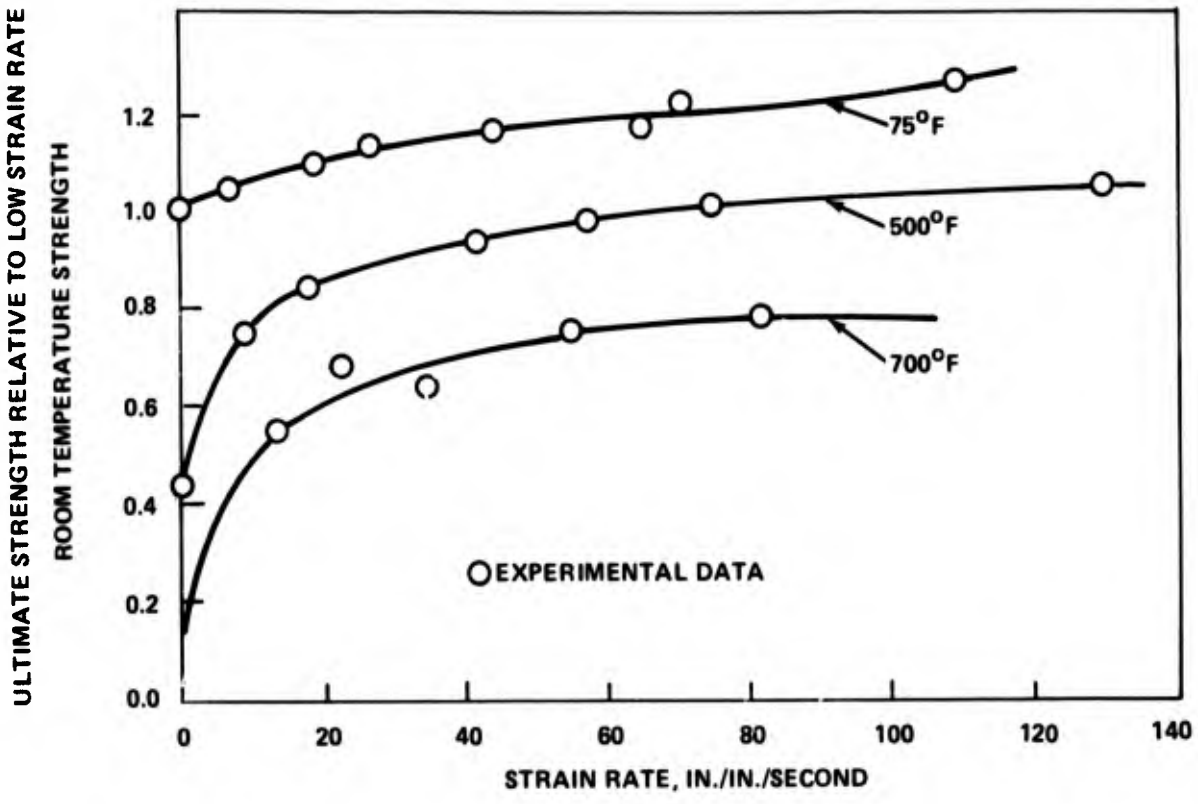

FIG. A-7 EFFECT OF STRAIN RATE ON ULTIMATE STRENGTH OF ALUMINUM ALLOY 6061-T6

value dependent on temperature for strain rates greater than about 50 in/in/second. A previously discussed study[74] also studied the effects of strain rate on strength for aluminum alloys 2014-T6, 2024-T3 and 7075-T6. These tests also show increases in strength due to strain hardening for increasing strain rates between .00005 and 1.0 in/in/second. This data corresponds to time at temperature greater than 10 seconds and temperatures of 300°F, 450°F and 600°F. The results of these studies show that the strength of aluminum alloys is increased by increases in the rate of load application, i.e. strain rate, for low strain rates and time at temperatures in domain three. The effect of strain rate on strength for time at temperature domain two is not clear although the strain rates must be high so that the loading is applied fast enough for the alloy to be in domain two.

The data reviews in this appendix indicated that complex changes effecting mechanical strength occur in aluminum alloys upon being

[74] Dotson, WADC Tech. Rep. 55-199, Op. Cit.

heated to relatively high temperature. Data does not exist for aluminum alloys heated by a simulated nuclear weapon thermal pulse to elevated temperature and held there for a time period equal to the blast arrival time of the weapons blast wave. Hence, it is necessary to make predictions based upon the limited amount of data that does exist for various aluminum alloys held at elevated temp-ratures for short times. There are several elements to be considered when making an extrapolation of existing data to a nuclear weapon effect case. One consideration is the time at temperature for which an aluminum structure remains at an elevated temperature before blast arrival. If this time is very short, i.e. less than a few seconds, the aluminum alloy will be in domain two and it can be assumed that tensile strength at temperature is proportional to the shear modulus. If this time is greater than a few seconds the alloy will be in domain three. Here, a significant decrease of tensile strength with increased temperature occurs and existing data for 10 second holding time or for moderately rapid temperature rise should be used as a guide. Another consideration is the temperature history of the structure at blast arrival. If this temperature has dropped significantly from a higher value, then the data shown in Figure A-6 for room temperature might be used for reference. The last consideration is the strain rate induced by the deforming blast load. Since this is expected to be relatively large, the existing data for time at temperature domain two would be the most appropriate. If data for time at temperature domain three at a low strain rate is used, it will give a conservative result as shown by Figure A-7. This may be increased to account for a higher strain rate or used as is to keep the results within safe limits.

APPENDIX B

METHODS AND EQUATIONS FOR COMPUTING BLAST-THERMAL STRESSES IN SIMPLE ELEMENTS

The calculation of elastic stresses and displacements in structures which are subjected to the nonuniform heating and blast provided by a nuclear weapon explosion is a very complicated problem. Both the stress and thermal equations describing the action of the thermal and pressure pulses on the structure are in general nonlinear partial differential equations. Thus, closed form solutions for either the stress or temperature acting alone will exist for only a mathematical model which includes simplifying assumptions and/or an idealized geometry. Because of the mathematical difficulties involved, numerical analysis is usually resorted to as an aid in solving these problems. Furthermore, the temperature and stress equations are in fact coupled. That is, the stress equations are effected directly because of thermal expansion and indirectly through the temperature dependence of the elastic constants. The heat conduction equation which governs temperature is likewise effected by compressive heating caused by the straining in the body. Because of the difficulties in obtaining a general solution for blast-thermal effects in structures, the first problem in computing these effects is in determining the necessary simplifying assumptions to make in building a mathematical model to represent the structural element being analyzed. Simplifying assumptions were made for the simple elements analyzed herein and mathematical analysis including computer programs was derived. This appendix will outline these assumptions and state the resulting equations. The details of the derivation of these equations and their associated computer programs are given in the references. Results computed from the programs are given in the main body of this report.

A principal assumption will be made in all cases to uncouple the stress and temperature problems. It is assumed that the temperatures are uneffected by stresses and strains hence the temperature distribution history can be computed separately and used in subsequent stress computations. It will be initially assumed that elastic constants are independent of temperature. However an estimate of the effect of varying elastic constants was given in the main body of this report. The thermophysical properties will also be assumed constant in all cases. An assumption that can sometimes be made in stress calculations is that the loading is quasi-static. That is, if the thermal and mechanical loadings are applied slowly enough, the effects of inertia within the body may be neglected. This allows the

time derivative terms to be dropped from the governing equation and the calculations are considerably simplified. Since the nuclear weapon blast pressure pulse is applied rapidly, the quasi-static assumption does not usually hold in blast problems, hence both the dynamic and quasi-static socutions will be given. However, the quasi-static assumption does hold in many cases for thermal stresses developed by the nuclear weapon thermal pulse. The equations given in this appendix are valid for quite general thermal or pressure pulses. The thermal and pressure pulses for a nuclear weapon explosion are given in the main body o. this report. It is these which are incorporated into the computer programs to calculate weapon effects.

1. Rectangular Plate Simply Supported on All Edges

The classical assumptions for bending stresses in a thin plate are made for this simple element. These assumptions are,

(1) Perpendiculars to the median plane in the thickness direction before deformation remain perpendicular after deformation, i.e., the shearing strains are zero at the median plane.

(2) The normal stresses in the thickness direction are negligible ($\sigma_z = 0$).

(3) The bending stresses are zero on the median plane ($z = L/2$).

A thin plate assumption implies that the deflections resulting from thermal or mechanical loading should be less than the thickness of the plate. It is further assumed that the plate is uniformly heated and pressured by the thermal and pressure pulses. Hence temperature is a function of time and the thickness direction (z) only and pressure is a function of time alone. Under the above assumptions, the following partial differential equation was derived[75] to describe the effect of a thermal-blast interaction in a rectangular plate.

$$D\nabla^4 w + \rho \cdot L \cdot \frac{\partial^2 w}{\partial t^2} = P - \frac{1}{1-\mu} \nabla^2 Mt \qquad \text{(B-1)}$$

Here, D is the structural rigidity ($D = EL^3/12(1-\mu^2)$) and Mt is the thermal moment due to the temperature gradient through the plate. i.e.,

$$Mt = a \cdot E \cdot \int_{-L/2}^{L/2} T \cdot Z \cdot dZ \qquad \text{(B-2)}$$

75 Koch, J.E., and Koplik,B., "Equations to Determine Displacements and Stresses in Certain Structural Elements When Exposed to the Thermal and Blast Effects of a Nuclear Event," N. Eastern Research Associates No. RR-NA-9, Dec 1969.

where a is the coefficient of thermal expansion and E is Young's Modulus. The values of temperature, T, as a function of time and thickness are found independently using the methods previously given in this report.

The quasi-static solution results by assuming that the time dependent term, $\frac{\partial^2 w}{\partial t^2}$, is negligible in equation (B-1). The resulting governing partial differential equation is,

$$D\nabla^4 w = p - \frac{1}{1-\mu}\nabla^2 Mt \qquad \text{(B-3)}$$

The boundary conditions for a simply supported plate are,

$$w = 0$$

$$D\nabla^2 w + \frac{Mt}{1-\mu} = 0 \qquad \text{(B-4)}$$

on all boundary edges of the plate. The equations (B-3) and (B-4) are linear hence the thermal and mechanical loadings can be considered separately and the principle of superposition used to combine the solutions. For the thermal loading acting along, p = 0 and equations (B-3) and (B-4) can be solved for the thermal displacement, w_{th}. The following solution was obtained[76] with the aid of Fourier Analysis.

$$w_{th} = \frac{16\ Mt}{(1-\mu)D\pi^4} \sum_{m=1,3,odd}^{\infty} \sum_{n=1,3,odd}^{\infty} \frac{\sin\frac{m\pi x}{a_1} \cdot \sin\frac{n\pi y}{b_1}}{m\cdot n\cdot\left[\left(\frac{m}{a_1}\right)^2 + \left(\frac{n}{b_1}\right)^2\right]} \qquad \text{(B-5)}$$

In equation (B-5), a_1 and b_1 are the length and width of the plate. For the mechanical loading acting alone, Mt=0 and equations (B-3) and (B-4) can be solved for the mechanical displacement, Wp. Here, Fourier Analysis was also used to obtain the following solution.[77]

$$W_p = \frac{16\ P}{D\pi^6} \sum_{m=1,3,odd}^{\infty} \sum_{n=1,3,odd}^{\infty} \frac{\sin\frac{m\pi x}{a_1} \sin\frac{n\pi y}{b_1}}{m\cdot n\cdot\left[\left(\frac{m}{a_1}\right)^2 + \left(\frac{n}{b_1}\right)^2\right]^2} \qquad \text{(B-6)}$$

[76] Koch, North Eastern Res. Assoc. No.-RR-NA-13, Op. Cit.
[77] Koch and Koplik, North Eastern Res. Assoc. No. -RR-NA-9, Op. Cit.

Hence for the synergistic problem of blast and thermal occurring simultaneously,

$$W - W_{th} + W_p \tag{B-7}$$

The plate stresses can be calculated by differentiating equation (B-7) and using the result in the following general relationships.

$$\sigma_x = - \frac{E\,Z}{1-\mu^2}\left[\frac{\partial^2 W}{\partial_x^2} + \mu \frac{\partial^2 W}{\partial_y^2}\right] + \frac{Nt}{L(1-\mu)} - \frac{a \cdot E \cdot T}{1-\mu}$$

$$\sigma_y = - \frac{E \cdot Z}{1-\mu^2}\left[\frac{\partial^2 W}{\partial_y^2} + \mu \frac{\partial^2 W}{\partial_x^2}\right] + \frac{Nt}{L(1-\mu)} - \frac{a \cdot E \cdot T}{1-\mu} \tag{B-8}$$

$$\tau_{xy} = - \frac{E \cdot Z}{1+\mu} \frac{\partial^2 W}{\partial_x \partial_y}$$

Where Nt is the edge force due to the thermal gradient through the plate, i.e.,

$$Nt = a \cdot E \cdot \int_{-L/2}^{L/2} T \cdot dZ \tag{B-9}$$

The principal stresses can be computed from the stresses given in equation (B-8) as follows,

$$\sigma_p = \frac{\sigma_x + \sigma_y}{2} \pm \sqrt{\left(\frac{\sigma_x - \sigma_y}{2}\right)^2 + \tau_{xy}^2} \tag{B-10}$$

The dynamic solution results by solving equation (B-1) subject to the boundary conditions for a simply supported plate given in equation (B-4). This solution results by using an infinite series expansion and integral transformation techniques. In this case a multiple finite Fourier sine transformation was employed. The details of arriving at the following results are given in the references.[78]

[78] Koch and Koplik, North Eastern Res. Assoc. No. RR-NA-9, Op. Cit.

(1) The natural frequencies of a free vibration are,

$$\omega_{mn} = \left[\left(\frac{n\pi}{a_1}\right)^2 + \left(\frac{m\pi}{b_1}\right)^2 \right] \sqrt{\frac{D}{\rho \cdot L}} \qquad \text{(B-11)}$$

(2) The Fourier transformed frequency, ωss, is given by a convolution (Faltung) integral, i.e.,

$$\omega ss = \frac{4}{\omega_{mn} \rho \cdot L \cdot \left(\frac{n\pi}{a_1}\right)\left(\frac{m\pi}{b_1}\right)} \int_0^t \left[P(\varepsilon) + \frac{Mt(\varepsilon)}{1-\mu} \left(\left[\frac{n\pi}{a_1}\right]^2 + \left[\frac{m\pi}{b_1}\right]^2 \right) \right] \cdot \sin \omega_{mn}(t-\varepsilon) \cdot d\varepsilon \qquad \text{(B-12)}$$

(3) The resulting dynamic displacement is,

$$w = \frac{4}{a_1 \cdot b_1} \sum_{n=1,3,odd}^{\infty} \sum_{m=1,3,odd}^{\infty} \omega ss \cdot \sin\left(\frac{n\pi x}{a_1}\right) \cdot \sin\left(\frac{n\pi y}{b_1}\right) \qquad \text{(B-13)}$$

The dynamic displacement at any time is found by solving equations (B-11) and (B-12) in turn given the thermal and mechanical loads, Mt(ε) and P(ε) up to that time. The corresponding plate stress is calculated by substituting the computed displacements into the stress-displacement equations (equations (B-8) and B-10)).

Although the dynamic solution for a simply supported rectangular plate has been given in integral form, it still remains a difficult task to obtain numerical answers to problems. This work is alleviated by using numerical methods in solving the above equations. Thus, the temperature and pressure are given at a number of discrete points in time and it is assumed that values between these points can be found by linear interpolation. Then, the convolution integral, equation (B-12), can be integrated in sections corresponding to the piecewise linear pressure and temperature loads. The computed value of this integral is then used directly in equation (B-13) to find the dynamic displacement, and after double differentiation, in equation (B-8) to compute the dynamic stresses. A computer program to perform these computations for the temperature and pressure pulses of a nuclear weapon explosion is described in the references.[79]

[79] Koch, J.E., "Equations and Computer Programs to Determine the Displacements and Stresses in Certain Structural Elements When Exposed to the Thermal and Blast Effects of a Nuclear Event," North Eastern Research Associates No. RR-NA-11, Feb. 1970.

2. Rectangular Plate, Simply Supported or Clamped, and Prestressed by A Thermal or Mechanical Load

An alternative approach to computing stresses in a rectangular plate is to solve the governing partial differential equation by numerical methods based on the use of finite differences. This approach will be outlined in solving the problem of blast stresses in a thin rectangular plate where an initial thermal and/or mechanical load may also be specified. Thus, the thermal problem in this approach is reduced to merely specifying an initial temperature level to which the plate has been heated above its thermal stress-free temperature. The initial elevated temperature then produces a compressive force in the plane of the plate since the edges are not free to move axially. For a uniformly heated plate without temperature gradients, this force per unit width is given by,

$$F = \frac{a \cdot E \cdot L \cdot T}{1-\mu} \tag{B-14}$$

The force, F, due to constraining the plate against axial movement was not developed in the previous plate analysis where the edges were not constrained against axial movement. However, the present analysis does not allow for thermal stresses that are developed by a thermal gradient in the thickness direction of the plate. (In the previous analysis, this gradient caused a thermal moment, given by equation (B-2), and a thermal edge force, given by equation (B-9) to be developed.) Since the blast usually arrives significantly later than the time of maximum thermal gradient for nuclear weapon effects problems, this limitation may not be important in studying blast-thermal effects. For example, Figure 13 shows that thermal gradients may become very much reduced with time. The following partial differential equation for the prestressed rectangular plate is taken from the references.[80]

$$D \cdot \nabla^4 W - (Fx-F) \frac{\partial^2 W}{\partial x^2} - (Fy-F) \frac{\partial^2 W}{\partial y^2} + \rho \cdot L \cdot \frac{\partial^2 w}{\partial t^2} = P \tag{B-15}$$

Here, Fx and Fy are the initial inplane tension forces per unit width in the x and y directions, respectively. The solution of equation (B-15) is accomplished starting with expressing all its terms in finite differences. By symmetry, only 1/4 of the plate was required for analysis. This region was divided into 16 nodal points and a finite difference equation derived for each nocal point. The resulting system of equations was solved for two edge boundary conditions. (1) A simple support, technically a hinged end, where the displacement

---

[80] Cost and Griffin, U. S. Army Missile Command Tech. Report RL-72-18, Op. Cit.

and moment of forces vanish on the boundary, i.e. $W = \frac{\partial^2 W}{\partial x^2} = \frac{\partial^2 W}{\partial y^2} = 0$. The simple support of this problem differs from that of the previous problem in that here the ends are constrained against axial movement. (2) A clamped, technically a built-in end, where the displacement and its slope are zero on the boundary, i.e., $W = \frac{\partial W}{\partial x} = \frac{\partial W}{\partial y} = 0$. The resulting system of finite difference equations was solved by a modal superposition technique. That is, the mode shapes and natural frequencies are computed for a free vibration and these are used to construct a modal matrix. The displacement is then assumed to consist of the product of the modal matrix and generalized coordinates, η. The generalized coordinates are found by substituting the assumed solution into the original system of equations, i.e., allowing for the presence of the uniform pressure on the plate. Since a diagonal matrix is produced by matrix manipulation, an integral solution for the generalized coordinates exists. This solution is valid for any uniform pressure loading. However, a simpler but approximate method has been devised to obtain generalized coordinates for the nuclear weapon blast pressure pulse. An upper bound of the displacement is estimated on the basis that all modal contributions reach a maximum value at the same time. The generalized coordinates can then be estimated by integrating the general solution for a single degree of freedom, mass-spring-dashpot oscillator subject to a time-varying force. The force in this case is the following exponential function which approximates the nuclear weapon blast pressure which is given in equation (20)

$$P = P_{max}\, e^{-2.386t/PDUR} \qquad \text{(B-16)}$$

The generalized coordinates are found by integrating the general solution for the single degree of freedom system. They are computed by maximizing the following expression for time greater than zero.

$$\eta_i = \left\{ \frac{P_{max}}{M_i \omega_i} \; \frac{\frac{2.386}{PDUR} \sin \omega_i t - \omega_i \cos \omega_i t + \omega_i e^{-2.386 \cdot t/PDUR}}{\left(\frac{2.386}{PDUR}\right)^2 + \omega_i^2} \right\} \qquad \text{(B-17)}$$

In equation (B-17), M_i are the coordinates of the generalized mass matrix and ω_i are the natural frequencies of (free) vibration. The displacement of the rectangular plate is found by computing the modal matrix for a free vibration and the generalized coordinates by equation (B-17). The details of making these calculations and a computer program to perform them are described in the previous reference.[81] Here, it is claimed that the upper bound of displacement computed is within 15 percent of the exact solution for many cases when a comparison was made. An examination of equation (B-17)

[81] Ibid

shows that the generalized coordinates are increasingly independent of the positive phase duration for natural frequencies above about 10 cycles/second.

Equation (B-11) shows that the natural frequencies are directly proportional to the plate thickness, L, and inversely proportional to the plate length and width, a_1 and b_1. Thus if a plate is sufficiently thick or short its natural frequencies will be high enough that the peak dynamic response is independent of the positive phase duration. In this case, the plate responds only to the maximum pressure of the blast, i.e., to the peak overpressure or peak reflected pressure. This is the case for many ship structures or systems which are threatened by a nuclear weapons air blast. That is, although these structures must be relatively thin to be threatened their natural frequencies of vibration are usually high enough to insure a dynamic response.

The stresses are calculated from equations (B-8) but omitting the terms involving Nt and using finite differences for the derivatives of displacement. The two above analyses for a simply supported rectangular plate have important differences in boundary conditions. In the second analysis the plate is uniformly preheated above its no stress temperature causing a compressive force to be developed (see equation B-14). This force develops because the plate is not free to move in an x or y direction against its boundaries. In the first analysis, no such force is developed in uniformly heating the plate because this plate is free to move outward to relieve this force.

When the in-plane compressive thermal force is allowed, the possibility exists that the plate will buckle. The force required to buckle a rectangular plat plate with various edge restraints is given by the following equation.

$$Ncr = \frac{\pi^2 \cdot D \cdot Kb}{(ab)^2} \qquad \text{(B-18)}$$

In equation (B-18), Kb is the buckling coefficient which depends on edge conditions and ab is the shortest of the plate edges, a_1 or b_1. The buckling coefficient for various boundary conditions is given in the references.[82] If equation (B-14) for the thermal force is set equal to equation (B-18) for the buckling force, the temperature rise which causes buckling will be obtained. This is,

$$Tb = \frac{\pi^2 \cdot Kb \cdot L^2}{12(1+\mu) \cdot a \cdot (ab)^2} \qquad \text{(B-19)}$$

An examination of equation (B-20) shows that the buckling temperature for aluminum is very low for thin structures. For example, the

---

[82] Cost and Griffin, U.S. Army Missile Command Tech. Rep. RL 72-18, Op. Cit.

buckling coefficient for a simply supported plate is about 4.5 and the coefficient of expansion and Poisson's ratio are about $1.9 \times 10^{-5} C^{-1}$ and 0.333, respectively. Hence, the temperature rise to cause buckling of a 1/8 inch thick plate, 12 inches long, computed from equation (B-19), is only 16°C. Although this plate buckles when heated only 16°C above its zero stress condition, this does not necessarily mean the plate has lost all of its load bearing capability.

3. Circular Plate Simply Supported on Its Boundary

The analysis leading to the quasi-static and dynamic response predictions for a rectangular plate, equations (B-1) to (B-13), was repeated for a circular plate. Equation (B-1) in cylindrical coordinates was integrated for the simply supported boundary condition and expressions were derived for the quasi-static and dynamic stress and displacement. The details of this derivation and the resulting equations are given in the references.[83] A computer program was written to compute these displacements and stresses in circular plates subjected to the thermal and pressure pulses of a nuclear weapon explosion. This program is also given in the references.[84] Here it was also indicated that results for a circular and rectangular plate of similar dimensions are also similar in magnitude. Hence, there are no features of a circular plate solution which are not present in the rectangular plate results.

4. Beams on Three Types of Support

Equations will be given to determine the quasi-static or dynamic displacement or stress for a beam subjected to a spacially uniform but time dependent pressure and a time dependent temperature which is uniform along its length but varies with depth. In addition to a simply supported edge condition, a cantilever beam and a beam with both ends clamped will be analyzed. The classical assumptions for bending stresses in a thin plate will also be made here with the additional assumption that the normal stress in the width direction is also negligible ($\sigma y \cong 0$), i.e. the beam is assumed to be narrow. Under these assumptions, the classical thermo-elastic equation for a beam of constant cross sectional area is given[85] as follows:

$$E \cdot I \frac{\partial^4 w}{\partial x^4} + \rho Ac \frac{\partial^2 w}{\partial t^2} = P \cdot B - \frac{\partial^2 Mt}{\partial x^2} \qquad \text{(B-20)}$$

In equation (B-20), I is the moment of inertia and Ac is the cross sectional area of the beam. Note that equation (B-20) is considerably simpler than equation (B-1) for the rectangular plate. The primary simplification resulted because the displacement is now a function of

[83] Koch and Koplik, N. Eastern Res. Assoc. No. RR-NA-9, Op. Cit.
[84] Koch, North Eastern Res. Assoc. No. RR-NA-11, Op. Cit.
[85] Koch and Koplik, N. Eastern Res. Assoc. No. RR-NA-9, Op. Cit.

only one coordinate, x, instead of both x and y. The following three types of boundary conditions will be considered for the beam.

(1) Both ends simply supported.
On each end, x=0 and x=B

$$W = 0$$

$$E \cdot I \cdot \frac{\partial^2 W}{\partial x^2} - Mt = 0 \qquad \text{(B-21)}$$

(2) The cantilever beam
On the supported end, x = B.

$$W = 0$$

$$\frac{\partial W}{\partial x} = 0$$

On the free end, x = 0.

$$-E \cdot I \cdot \frac{\partial^2 W}{\partial x^2} - Mt = 0 \qquad \text{(B-23)}$$

$$-E \cdot I \cdot \frac{\partial^3 W}{\partial x^3} - \frac{\partial Mt}{\partial x} = 0$$

(3) Both ends clamped
On each end, x=0 and x=B.

$$W = 0$$

$$\frac{\partial W}{\partial x} = 0 \qquad \text{(B-24)}$$

The quasi-static solution results by assuming that the loads are applied slowly such that the time dependent term, $\frac{\partial^2 W}{\partial t^2}$, is negligible. Also, for a uniformly applied thermal load, the thermal moment, Mt, will not vary in the x direction. Hence the beam equation for the quasi-static case reduces to,

$$\frac{d^4 W}{dx^4} = \frac{P \cdot B}{E \cdot I} \qquad \text{(B-25)}$$

Equation (B-25) can be easily integrated with the constants of integration easily evaluated for each of the above 3 boundary conditions. The beam stress can be calculated by using the displacement result in

the following general result for thin narrow beams.

$$\sigma x = -EZ \frac{\partial^2 W}{\partial x^2} + \frac{Nt}{Ac} - a \cdot E \cdot T \qquad \text{(B-26)}$$

The result of solving equations (B-25) and (B-26) for the quasi-static displacement and stress for beams on three types of support is given in the following equations.

(1) Both ends simply supported

$$W = \frac{P \cdot X}{24E \cdot I} (x^3 - 2 \cdot B \cdot X^2 + B^3) + \frac{Mt \cdot X}{2E \cdot I} (B-X) \qquad \text{(B-27)}$$

$$\sigma x = \frac{P}{2 \cdot I} X (B-X) Z + \frac{Mt \cdot Z}{I} + \frac{Nt}{Ac} - \alpha \cdot E \cdot T$$

(2) The cantilever beam

$$W = \frac{PX^2}{24E \cdot I} (x^2 - 4XB + 6B^2) - \frac{Mt \cdot x}{2E \cdot I} (B-X) \qquad \text{(B-28)}$$

$$\sigma x = \frac{P}{2 \cdot I} X (B-X) Z + \frac{Mt \cdot z}{I} + \frac{Nt}{Ac} - \alpha \cdot E \cdot T$$

(3) Both ends clamped

$$W = \frac{PX^2}{24E \cdot I} (B-X)^2 \qquad \text{(B-29)}$$

$$\sigma x = \frac{P}{12 \cdot I} (6X^2 - 6X \cdot B + B^2) Z + \frac{Nt}{Ac} - \alpha \cdot E \cdot T$$

The dynamic solution for the displacement of a beam of constant cross-sectional area and a uniform thermal load over its length requires the solution of the following partial differential equation.

$$E \cdot I \frac{\partial^4 W}{\partial X^2} + \rho \cdot Ac \cdot \frac{\partial^2 W}{\partial t^2} = P \qquad \text{(B-30)}$$

Equation (B-30) will be solved using the modal series solution technique where the modes are the individual modes of a free vibration. The assumed form of this solution is,

$$W = \sum_{n=1}^{\infty} Wn(x) \cdot Tn(t) + \sum_{i-1}^{4} gi(x) \cdot fi(t) \qquad \text{(B-31)}$$

In equation (B-31), Wn are the engenfunctions of the homogeneous form of equation (B-31), i.e., of the free vibration problem. Tn are found by substituting the assumed solution, equation (B-31) into the original equation, equation (B-30). The gi functions are chosen to satisfy the inhomogeneous boundary conditions while the fi functions represent the time dependency of the inhomogeneous conditions.

The homogeneous solution of equation (B-30) is easily accomplished by assuming a solution of the form $w = Wn\, e^{i\omega t}$ where ω is the natural circular frequency. The following solutions for the homogeneous eigenfunctions are derived[86] for each of the three beam supports. Note that the boundary conditions for the homogeneous problem are given by equations (B-21) - (B-24) but with terms involving the thermal moment, Mt, equal to zero. The natural circular frequencies are found from the eignevalues, λn, of the homogeneous solution through the following relationship.

$$\omega n = \lambda n^2 \sqrt{\frac{EI}{\rho Ac}} \tag{B-32}$$

(1) Both ends simply supported

$$\lambda n = \frac{n \cdot \pi}{B} \tag{B-33}$$

$$Wn = \sin \lambda n \cdot x$$

(2) Cantilever beam

λn are the roots of the equation,

$$1 + \cos(\lambda n \cdot B) \cdot \cosh(\lambda n \cdot B) = 0 \quad \text{and}$$

$$Wn = \frac{\sin(\lambda n \cdot x) - \sinh(\lambda n \cdot x)}{\sin(\lambda n \cdot B) + \sinh(\lambda n \cdot B)} - \frac{\cos(\lambda n \cdot x) - \cosh(\lambda n \cdot x)}{\cos(\lambda n \cdot B) + \cosh(\lambda n \cdot B)} \tag{B-34}$$

(3) Both ends clamped

λn are the roots of the equation

$$1 - \cos(\lambda n \cdot B) \cdot \cosh(\lambda n \cdot B) = 0 \quad \text{and} \tag{B-35}$$

$$Wn = \frac{\sin(\lambda n \cdot x) - \sinh(\lambda n \cdot x)}{\sin(\lambda n \cdot B) \sinh(\lambda n \cdot B)} - \frac{\cos(\lambda n \cdot x) - \cosh(\lambda n \cdot x)}{\cos(\lambda n \cdot B) - \cosh(\lambda n \cdot B)}$$

[86] Koch and Koplik, N. Eastern Res. Assoc. No. RR-NA-9, Op. Cit.

The inhomogeneous solution proceeds using the assumed form of the solution, equation (B-31), to solve the governing equation, equation (B-30). By using the initial conditions, $w = \frac{\partial w}{\partial x} = 0$ for all x, and the fact that the modes of the free vibration are orthogonal, the following result is derived in the previous reference[87] for the functions, Tn.

$$Tn = \frac{Kn}{E \cdot I \cdot In}\left[Mt(o)\cos \omega nt + \frac{\dot{Mt}(o)}{\omega n}\sin \omega nt + \frac{1}{\omega n}\int_o^t \ddot{Mt}(\varepsilon)\sin \omega n(t-\varepsilon)\,d\varepsilon\right]$$

$$+ \frac{Jn}{\rho Ac \cdot \omega n \cdot In}\int_o^t P(\varepsilon)\cdot \sin \omega n(t-\varepsilon)\,d\varepsilon \qquad \text{(B-36)}$$

In the above equation, a dot over a variable denotes a derivative with respect to time. The auxiliary functions, Kn, In, and Jn have the following definitions.

$$In = \int_o^L Wn^2 \cdot dx$$

$$Jn = \int_o^L Wn \cdot dx \qquad \text{(B-37)}$$

$$Kn = \int_o^L g4 \cdot Wn\, dx$$

In equations (B-37), g4 is the fourth of the gi functions which satisfy inhomogeneous boundary conditions. The dynamic solution for each of the three types of support is completed by choosing the functions gi and fi to satisfy the particular boundary conditions of that beam support. The following result was given[88] and only the functions g4 and f4 contribute to the solution.

(1) Both ends simply supported.

$$fy = -\frac{Mt}{E \cdot I}$$

$$g4 = \frac{x}{2}(x-B) \qquad \text{(B-38)}$$

---

87 Ibid
88 Ibid

(2) Cantilever beam

$$f4 = -\frac{Mt}{E \cdot I} \qquad (B\text{-}39)$$

$$g4 = \frac{x^2}{2}$$

(3) Both ends clamped

$$f4 = 0. \qquad (B\text{-}40)$$

$$g4 = 0.$$

and, in addition, Kn is also zero for the clamped ends.

Thus, equation (B-31) with the various functions given by equations (B-32) - (B-40) provides the complete solution for the dynamic displacement for beams on 3 types of supports.

The corresponding beam stress is gotten from the displacement by use of equation (B-26). These equations for computing the static or dynamic displacement or stress have been programmed for solution by a digital computer. These computer programs are listed and described in the references.[89]

5. Constrained or Unconstrained Beam Column

This problem is similar to that of the previous beams in that these beams are also subjected to a uniform time dependent pressure and a time dependent temperature which is uniform along its length but varies depthwise. However, the beam-column will be constrained against movement in its axial (x) direction, or if its ends are free, a prescribed time dependent axial force will be allowed. Displacement and stress equations will be given for the beam-column on the three types of supports previously described. In fact, the derivation of equations for this case will parallel that of the beams previously analyzed.

The describing partial differential equation for the beam column using the previously given assumptions for bending stress in a narrow thin beam of constant cross-sectional area is given in the references[90] as follows.

$$E \cdot I \frac{\partial^4 w}{\partial x^2} - F(t) \frac{\partial^2 w}{\partial x^2} + \rho \cdot Ac \frac{\partial^2 w}{\partial t^2} = P \cdot B - \frac{\partial^2 Mt}{\partial x^2} \qquad (B\text{-}41)$$

---

89 Koch and Koplik, N. Eastern Research Assoc. No. RR-NA-11, Op. Cit.
90 Koch, North Eastern Research Assoc. No. RR-NA-14, Op. Cit.

In Equation (B-41), F(t) is the axial force which may be prescribed or may be due to constraining the ends. Equation (B-41) is similar to equation (B-20) except for the term involving the axial force. Also, the assumption that the thermal load is uniform in the length (x) direction eliminates the term involving the second derivative of thermal moment. Finally, it will be assumed that the time varying axial force, F(t), can be replaced by piecewise constant forces. Therefore, the solution will consist of integrating equation (B-41) for a constant force, F. It will be necessary to resort to numerical methods to include time-varying axial forces. This is accomplished by dividing the total time into subintervals where the axial force remains approximately constant. Then, the computed values of beam displacement and velocity at the end of one subinterval represent the initial values of displacement and velocity for the next subinterval.

If the beam-column is constrained against axial motion of its end points, the resulting force, F(t) must be computed. This is done by applying the boundary condition that the axial displacement, u, is zero at each end. The following equation is given[91] to determine the relative displacement of the ends. F(t) is found for constrained ends by equating the relative displacement to zero.

$$ul-uo = \frac{1}{2}\int_{o}^{L}\left(\frac{\partial w}{\partial x}\right)^2 dX + \frac{Nt - F}{A \cdot E} B \qquad \text{(B-42)}$$

Note that the displacement, W, is required in computing the axial force, F. Hence equation (B-42) must be solved simultaneously with equation (B-41). Also the problem exists of defining subintervals to keep F approximately constant while ul-uo approaches zero. A systematic method of computing displacements for axial forces developed by constrained ends is given in the previous reference.[92]

The boundary conditions given by equations (B-21) - (B-24) will be used for the beam column depending on the type of support. The beam stress is computed from the following equation when an axial force is present.

$$\sigma x = -EZ\frac{\partial^2 W}{\partial x^2} + \frac{Nt - F}{Ac} - \alpha \cdot E \cdot T \qquad \text{(B-43)}$$

The quasi-static integration of equation (B-41) is easily accomplished by treating the axial force F as a constant. The following equations are derived[93] for the three types of edge boundary conditions.

---

91 Ibid
92 Ibid
93 Ibid

(1) Simple support

$$W = -\left(\frac{E\cdot I\cdot P\cdot B}{F^2} + \frac{Mt}{F}\right)\left[\frac{(\cos \beta B-1)\cdot \sin \beta X-\sin \beta B\cos \beta X}{\sin \beta B}\right] - \frac{PBX(B-X)}{2F} \tag{B-44}$$

$$\sigma x = EZ\left[\left(\frac{E\cdot I\cdot P\cdot B}{F^2} + \frac{Mt}{F}\right)\beta^2\ \frac{(\text{Cos } \beta B-1)\sin \beta X-\sin \beta L\cdot\cos \beta X}{\sin \beta B} - \frac{P\cdot B}{F}\right]$$

$$+ \frac{Nt - F}{Ac} - \alpha\cdot E\cdot T$$

where β is equal to $\frac{F}{E\cdot I}$

(2) Cantilever beam

$$W = -\frac{\frac{Mt}{E\cdot I} + \frac{P\cdot B}{F}(1-\beta\cdot B \sin \beta B)}{\beta^2 \cos \beta B}(1-\cos \beta X) - \frac{PB^2}{F\beta}(\beta X-\sin \beta X) + \frac{PBX^2}{2\cdot F} \tag{B-45}$$

$$\sigma_x = E\cdot Z\left[-\frac{\frac{Mt}{E\cdot I} + \frac{P\cdot B}{F}(1-\beta B \sin \beta B)}{\cos \beta B}\cos \beta X - \frac{PB^2\cdot\beta}{F}\sin \beta X + \frac{P\cdot L}{F}\right] +$$

$$+ \frac{Nt-F}{A} - \alpha\cdot E\cdot T$$

(3) Both ends clamped

$$W = \frac{PB^2}{2 \cdot F \cdot \beta} \left\{ \frac{\beta B \cos \beta B - \beta B \cdot \beta \sin \beta B}{\beta B \sin \beta B - 2 + 2 \cos \beta B} \right\} \left\{ - \frac{(1-\cos \beta B)}{\beta B - \sin \beta B} (Bx - \sin BX) + (1 - \cos \beta X) \right\}$$

$$+ \frac{P \cdot B^3}{2 \cdot F} \left\{ \frac{X^2}{B^2} - \frac{\beta X - \sin \beta X}{\beta B - \sin \beta B} \right\} \qquad \text{(B-46)}$$

$$\sigma_x = -EZ \left\{ \frac{P \cdot B^2 \beta}{2F} \left(\frac{\beta B \cos \beta B + \beta B - 2 \sin \beta B}{\beta B \sin \beta B - 2 + 2 \cos \beta B} \right) \left(\frac{1-\cos \beta B}{\beta B - \sin \beta B} \sin \beta X + \cos \beta X \right) \right.$$

$$\left. + \frac{P \cdot B}{F} \left(1 - \frac{\beta^2 \sin BX}{\beta B - \sin \beta B} \right) \right\} + \frac{Nt - F}{Ac} - \alpha \cdot E \cdot T$$

The relative axial displacement of the ends, ul-uo, can be computed from equation (B-42) for each of the above edge boundary conditions. For the constrained end case, ul-uo is zero and the resulting value of axial force can be computed.

The dynamic solution of the beam-column problem requires that equation (B-41) be integrated. This integration is carried out for a thermal load which is uniform in the length direction and for a constant axial force, F, in precisely the same manner as was previously done for the beam with unconstrained ends. Results of this integration will be outlined below while details of the derivation may be found in the references.[94] A modal series solution is assumed based on the individual modes of a free vibration. (See equation B-31.) The homogeneous solution is found by neglecting the right-hand side of equation (B-31) and assuming a solution of the form $w = Wn\, e^{TX} e^{i\omega_n t}$ where ω_n are the natural circular frequencies. The circular frequencies are related to the eigenvalues, γn, of the homogeneous solution by the following relationship

$$\omega_n = \gamma n^2 \sqrt{\frac{EI}{\rho Ac}} \sqrt{1 - \frac{P}{n^2 Pcr}} \qquad \text{(B-47)}$$

In equation (B-47), Pcr is the Euler or critical force for buckling of a beam-column. This is given by,

---

[94] Ibid

$$Pcr = \frac{\pi^2 E \cdot I}{B^2} \tag{B-48}$$

The parameter τn is related to the axial force through the following,

$$\tau n = -\frac{F \pm \sqrt{F^2 + 4EI\rho A c\omega^2}}{2\ EI} \tag{B-49}$$

The homogeneous solution for the beam-column on three types of supports is the following

(1) Both ends simply supported.

$$\gamma n = \frac{n\pi}{B}$$

$$Wn = \sin \gamma n\, x \tag{B-50}$$

(2) Cantilever beam

γn are the roots of the frequency equation,

$$(\gamma^4+\zeta^4)\ \cos \gamma B \cosh \zeta B - \gamma\zeta\,(\gamma^2-\zeta^2)\ \sin \gamma B \sinh \zeta B + 2\gamma^2\zeta^2 = 0. \tag{B-51}$$

$$Wn = \frac{\sin\gamma nx - \frac{\gamma n}{\zeta n}\sinh \zeta_n x}{\sin\gamma nB + \frac{\gamma n}{\zeta n}\sinh \zeta nB} - \frac{\cos\gamma nx - \cosh \zeta nx}{\cos\gamma nB - \frac{\zeta n^2}{\gamma n^2}\cosh \zeta nB}$$

(3) Both ends clamped.

γn are roots of the frequency equation

$$2\gamma\zeta\,(1 - \cos \gamma B \cdot \cosh\zeta B) + (\zeta^2-\gamma^2)\ \sin \gamma B \cdot \sinh\ \zeta B = 0 \tag{B-52}$$

$$Wn = \frac{\zeta n \sin \gamma nx - \gamma n \sinh\ \zeta nx}{\zeta n \sin \gamma nB - \gamma b \sinh\ \zeta nB} + \frac{\cos \gamma nx - \cosh \zeta nx}{\cos \gamma nB - \cosh \zeta nB}$$

In equations (B-51) and (B-52), the roots of the frequency equation, γn and ζn, are solved simultaneously with the following relationship between these roots and the parameter, τ, given in equation (B-49)

$$\gamma n = \tau n1$$
$$\zeta n = \tau n2 \tag{B-53}$$

In equation (B-53), $\tau n1$ and $\tau n2$ are the positive and negative roots of τn, respectively. (See equation (B-49).)

The inhomogeneous solution proceeds as outlined in the previous section, i.e., the assumed form of the solution, equation (B-31), is substituted into the governing equation, equation (B-41). The initial conditions for the beam-column are w=wo and $\frac{\partial w}{\partial r}$ = Vo for all x. Using the fact that the modes of the free vibration are orthogonal, the following result is derived for the functions, Tn.

$$Tn = Cn \cdot \cos \omega nt + \frac{Dn}{\omega n} \sin \omega nt + An \int_0^t F(\mathcal{E}) \sin \omega n(t-\mathcal{E})\, d\mathcal{E} + Bn \int_0^t Mt(\mathcal{E})$$

$$\sin \omega n(t-\mathcal{E})\, d\mathcal{E} \qquad \text{(B-54)}$$

The auxiliary functions, Cn and Dn, have the following definitions.

$$Cn = \frac{1}{In} \int_0^L wo \cdot Wn \cdot dx \qquad \text{(B-55)}$$

$$Dn = \frac{1}{In} \int_0^L vo\ Wn\ dx$$

An and Bn are mode constants. These are given in reference [22] as follows for the simply-supported edge condition only.

$$An = \frac{4}{n \cdot \pi \cdot \rho \cdot Ac\omega n} \qquad \text{(B-56)}$$

$$Bn = \frac{4 \cdot \omega n \cdot B^2}{(n\pi)^3 \cdot E \cdot I}$$

The dynamic solution is completed by choosing the functions gi and fi to satisfy the particular boundary condition of the edge support. The following results were derived in the references.[95] Functions gi and fi not specified are zero in all cases.

$$f4 = -\frac{Mt}{E \cdot I} \qquad \text{(B-57)}$$

$$g4 = \frac{x}{2}(X-B)$$

---

[95] Koch, N. Eastern Res. Assoc. No. RR-NA-14, Op. Cit.

(2) Cantilever beam

$$f3 = -\frac{Mt}{E \cdot I}$$

$$g3 = \frac{x^2}{2}\left(\frac{1+H^1 \cdot B}{1-H^1 \cdot B}\right) - \frac{x^3}{3}\frac{H^1}{1-H^1 \cdot B} \qquad \text{(B-58)}$$

where $H^1 = \frac{P \cdot B}{2E \cdot I}$

(3) Both ends clamped.

$$fi = 0$$
$$gi = 0 \qquad \text{(B-59)}$$

Thus, equations (B-47) - (B-49) when used in equation (B-31) allow the dynamic displacement to be computed for a beam column which has a constant axial force. The corresponding beam stress is computed using equation (B-43). A method has been devised to treat variable axial forces by dividing the total time nto subintervals of approximately constant axial force as previously mentioned. If the beam is constrained against axial movement, the resulting axial force can be computed from equation (B-42). Then, an additional problem exists of choosing subinterval time such that the axial forces remain approximately constant over a subinterval. Due to the complexities of the beam-column problem, four computer programs were written to compute the quasi-static and dynamic displacements, stresses and axial forces for the beam on simple supports only. The first two programs compute the axial force developed in the beam-column due to to the combined pressure and thermal pulses produced by a nuclear weapon explosion. One of these programs is for quasi-static and the other for dynamic analysis. The remaining programs compute the displacement and stress in a beam-column due to the combined pressure and thermal loads of a nuclear weapon explosion and a specified axial load. The axial load can either be that due to constraining the beam or any arbitrary loading. One of these programs is for quasi-static and the other for dynamic conditions. A listing of each of these programs is found in the references.[96]

[96] Ibid

DISTRIBUTION LIST

	No. of Copies
Assistant to the Secretary of Defense Atomic Energy Department of Defense Washington D. C. 20301 Attn: Honorable Donald R. Cotter	1
Director Defense Advanced Research Project Agency Architect Building 1400 Wilson Blvd. Arlington, Virginia 22209 Attn: Technical Library	1
Director Defense Civil Preparedness Agency Washington, D. C. 20301 Attn: Technical Library	1
Defense Documentation Center Cameron Station Alexandria, Virginia 22314	12
Director Defense Intelligence Agency Washington, D. C. 20301 Attn: Technical Library	1
Director Defense Nuclear Agency Washington, D. C. 20305	
Attn: SPSS	1
Attn: DDST	1
Attn: STST Archives	1
Attn: STTL Technical Library	2

	No. of Copies
Director of Defense Research and Engineering Department of Defense Washington D. C. 20301	
Attn: DD/T&SS	1
Attn: DD/S&SS	1
Attn: DD/TWP	1
Attn: AD/NP	1
Attn: AD/SW	1
Commander Field Command Defense Nuclear Agency Kirtland Air Force Base New Mexico 87115	
Attn: FCT	1
Attn: FCPR	1
Director Interservice Nuclear Weapons School Kirtland Air Force Base New Mexico 87115	
Attn: Technical Library	1
Director Joint Strat TGT Planning Staff Offutt Air Force Base Omaha, Nebraska 68113	
Attn: Stineo Library	1
Chief Livermore Division FLD Command DNA Lawrence Livermore Laboratory P.O. Box 808 Livermore, California 94550	
Attn: FCPRL	1
Commandant National War College Fort Lesley J. McNair Washington, D. C. 20315	
Attn: NWCLB-CB	1
Weapons Systems Evaluation Group 400 Army Navy Drive Arlington, Virginia 22202	
Attn: Document Control	1

No. of Copies

Assistant Chief of Staff For Operations & Plans
Department of the Army
Washington, D. C. 20310
Attn: Director of Chemical and Nuclear Operations 1
Attn: Technical Library 1

Commander
Ballistic Defense System Command
P.O. Box 1500
Huntsville, Alabama 35807
Attn: RDMSC-TFN Noah J. Hurst 1

Director
BMD Advanced Technical Center
Hunstville Office
P.O. Box 1500
Huntsville, Alabama 35807
Attn: CRDABH-S 1
Attn: 1CRDABH-X 1

Manager
BMD Program Office
1300 Wilson Boulevard
Arlington, Virginia 22209
Attn: John Shea 1

Chief of Res. Dev. & Acquisition
Department of tne Army
Washington, D. C. 20310
Attn: Technical Library 1

Chief of Naval Material
Navy Department
Washington, D. C. 20360
Attn: Mat 0323 1

Chief of Naval Operations
Navy Department
Washington, D. C. 20350
Attn: OP 985F 1
Attn: OP 03EG 1

Chief of Naval Research
Navy Department
Arlington, Virginia 22217
Attn: Technical Library 1

	No. of Copies
Officer-In-Charge Civil Engineering Laboratory Naval Construction Battalion Center Port Hueneme, California 93041 Attn: Technical Library	1
Commander Naval Electronic Systems Command Naval Electronic Systems CMD HQS Washington, D. C. 20360 Attn: PME 117-21A	1
Commander Naval Facilities Engineering Command Headquarters Washington, D. C. 20390 Attn: Technical Library	1
Commander Naval Missile Systems Engineering Station Port Hueneme, California 93041 Attn: Code 4923 (Hort Perry)	1
Superintendent Naval Postgraduate School Monterey, California 93940 Attn: Code 2124 Tech RPTS Librarian	1
Director Naval Research Laboratory Washington, D. C. 20375 Attn: Code 2027 Technical Library	1
Commander Naval Sea Systems Command Navy Department Washington, D. C. 20362 Attn: SEA Code 03511 Attn: SEA 09G32 Attn: SEA Code 03511, Carl H. Pohler	 2 2 1
Commander Naval Ship Engineering Center Center Building Hyattsville, Maryland 20782 Attn: NSEC 6105 (Y. H. Park) Attn: NSEC 6105 (R. Fuss) Attn: Technical Library	 1 1 1

	No. of Copies
Commander Naval Ship Research and Development Center Bethesda, Maryland 20034	
Attn: Code 745 (S. L. Wang)	1
Attn: Library	1
Commander Naval Undersea Center San Diego, California 92152	
Attn: Technical Library	1
President Naval War College Newport, Rhode Island 02840	
Attn: Technical Library	1
Commander Naval Weapons Center China Lake, California 93555	
Attn: Code 533 Technical Library	1
Commanding Officer Naval Weapons Evaluation Facility Kirtland Air Force Base Albuquerque, New Mexico 87117	
Attn: Technical Library	1
Director Strategic Systems Project Office Navy Department Washington, D. C. 20376	
Attn: NSP-43 Technical Library	1

	No. of Copies
Commander Harry Diamond Laboratories 2800 Powder Mill Road Adelphi, Maryland 20783	
Attn: AMXDO-BBI John A. Rosado	1
Attn: AMXDO-II Technical Library	1
Commander Picatinny Arsenal Dover, New Jersey 07801	
Attn: Technical Library	1
Director U. S. Army Ballistic Research Laboratories Aberdeen Proving Ground, Maryland 21005	
Attn: AMXBR-X Julius J. Meszaros	1
Attn: W. Taylor	1
Attn: Technical Library, Edward Baicy	1
Attn: J. H. Keefer	1
Attn: E. Quigley	1
Commander U. S. Army Engineer Center Fort Belvoir, Virginia 22060	
Attn: ATSEN-SY-L	1
Commander U. S. Army Material Command 5001 Eisenhower Avenue Alexandria, Virginia 22333	
Attn: Technical Library	1
Commander U. S. Army Material Command Foreign and Scientific Technical Center 220 7th St. N.E. Charlottesville, Virginia 22901	
Attn: Research & Concepts Branch	1
Commander U. S. Army Missile Command Redstone Arsenal Huntsville, Alabama 35809	
Attn: Technical Library	1
Commander U. S. Army Mobility Equipment R & D Center Fort Belvoir, Virginia 22060	
Attn: Technical Library	1

	No. of Copies
Commander U. S. Army Nuclear Agency Fort Bliss, Texas 78916 Attn: Technical Library	1
Commandant U. S. Army War College Carlisle Barracks, Pennsylvania 17013 Attn: Library	1
Commander Aeronautical Systems Division, AFSC Wright-Patterson AFB,Ohio 45433 Attn: Technical Library	1
Air Force Armament Laboratory, AFSC Eglin AFB., Florida 32542 Attn: DLOSL-Library	1
Air Force Cambridge Research Laboratories, AFSC L. G. Hanscom Field Bedford, Massachusetts 01730 Attn: SUOL AFCRL Research Library	1
Air Force Weapons Laboratory, AFSC Kirtland AFB., New Mexico 87117 Attn: SUI	1
Headquarters Air Force Systems Command Andrews Air Force Base Washington, D. C. 20331 Attn: Technical Library	1
Commander Armament Development & Test Center Eglin, Air Force Base, Florida 32542 Attn: Technical Library	1
Commander Foreign Technology Division, AFSC Wright-Patterson AFB., Ohio 45433 Attn: TD-BTA Library	1
SAMSO/DY Post Office Box 92960 Worldway Postal Center Los Angeles, California 90009 Attn: DYS	1

	No. of Copies
Commander In Chief Strategic Air Command Offutt AFB., Nebraska 68113	
Attn: OAI	1
Attn: NRI-Stineo Library	1
Division of Military Application U. S. Energy Research & Development Admin. Washington, D. C. 20545	
Attn: Doc Control for Test Office	1
University of California Lawrence Livermore Laboratory P.O. Box 808 Livermore, California 94550	
Attn: Technical Information Department L-3	1
Los Alamos Scientific Laboratory P.O. Box 1663 Los Alamos, New Mexico 87545	
Attn: Doc Control for Reports Library	1
Sandia Laboratories Livermore Laboratory P.O. Box 969 Livermore, California 94550	
Attn: Doc Control for Technical Library	1
Sandia Laboratories P.O. Box 5800 Albuquerque, New Mexico 87115	
Attn: Doc Con for 3141 Sandia RPT Coll.	1
Department of the Interior Bureau of Mines Building 20 Denver Federal Center Denver, Colorado 80225	
Attn: Technical Library	1
Aerospace Corporation P.O. Box 92957 Los Angeles, California 90009	
Attn: Technical Information Services	1
Analytic Services, Inc. 5613 Leesburg Pike Falls Church, Virginia 22041	
Attn: George Hesselbacher	1

	No of Copies
Battelle Memorial Institute 505 King Avenue Columbus, Ohio 43201 Attn: Technical Library	1
BDM Corporation 1920 Aline Avenue Vienna, Virginia 22180 Attn: Technical Library	1
Boeing Company P.O. Box 3707 Seattle, Washington 98124 Attn: Aerospace Library	1
University of California at Berkeley Room 8 2543 Channing Way Berkeley, California 94720 Attn: G. Sackman	1
EG&G, Inc. Albuquerque Division P.O. Box 10218 Albuquerque, New Mexico 87114 Attn: Technical Library	1
General Dynamics Corporation Electric Boat Division Eastern Point Road Groton, Connecticut 06340 Attn: I. H. Chan	1
General Electric Company Space Division Valley Forge Space Center Goddard Boulevard King of Prussia P.O. Box 8555 Philadelphia, Pennsylvania 19101 Attn: M. H. Bortner Space Science Laboratory	1
General Electric Company Tempo-Center for Advanced Studies 816 State Street (P.O. Drawer QQ) Santa Barbara, California 93102 Attn: DASTAC	1

	No. of Copies
IIT Research Institute 10 West 35th Street Chicago, Illinois 60616 Attn: Technical Library	1
General Research Corpporation P.O. Box 3587 Santa Barbara, California 93105 Attn: Benjamin Alexander	1
Institute for Defense Analyses 400 Army-Navy Drive Arlington, Virginia 22202 Attn: IDA Librarian Ruth S. Smith	1
Kaman Avidyne Division of Kaman Sciences Corp. 83 Second Avenue Northwest Industrial Park Burlington, Massachusetts 01803	
Attn: Technical Library	1
Attn: F. S. Criscione	1
Attn: R. Yeghiayan	1
Kaman Sciences Corporation P.O. Box 7463 Colorado Springs, Colorado 80933 Attn: Library	1
Lockheed Missiles & Space Company, Inc. P.O. Box 504 Sunnyvale, California 94088 Attn: Technical Library	1
Lockheed Missiles and Space Company 3251 Hanover Street Palo Alto, California 94304 Attn: Technical Information Center D/COLL	1
Martin Marietta Aerospace Orlando Division P.O. Box 5837 Orland, Florida 32805 Attn: G. Fotifo	1
McDonnell Douglas Corporation 5301 Bolsa Avenue Huntington Beach, California 92647 Attn: Robert W. Halprin	1

	No. of Copies
Mitre Corporation Route 62 and Middlesex Turnpike P.O. Box 208 Bedford, Massachusetts 01730 Attn: Library	1
Physics International Company 2700 Merced Street San Leandro, California 94577 Attn: Doc Con for Technical Library	1
Polytechnic Institute of Brooklyn Department of Aerospace & Applied Mechanics 333 Jay Street Brooklyn, New York 11201 Attn: J. M. Klosner	1
Rand Corporation 1700 Main Street Santa Monica, California 90406 Attn: C. C. Mow	1
Science Applications, Inc. 7850 Edgewater Drive Oakland, California 94621 Attn: D. F. Maxwell	1
Science Applications, Inc. 1651 Old Meadow Road McLean, Virginia 22101 Attn: John Mansfield	1
Science Application, Inc. P.O. Box 2351 La Jolla, California 92038 Attn: Technical Library	1
Stanford Research Institute 333 Ravenswood Avenue Menlo Park, California 94025 Attn: SRI Library Room G021	1
TRW Systems Group One Space Park Redondo Beach, California 90278 Attn: Technical Information Center/S-1930	1

	No. of Copies
TRW Systems Group San Bernadino Operations P.O. Box 1310 San Bernadino, California 92402 Attn: Greg Hulcher	1
URS Research Company 155 Rovet Road San Mateo, California 94402 Attn: Ruth Schneider Attn: Technical Library	1 1
Westinghouse Electric Company Marine Division Hemdy Avenue Sunnyvale, California 94008 Attn: W. A. Volz	1